MODELLING ADVECTION OF COD EGGS & LARVAE ON THE NEWFOUNDLAND SHELF

FRASER DAVIDSON

MODELLING ADVECTION OF COD EGGS & LARVAE ON THE NEWFOUNDLAND SHELF

By

©Fraser Davidson, B.Sc.

A thesis submitted to the School of Graduate Studies in partial fulfillment of the requirements for the degree of Master of Science

Department of Physics

Memorial University of Newfoundland

July, 1994

St. John's Newfoundland Canada

ISBN 0-315-96077-9

Abstract

In this thesis I investigate the drift and retention of cod eggs and larvae on the Newfoundland Shelf using two different mathematical methods. The first is an analytical model that solves the advection-diffusion equation for a patch of larvae in a spatially homogeneous, time-dependent current for the proportion of larvae retained on the shelf. We show that there is a weak correlation between retention of larvae and recruitment of northern cod. Furthermore, we demonstrate the sensitivity of retention to location of the larvae relative to the shelf break.

In the second method we use a two-dimensional velocity field to study the interannual variations of cod egg and larval dispersion on the Newfoundland and Labrador shelf. This model uses a steady state mean flow derived from a diagnostic calculation of objectively analysed density data for the Northeast Newfoundland Shelf. Time-dependent currents are generated using a slab model driven by observed winds, following the approach of Pollard-Millard (1970). We study the advection of the eggs and larvae using numerical Lagrangian drifters seeded throughout the Newfoundland Shelf region. We identify favourable and unfavourable zones of retention on the Newfoundland shelf. We show that northerly, shelf break spawning locations are more favourable than southerly shelf break spawning locations for northern cod (*Gadus*

Morhua in NAFO divisions 2J3KL).

Contents

List of Figures

List of Tables

Acknowledgements

I would like to extend my sincerest appreciation to my supervisors Dr. Brad de Young and Dr. Joe Wroblewski. I am grateful to Joe's enthusiasm, encouragement, and guidance throughout my course of studies. I would like to extend my gratitude to Brad for focussing my research and his encouragement for me to present a talk as well as attend conferences. I would like to thank both my supervisors for their many patient and thoughtful and stimulating reviews of this thesis.

I am grateful to the knowledge and kind disposition of Allan Goulding, Ken Forward, Fred Perry, Todd Wareham, Paul Fardy and Ying Ren, the programmers in the Physical Oceanography group and Memorial University. Stimulating discussion's demystified the world of computing and increased the efficiency of my programming. I am also indebted to Drs. Richard Greatbatch, Kevin Lamb and Alex Hay who imparted to me some of their knowledge of ocean circulation and fluid dynamics.

I am grateful to my parents for their support and encouragement. I would like to thank my fellow class mates, Youyu Lu and Guoqing Li for their friendship and support throughout my studies at Memorial University.

Last but certainly not least, I would like to thank my Grand-mother, Mrs. J. B. Moore for all her support and kind encouragement throughout my post secondary

education.

This work was supported by the Ocean Production and Enhancement Network (OPEN), one of the Networks of Centres of Excellence funded by the Natural Science and Engineering Research Council of Canada (NSERC). Financial support from the School of Graduate Studies at MUN, in the form of a Graduate Fellowship, is also acknowledged.

Chapter 1

Introduction

1.1 Overview

Numerical modelling in physical oceanography is a fundamental tool for understanding the property distributions and circulation of sea water. It can be helpful in the interpretation of spatially and temporally limited observations of circulation. However, a representative model of ocean currents must be based upon observations. Since we cannot resolve physical processes continuously in time and space, we are restricted to describing the processes that the model and observations can resolve. Such models may be, initially at least, somewhat simplistic. However, they can span a range of time-dependent components of the real flow over a broad spatial scale. Applications

of ocean circulation models include enhanced search and rescue operations, determination of oil spill trajectories, improved designs of offshore structures and assessment of the environmental impact of chemical spills.

Ocean circulation models are also useful in fisheries oceanography. One possible application of such models is in the assessment of the success of spawning strategies of fish. In the simplest models, eggs and larvae may be treated as passive drifters. Egg and larval drift determines if larvae reach suitable nursery grounds, thereby increasing their chance of survival (Hjort 1914). While the physical environment plays an important role, biological processes such as predation and first feeding cannot be neglected in providing an explanation of larval survival. Before including these biological processes in a model, it is constructive to look first at how environmental variability can influence a fish population.

In this thesis, we explore direct links between environmental variability and the spawning success of a cod population. We look first at a simple analytical model of advection of cod eggs and larvae. We then proceed to apply a circulation model of the Northeast Newfoundland shelf to examine the success of different spawning strategies for Northern Cod (*Gadus morhua* in NAFO division 2J3KL).

1.2 Circulation on the Newfoundland Shelf

The Newfoundland and Labrador Shelf is one of the broadest continental shelves on Earth (Figure 1.1). It ranges from Hudson Strait to the tail of the Grand Banks along the eastern coasts of Labrador and Newfoundland. The ocean circulation in this region was first described by Smith *et al.* (1937) through work carried out by the International Ice Patrol (IIP). The source water of the Labrador Current is a combination of the cold and fresh Baffin Land Current ($< -1°C$, $33.0 - 33.5$ ppt) with Hudson Bay outflow for the inner shelf region ($< 1°C$, 33.0 ppt), (Smith *et al.* 1937) and a combination of the Baffin Land Current with the warmer, saltier ($3-4°C$, 34.8 ppt) West Greenland Current on the outer shelf region (Kollemeyer *et al* 1967, Smith *et al.* 1937). The contribution of the West Greenland Current to the total transport of the Labrador Current is approximately 10% (Sutcliffe *et al.* 1983). The Labrador Current flows southward from Hudson Strait along the Labrador Coast and appears as two branches at Hamilton Bank. (Smith *et al.* 1937, Lazier and Wright 1993). The main branch of the Labrador Current flows over the upper shelf break following the 500 m isobath (Figure 1.1) and contains 90% of the total transport of 5-6 Sv (Moynihan and Anderson 1971, Petric and Anderson 1983)(1 Sv = $10^6 m^3 s^{-1}$). The main branch is a narrow jet of water 50 km in width (Lazier and Wright 1993)

coinciding with a strong density front (Smith *et al.* 1937, Allen 1979, Lazier and Wright 1993) dividing the brackish, cold shelf waters from the warmer, saltier North Atlantic waters.

Just north of the Grand Banks, the Labrador current splits into three parts, flowing through the Avalon Channel with 0.6 Sv (Petrie and Anderson 1983), the Flemish Pass with 4.2 Sv (Greenberg and Petrie 1988) and eastwardly north of the Flemish Cap (Mathews 1914) with 3.2 Sv (Greenberg and Petrie 1988). Currents on the Grand Banks are irregular and weak (de Young and Tang 1988). Drifter and iceberg studies on the Grand Banks (Petrie 1985, Petrie and Isenor 1985) indicate no clear mean circulation pattern on the Grand Banks, although they do point to a generally southerly flow there. Some of the westward flow north of Flemish Cap circulates anticyclonically around Flemish Cap and rejoins the main branch that came through the Flemish Pass. At the southern end of the Grand Banks, a fraction of the main branch flow is entrained directly into the Gulf Stream and the North Atlantic Current. The remaining 3 Sv (McLellan 1957) flows westwards off the southern flank of the Grand Banks (Chapman and Beardsley 1989).

There have been several circulation models to explain different features of the Labrador Current. Observations of significant bottom velocities for the main and inshore branch prompted Greenberg and Petrie (1988) to apply a barotropic model

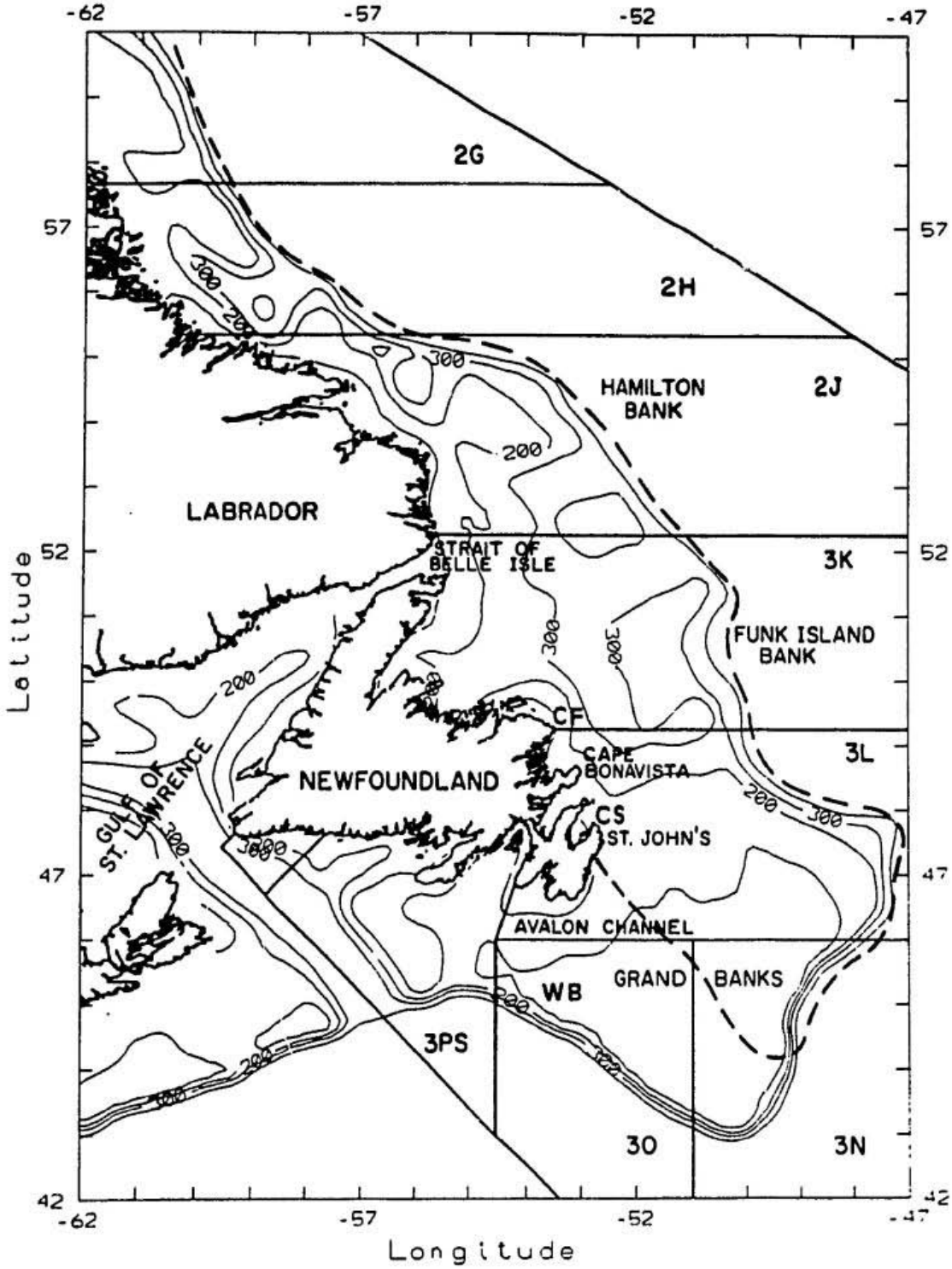

Figure 1.1: Overview of the Newfoundland Shelf region. WB refers to Whale Bank. CF refers to Cape Freels, and CS refers to Cape St. Francis.

to the Newfoundland shelf circulation. Bottom velocities through Flemish Pass are roughly 80% of the mean flow though the Pass. The barotropic model qualitatively describes the circulation on the Newfoundland Shelf with the inshore and offshore branch, as well as flow through the Avalon Channel and the Flemish Pass around the Grand Banks. Model flow on the Grand Banks is weak and westwards. Measurements of modelled transport and observed transport showed reasonable agreement. While the barotropic model approach explains some of the general circulation features on the Newfoundland Shelf, such as topographically steered flow, it includes neither density gradients nor seasonal density variations. Satellite images showing undulations of pack ice edges with horizontal length scale of 75 km above the main branch of the Labrador Current on four consecutive winter days suggest baroclinic instability at the shelf break (LeBlond 1982). In the Avalon Channel, during periods of increased stratification the flow is baroclinically unstable (Anderson 1986).

The temperature and salinity jump between shelf waters and North Atlantic waters is about $3°C$ and 1 ppt respectively. Shelf water salinity varies greatly due to spring freshwater runoff as well as melting of sea ice. Harmonic analysis of data from Station 27 in the Avalon Channel by Petrie *et al.* (1991) reveals that the amplitude of the seasonal cycle at the surface is 7°C and 0.7 ppt for temperature and salinity respectively. The seasonal variations decrease greatly with depth, so that at the

bottom of the Avalon Channel, temperature and salinity vary only slightly during the year by 1°C and 0.1 ppt respectively. Noting the salinity minimum at Station 27 in September in the Avalon Channel, Bailey (1961) reasoned that the bulk of low salinity water originated from Southern Labrador, assuming an advection velocity of 10 cm s^{-1}. Doubling this velocity to 20 cm s^{-1} would mean that the fresh water originated from as far north as Davis Strait (Petrie and Anderson 1983). Myers et al. (1990) compared surface salinity at Station 27 with Hudson Bay runoff, Ungava Bay runoff and ice-melt on the Newfoundland and Labrador Shelf. They conclude that ice-melt on the Newfoundland and Labrador Shelf is the leading cause of the September salinity minimum at Station 27. Hudson Bay and Ungava Bay runoff had little effect on Station 27 salinity. Thus each spring a pulse of fresh water stemming from spring runoff and ice melting is advected down the Labrador and Newfoundland Shelf. On the shelf, the cold fresh water layer reaches down to around 200 m while underneath lies warmer but saltier water that has been advected from offshore (Lazier and Wright 1993). During the summer, the surface heats up, leaving a cold arctic water layer at mid depths, the Cold Intermediate Layer (Petrie *et al.* 1992). This layer of cold water is thought to affect the migration and distribution of cod (Templeman 1966).

Variability of the Labrador Current is probably quite significant. The seasonal variations of the flow are comparable to the mean flow (Lazier and Wright 1993).

The main branch of the Labrador Current shows a minimum in velocity in March and April and a maximum in October (Lazier and Wright 1993). The variation in total flow which reaches 5 Sv is caused by the Joint Effect of Baroclinicity and Relief (JEBAR) (Lazier and Wright 1993). This variation is probably driven by the strong seasonal cycle in fresh water flux into the Labrador Current, since freshening of the shelf waters draws in water from offshore. Although wind forcing may not affect the net transport of the Labrador current, it can certainly shift the position of the very narrow (50 km) main branch of the Labrador Current with respect to bottom topography.

One way to account for density fronts in a circulation model is by diagnosing the circulation from a given density field (de Young *et al.* 1993a). They used an objectively analysed set of seasonally binned observations from all available data for the Northwest Atlantic from 1910 to 1989 (de Young *et al.* 1994b). Care was taken to ensure that the strong density gradients associated with the main branch of the Labrador Current were not smeared by the objective analysis process. Diagnosing this density field yields a steady state, 3-D current field that represents the seasonal averaged flow over a period of 79 years. The resulting surface circulation field is similar to that of Greenberg and Petrie (1988), thus suggesting that upstream boundary conditions and topography steering dominate in determining the circulation pattern

in this region.

To date, there have been no shelf circulation models for the Newfoundland Shelf that permit resolution of baroclinic-instability-driven-eddies. This would be necessary to resolve the time-dependent variations that have amplitudes of the order of the mean flow of the Labrador Current main branch. For the present we must be content with diagnostic or barotropic models. We have briefly summarised the hydrographic environment of the Newfoundland and Labrador Shelf, as well as some of the models describing the circulation for this shelf. Our main regional focus is the Northeast Newfoundland Shelf, for which we shall examine the link between circulation and dispersion of cod eggs.

1.3 Biology of northern cod

Atlantic cod, *Gadus Morhua*, are adapted for bottom feeding, living in waters ranging from the cool-temperate to subartic waters and are found in depths ranging from the surface to 450 m (Scott and Scott 1988). On the Northeast Newfoundland Shelf, cod mainly spawn close to the bottom near the shelf break in water depths greater than 250 m with ambient temperatures around 3°C (Templeman 1981). Spawning times extend from April to July (Myers *et al.* 1993). On average a female cod may

release $\frac{1}{4}$ million eggs per batch several times per spawning season (Kjesbu 1988). Survival rates for eggs and larvae are very low, with, perhaps, only one egg in a million surviving to the adult stage. Eggs are positively buoyant and start rising slowly in the water column. Egg density varies with surrounding water density and decreases with development (Anderson and de Young 1994). In 5 to 10 days, eggs rise into the top 50 m layer of the ocean (Anderson and de Young 1994). The egg stage ends at hatching, which occurs after 40 days in 0°C water and after 20 days in 2°C water (Page and Frank 1989). At hatching, the yolk sack is the only source of energy for the larvae for the next 5 days, after which larvae must forage or starve. For cod on the Northeast Newfoundland shelf, there is a dearth of information on the vertical distribution of cod eggs and larvae (Helbig *et al.* 1992). Given the stratification and the vertical diffusivity of a water column, we can predict larvae and egg distribution if we know the egg or larval density (Anderson and de Young 1994, Kjesbu 1992) as well as the swimming ability of the larvae (Sclafani *et al.* 1993). From egg and larval densities, we can infer that healthy eggs prior to hatching and larvae are in the surface layer for most waters on the shelf. Larval mobility is very limited (≤ 0.2 cm s^{-1}) (Sclafani *et al.* 1993).

Metamorphosis of cod larvae into juvenile fish is a gradual process that may be demarcated by the descent of larvae out of the surface layer (Pepin and Myers 1991).

This descent occurs 5 to 9 months after spawning (Brown *et al.* 1989). Juveniles differ from adults by readily withstanding sub zero degrees water due to higher production of anti-freeze proteins (Goddard *et al.* 1993). This enables them to overwinter in the cold inshore water of Newfoundland bays. Juveniles do not associate with adult cod due to predation risk, but by age three they join the adult cod population and become harvestable by the fishery. The newly recruited cod do not reach full maturity till age 7 (Harris *et al.* 1991), when they become reasonably proficient spawners. Cod in nature may reach the age of 25 or older in the absence of a fishery. Northern Cod have been observed to migrate and spawn in large groups (Rose 1993).

A group of cod that spawn together is referred to as a population. A stock may be composed of one or more populations. The physical requirements for the spawning ground of a population is that there be a current system that transports eggs and larvae to suitable nursery grounds (Iles and Sinclair 1982). The size of the population depends upon the size of the spawning grounds as well as the characteristics of the current. On the Newfoundland Shelf, favourable spawning locations are regions from which released eggs and larvae are retained shoreward from the 500 m isobath. Variability in the size of the retention zone due to variable wind driven currents, buoyancy driven currents and time of spawning may reflect variability in the recruitment to that population. Suitable spawning environments are spatial and

temporal windows of opportunity, in which the survival success of the year class is determined (Bakun *et al.* 1982).

1.4 Modelling Larval Dispersion

Many studies regarding the links between retention of larvae and the environment have been carried out for several species of fish outside of the Labrador and Newfoundland shelf region. Location and timing of spawning with respect to hydrodynamic features is important in ensuring transport from the spawning grounds to the nursery grounds where larvae and juveniles may grow (Hjort 1914, Iles and Sinclair 1988, de Young and Rose 1993).

Wind driven currents may be important to larval transport. Nelson *et al.* (1976) demonstrated the relationship between Ekman on-shelf transport of Cape Hatteras (US) and the number of year old menhaden (*Brevoortia tyrannus*). Years of high on-shelf transport correspond to years of good recruitment. In a study on Japanese sardine larval transport with respect to the Kuroshio Current, Kasai *et al.* (1992) showed that offshore Ekman transport and spawning distance from the Kuroshio axis were important factors in enabling larvae to reach their nursery grounds.

For North Sea herring (*Clupea harengus L.*), Bartsch *et al.* (1989) used a 3

dimensional baroclinic circulation model to illustrate the eastward advection of herring larvae. Their nonlinear model was forced by seasonal mean densities, three hour winds, three hour pressure fields as well as the M_2 tide. Tracers with a given diurnal vertical migration were inserted into the model flow field to simulate herring larvae. The authors were able to simulate the drift of larvae from northeast Scotland and the Yorkshire coast to the Danish coast and into the German Bight. They found that for model tracers to enter the German Bight, as observed, required adjustment of vertical migration, indicating that for herring larvae in the North Sea, the amplitude of their diurnal vertical migration as well as their mean depth are important factors for successful drift to their nursery grounds.

For fish with reproductive strategies such as cod where millions of eggs are released from a female during the spawning season, proximity to suitable concentrations of prey at time of first feeding is important. Fortier *et al.* (1992) show that capelin (*Mallottus villosus*) and sand lance (*Ammodytes sp.*) larvae in the northwestern Gulf of St. Lawrence depend on high concentrations of prey occurring in the Gaspé coastal current jet and subsequent transport into the Anticosti Gyre which is their nursery ground.

To simulate cod and haddock larval drift on Georges Bank, Werner *et al.* (1993) apply a 3-dimensional nonlinear time-dependent diagnostic circulation model (Lynch

et al. 1991) forced by inflow boundary conditions and the M_2 tide. They test the importance of hydrodynamic features and larval behaviour to the retention of eggs spawned on the Northeast Peak of Georges Bank. Eggs released in the top 10 m of the water column are swept off the Bank by the wind driven component of flow. Eggs released below 30 m have a greater chance of being retained on the Bank. Eggs released at 50 m are retained. Their model emphasises the importance of vertical distribution in the water column on larval drift.

There have been two previous attempts at exploring the mechanistic links between the environment and the recruitment of cod in the Newfoundland Shelf region. Myers and Drinkwater (1988) applied a simple 1-dimensional Lagrangian drift model using the cross shelf Ekman component of velocity. They attempted to find a correlation between the number of larvae within a 50 km distance from shore and recruitment. Their results showed no relationship, however their method ignored along-shore currents and spatial inhomogeneity of the mean flow field. Helbig *et al.* (1992) used the barotropic velocity field of Greenberg and Petrie (1988) with an additional wind driven component of flow to examine tracks of passive drifter seeded on the Newfoundland shelf. They demonstrated that the advection of eggs and larvae from the Northeast Newfoundland Shelf to the bays of Northeast Newfoundland required appropriate wind forcing. They also demonstrated that under mean barotropic

flow cod eggs on the Newfoundland Shelf drift around the Grand Banks rather than onto the Grand Banks. This reinforced the hypothesis that cod on the Northeast Newfoundland Shelf may be treated as a separate population from cod on the Grand Banks (de Young and Rose 1993).

1.5 Objectives of this study

In this thesis we are interested in determining how physical factors influence year to year variability in survival of the cod eggs and larvae.

Chapter 2 presents a semi-analytical model of retention of larvae on the Northeast Newfoundland Shelf (de Young and Davidson 1994). Using an idealised, time-dependent homogeneous circulation field, we investigate interannual variability of retention of cod eggs and larvae on the shelf. We discuss the sensitivity of the model to cod spawning locations. As well, we summarise cod recruitment data for the Northeast Newfoundland Shelf.

In chapter 3 we present the numerical model used to solve the advection-diffusion equation for a two-dimensional, time-dependent flow field. The flow field consists of a time-dependent, Pollard-Millard slab model with wind-driven currents, superimposed on a steady state circulation field taken from the diagnostic model of

de Young *et al.* (1993a) as applied to the Newfoundland Shelf. We make use of a Lagrangian tracking model to examine interannual variability in larval drift paths. To analyse dispersion of a patch of drifters we use a geometrical method to estimate the area and shape of a set of passive drifters. This geometrical scheme is presented in Appendix C. In Chapter 3 we also discuss year-to-year variations in retention of eggs and larvae in different shelf region, drift trajectories, displacement of larvae and we identify ideal spawning locations based on passive drift.

In chapter 4 we conclude with a discussion of the relative merits of spawning locations in view of our model results. We discuss the limitations of our model and future research possibilities on the drift of cod eggs and larvae.

Chapter 2

Analytical Retention Model

2.1 Introduction

In this chapter we present an analytical solution to a model of retention of cod larvae on the Newfoundland and Labrador shelf. The egg and larval stage is crucial to the survival of a fish population (Hjort 1914, Iles and Sinclair 1982). Advection may play a critical role in their survival. We shall explore the fundamental characteristics that govern the retention of cod larvae on the Newfoundland and Labrador Shelf. We extend a model of Kasai *et al.* (1992), originally developed to explain the importance of spawning locations of Japanese Sardines (*Sardinops melanosticus*) for retention of larvae shoreward from the Kuroshio Current. They solve a one-

dimensional, advection-diffusion equation with constant velocity for a given initial Gaussian distribution of passive drifters. They define a 'Retention Rate' R as the proportion of eggs and larvae shoreward from the Kuroshio Current at a given time t. Here, we shall extend this model by making it two-dimensional and including a time-dependent wind driven velocity component. We shall rename the 'Retention Rate' of Kasai *et al.* (1992) as 'Retention Ratio' since it expresses a ratio of larvae retained in a specific area over all larvae. We explore the influence of spawning ground location, diffusivity, size of egg patch, the mean Labrador Current and the wind-driven current on the retention of cod larvae on the Newfoundland Shelf through the use of an analytical model.

Since the Newfoundland and Labrador Shelf topography is complex and mean flow in the region is topographically steered, we must use an idealised topography. The shelf is simplified to a rectangular shape with a length of 1000 km and a width of 240 km (see Figure 2.1). The mean flow of the Labrador current is simplified to a homogeneous flow in the along-shelf direction, with a fixed velocity of 0.2 ms^{-1}. We shall consider the flow to be an average of the horizontal currents over the top 50 m.

The retention ratio R is the proportion of larvae on our rectangular shelf at a given time. The shelf has three open boundaries and one land boundary. We shall consider the drift of a patch of passive cod eggs and larvae starting in the

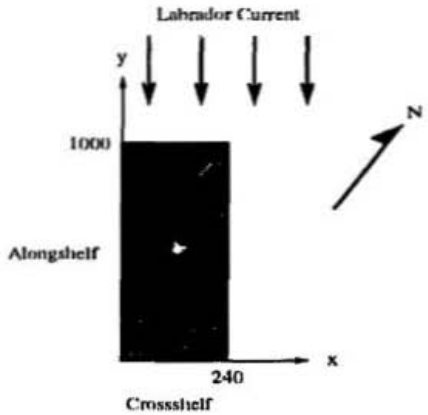

Figure 2.1: The model domain and axis orientation showing the shelf (shaded region) and the direction of the mean flow (0.20 ms^{-1}), representing the southeastward flowing Labrador Current.

Northeast corner of the shelf and examine the retention ratio. For sardine larvae in the Kuroshio current system, Kasai *et al.* (1992) considered the region inshore from the Kuroshio current axis as being the favourable environment for successful development of eggs and larvae. On the Newfoundland and Labrador Shelf, the main branch of the Labrador current separates the favourable shelf waters from the less favourable deep ocean waters. Since the main branch coincides with the shelf break, we use the shelf break as the demarcation zone for retention. Although we have greatly simplified the topography, we have maintained the basic features of the

system; i.e., a long shelf that is hundreds of kilometres broad.

We shall assume that the eggs are in the surface Ekman layer (Helbig *et al.* 1992). Hence we shall use an average wind-driven Ekman velocity, averaged over the top 50 m of the water column (Gill 1982). Anderson and de Young (1994) showed that eggs take up to 5-10 days to reach the surface layer, where they remain until after hatching. The time from spawning to hatch is about 20-30 days at these temperatures. Young larvae can be treated as passive drifters until they are 60 days old.

2.2 Model Development

The time rate of change of larval concentration in a given volume is equal to the advection and diffusion of larvae out of this volume. The two-dimensional advection-diffusion equation is,

$$\frac{\partial C}{\partial t} + u\frac{\partial C}{\partial x} + v\frac{\partial C}{\partial y} = \kappa_h \left(\frac{\partial^2 C}{\partial x^2} + \frac{\partial^2 C}{\partial y^2} \right) \quad , \tag{2.1}$$

where $C(x, y, t)$ is concentration, t is time, $u(t)$ and $v(t)$ are the x and y components of velocity and κ_h is the horizontal diffusivity. The advection-diffusion equation can be solved by analogy to the simple one-dimensional diffusion equation

$$\frac{\partial C}{\partial t} = \kappa_h \frac{\partial^2 C}{\partial x^2} \quad , \tag{2.2}$$

which has the solution,

$$C = \frac{1}{\sqrt{4\kappa_h t}} e^{\frac{-x^2}{4\kappa_h t}} \quad . \tag{2.3}$$

To solve the two-dimensional, advection-diffusion equation we use the following transformation of coordinates,

$$\hat{x} = x - \int_0^t u(t')dt' \quad , \tag{2.4}$$

$$\hat{y} = y - \int_0^t v(t')dt' \quad , \tag{2.5}$$

$$\hat{t} = t \quad . \tag{2.6}$$

By the chain rule of differentiation, we find

$$\frac{\partial}{\partial x} = \frac{\partial}{\partial \hat{x}} \quad , \tag{2.7}$$

$$\frac{\partial}{\partial y} = \frac{\partial}{\partial \hat{y}} \quad , \tag{2.8}$$

$$\frac{\partial}{\partial t} = \frac{\partial}{\partial \hat{t}} - u\frac{\partial}{\partial \hat{x}} - v\frac{\partial}{\partial \hat{y}} \quad . \tag{2.9}$$

In the modified coordinates, the advection-diffusion equation is expressed as a simple diffusion equation: B

$$\frac{\partial C}{\partial \hat{t}} = \kappa_h \left(\frac{\partial^2 C}{\partial \hat{y}^2} + \frac{\partial^2 C}{\partial \hat{y}^2} \right) \quad . \tag{2.10}$$

The solution approach that we follow is similar to that taken by Kasai *et al.* (1992), except that we make fewer simplifying assumptions. We assume, as do they, that the initial distribution of the spawning eggs is given by a Gaussian distribution. This produces solutions for the retention ratio in terms of error functions. We do not assume that the velocities u and v are constant in time. Both velocity components are time-dependent yet spatially uniform.

Transforming the standard solution of the diffusion equation (2.3) into the original coordinates x and y, making the substitution $t = T + t_o$ yields

$$C = \frac{1}{\sqrt{4\kappa_h(T + t_0)}} \exp \left(\frac{-(y - \int_0^{T+t_o} v(t)dt)^2 - (x - \int_0^{T+t_o} u(t)dt)^2}{4\kappa_h(T + t_0)} \right) \quad . \tag{2.11}$$

T is the time after the initial spawning when the variance of the distribution of the patch in the x and y direction is $4\kappa_h t_0$. t_0 is the time taken to evolve from a singularity to the initial patch distribution. Letting $\alpha = 4\kappa_h t_0$, and then simplifying the solution we obtain

$$a = 4\kappa_h t + \alpha \ , \tag{2.12}$$

$$cx = \int_0^T u(t')\, dt' + x_o \ , \tag{2.13}$$

$$cy = \int_0^T v(t')\, dt' + y_o \tag{2.14}$$

and allowing for reflection of the larval patch at the coast $x = 0$ gives

$$C = \frac{1}{\sqrt{a}} \exp\left(\frac{-(y-cy)^2}{a}\right) \times \left\{\exp\left(\frac{-(x-cx)^2}{a}\right) + \exp\left(\frac{-(x+cx)^2}{a}\right)\right\} \ . \tag{2.15}$$

where a is the time-dependent variance of the larval distribution, and cx and cy are the coordinates of the patch centre. The retention ratio is the proportion of eggs on the shelf to the total number of eggs, and is given by

$$R(t) = \frac{\int_{As} C(x,y,t)\, dA}{\int_{Aw} C(x,y,t)\, dA} = \frac{\int_0^L \int_0^l C(x,y,t) dx dy}{\int_{-\infty}^{\infty} \int_0^{\infty} C(x,y,t)\, dx\, dy} \ , \tag{2.16}$$

where As and Aw represent the area of the shelf and the whole region respectively, l is the cross-shelf width and L is the along-shelf length. Note that the coordinate system is set such that y is along-shelf and x is cross-shelf (Figure 2.1).

Making the substitution

$$\sigma = (y - cy)/(\sqrt{a}) \qquad dy = \sqrt{a} d\sigma$$

$$\phi = (x - cx)/(\sqrt{a}) \qquad dx = \sqrt{a}d\phi$$

$$\varphi = (x + cx)/(\sqrt{a}) \qquad dx = \sqrt{a}d\varphi$$

and applying the following boundary conditions:

$$y = L \rightarrow \sigma = (L - cy)/\sqrt{a}$$

$$y = 0 \rightarrow \sigma = -cy/\sqrt{a}$$

$$x = l \rightarrow \phi = (l - cx)/\sqrt{a}$$

$$x = 0 \rightarrow \phi = -cx/\sqrt{a}$$

$$x = l \rightarrow \varphi = (l + cx)/\sqrt{a}$$

$$x = 0 \rightarrow \varphi = cx/\sqrt{a}$$

then the retention ratio for the model domain is

$$R(T) = \int_{-cy/\sqrt{a}}^{(L-cy)/\sqrt{a}} e^{-\sigma^2} d\sigma \times \left(\int_{-cx/\sqrt{a}}^{(l-cx)/\sqrt{a}} e^{-\phi^2} d\phi + \int_{cx/\sqrt{a}}^{(l+cx)/\sqrt{a}} e^{-\varphi^2} d\varphi \right) \qquad (2.17)$$

If we define the error function such that

$$erf\,(a, b) = \frac{2}{\sqrt{\pi}} \int_a^b e^{-z^2} dz \qquad (2.18)$$

where z is just a dummy variable, then the retention ratio becomes

$$R(T) = \frac{\pi}{4} erf\left(\frac{-cy}{\sqrt{a}}, \frac{(L-cy)}{\sqrt{a}}\right) \times \left\{ erf\left(\frac{-cx}{\sqrt{a}}, \frac{(l-cx)}{\sqrt{a}}\right) + erf\left(\frac{cx}{\sqrt{a}}, \frac{(l+cx)}{\sqrt{a}}\right) \right\} \tag{2.19}$$

where a, cx and cy depend on T, as in equations (2.12), (2.13) and (2.14). Note that we are primarily interested in the region close to the shelf break. The reflection condition at the coastline is negligible when considering larval drift at the shelf break since the wind-driven current cannot transport particles across the width of the shelf within the time frame that we are considering, approximately 50 days. The average wind-driven currents are on the order of 1 cm s^{-1}.

2.3 Model Analysis

Detailed information on the spawning location of cod is sparse though in a summary of cod recruitment and distribution de Young and Rose (1993) concluded that most of the spawning occurs in water 300-600 m deep, near the shelf break. A recent paper by Hutchings and Myers (1993) questions this conclusion, using trawl catch data to show that spawning cod have also been found on the inner part of the shelf. We shall assume that the majority of cod spawn on the outer part of the shelf, near the shelf break (Templeman 1966). Recruitment data for comparison with model results

were obtained from the Department of Fisheries and Oceans sequential population analysis (Hilborn and Walters 1992) of the cod in the 2J3KL region (Figure 1.1) of the Newfoundland Shelf (Baird *et al.* 1992).

Wind data used in the model was measured at hourly intervals at St. John's. Wind speeds measured on land may underestimate the wind speed blowing across the ocean (de Young *et al.* 1993b). Wind data at St. John's show good agreement with wind data collected at the mouth of Conception Bay (de Young *et al.* 1993b). We shall assume the wind stress to be uniform over the entire Newfoundland Shelf. Wind stress was computed using the drag formulation developed and tested by Large and Pond (1981). We have filtered the wind stress data using a low-pass filter, to remove energy at periods below half a day. The wind stress was then converted to the vertical averaged velocity for the Ekman layer by

$$< u_{EK} > \quad = \quad \frac{\tau^y}{\rho f H} \tag{2.20}$$

$$< v_{EK} > \quad = - \quad \frac{\tau^x}{\rho f H} \tag{2.21}$$

Here τ^y and τ^x are the wind stress components in the x and y direction, H is the depth of the Ekman layer assumed to be 50 m, f is the coriolis parameter (assumes constant at $10^{-4} s^{-1}$), ρ is the density of sea water (set at 1024 $\mathrm{kg\,m^{-3}}$) and $< u_{EK} >$

and $< v_{EK} >$ are the horizontal velocity components averaged over the depth H of the Ekman layer.

The model velocity field consists of the Ekman components, with -0.2 ms^{-1} added to the v component to represent the Labrador Current. The time step in model was twelve hours. Integrations of the retention ratio over time were carried out for two drift periods of 50 days starting 1 April and 21 May. These drift periods were chosen to cover the spawning period of the cod (Templeman 1966, May 1966) and to test sensitivity of the model to the timing of the release of the patch.

The starting egg mass was initially located in the northeast corner of the model domain (Figure 2.2), corresponding roughly between the southern Labrador shelf and the north end of the Northeast Newfoundland shelf. Some sample trajectories for the centre of mass of larvae patches are shown in Figure 2.2. The cross-shelf component of the wind-driven current is more important than the along-shelf wind driven component of flow in determining retention over a period of 50 days since patches are along the eastern boundary of the shelf. The two plots in Figure 2.2 show trajectories for years when the retention was high (1975) and low (1981), illustrating the differences in the trajectories for these two years. This particular model run is from 21 May to 10 July covering the time when larvae are present on the shelf. The halfway point of the drift curves, marked with a circle in Figure 2.2, show that 1981

and 1975 are very different in the first half of the period, but are quite similar in the second half. This sensitivity to the timing of the drift of larval patches complicates somewhat the interpretation of our results.

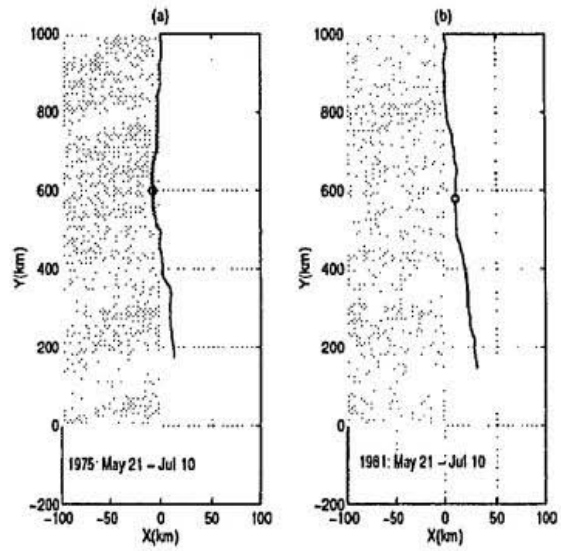

Figure 2.2: Sample trajectories of the egg patch centroid for (a) 1975 and (b) 1981. The period for the simulation is from 25 May to 10 July. The halfway point in the simulation is shown with an open circle. The shaded area represents the shelf.

As a retention index suitable for comparison with recruitment data we average the retention ratio over the period of the model run R_{av}. This averaged retention ratio $R_{av}(yr)$ takes in account the time that the larval patch spent on or off the shelf which cannot be accounted for by using the retention ratio at 50 days (i.e., R(50d)) in the model run. To analyse the sensitivity of the averaged retention ratio $R_{av}(yr)$, we plot

for all years in the model run $R_{an}(yr)$ against horizontal diffusivity and initial larval patch radius. Figure (2.3a) refers to an initial starting position at the shelf break and Figure (2.3b) refers to eggs starting 50 km inshore from the shelf break. Increasing the initial patch radius reduces year to year variability in retention. Initial patch radius is particularly important for patches initially centred at the shelf break where the effect of increasing the patch radius increases retention during years of onshore wind-driven currents and decreases retention during years of offshore wind-driven currents. For a small egg patch, retention of larvae on the shelf is highly variable since the currents only need to advect the patch slightly to alter the proportion of eggs on the shelf. For a patch radius of 5 km, the standard deviation of the yearly averaged retention ratio (R_{an}) is 0.2 with a mean of 0.3. Increasing the radius to 100 km raises the mean by a factor of 2 and reduces the standard deviation by a factor of 3. For larval patches seeded at the shelf break in the absence of the cross-shelf component of flow, diffusion and patch radius have no effect on retention. If a patch remains centred at the shelf break changing the radius or the diffusivity coefficient does not alter the proportion of shelf bound larvae.

Dependence on the diffusivity coefficient is limited (Figure 2.4). Increasing diffusion decreases slightly interannual variability in retention. For years of high retention, a horizontal diffusivity coefficient of 100 m^2s^{-1} decreases the yearly averaged

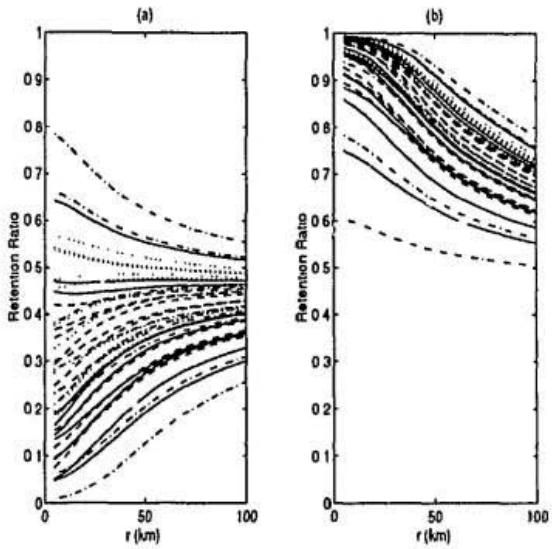

Figure 2.3: Dependence of the averaged retention ratio R_{av} on initial patch radius r for years 1953 to 1992 of the model run. The model run spans 50 days starting 1 April. In (a) initial egg mass position is at the shelf break. In (b) initial egg mass is located 50 km inshore from the shelf break.

retention rate by 3 % over the non diffusive case.

An important factor regarding retention is the timing of spawning. Figure 2.5 is the same plot as Figure 2.3 except that the model run starts 50 days later, on 21 May rather than 1 April. From the years 1953 to 1992 the standard deviation around the mean of the averaged retention ratio R_{av} during the period 1 April to 20 May is twice that of the period from 21 May to 10 July. This indicates that spawning success early in the season would be more variable than later in the spawning season, if wind-driven retention is an important factor. As well, there is no correlation between model runs

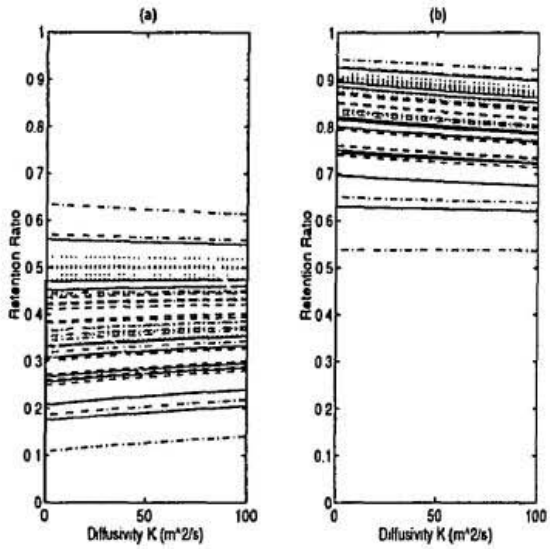

Figure 2.4: Dependence of retention ratio R on diffusivity κ_h. For (a) the initial egg mass position is at the shelf break. For (b) the initial egg mass position is inshore (50 km) from the shelf break.

that start early in the spawning season (April-May) and those that start 50 days later. Thus model results depend strongly on time of spawning.

We would like to compare model results to recruitment. We have developed a model pertaining to an idealised spawning population of cod that spawn at the same place at the same time each year in an idealised marine environment. Although the currents may not be entirely realistic, we believe that the variability of the wind at St. John's reflects the variability of wind over the Newfoundland Shelf. Our results concerning retention applies to cod populations spawning between the southern

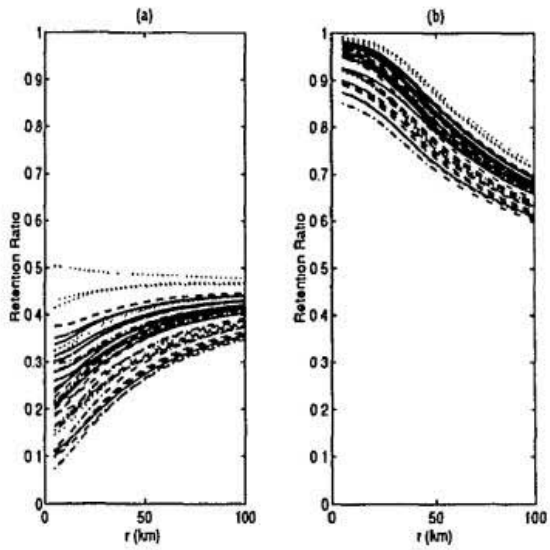

Figure 2.5: Same as for Figure 2.3 but with model runs starting 50 days later on 21 May.

Labrador Shelf and the north end of the Northeast Newfoundland Shelf. However the only reliable source of recruitment information is for the entire 2J3KL region (de Young and Rose 1993).

The recruitment data used is from sequential population analysis (Hilborn and Walters 1992) of cod in the 2J3KL region. A year class is the group of fish born in the same year. Sequential population analysis is based on summing catch at age throughout the years for each year class to estimate the number of fish of a year class that the enter fishery at the age of 3. For this analysis, it is necessary to assume an arbitrary function of age for the natural mortality of fish. Thus the recruitment data

is a measure of the number of fish that 'recruit' into the fishery, that is, fish that can be caught. Recruitment represents the survival success of cod, at the egg, larval and juvenile stages.

Cod recruitment data derived from observations of trawl catches is subject to misreporting of trawler catches. As well, effects of management and reporting policies may install trends in the data. Prior to the extension of the jurisdiction of coastal waters to 200 miles in 1977, undersampling and misrepresentation of catch may have resulted in misclassification of age classes prior to 1977 (Pinhorn and Halliday 1990).

A plot of the retention ratio over the period 1960 to 1990 shows the interannual variability in the retention ratio, normalised by the maximum since it is the variability itself in which we are interested (Figure 2.6). Also plotted in Figure 2.6 is the recruitment index for the 2J3KL cod stock (Figure 1.1). This recruitment index has been normalised by the number of adults (thus density dependent effects are removed), and also by the maximum in the record. The time series shown in Figures 2.6 have a cross correlation coefficient r of 0.34 which is only marginally significant, at the 90% level. Removing the stock recruitment relationship (normalising recruitment by biomass) does not make much difference to this overall correlation.

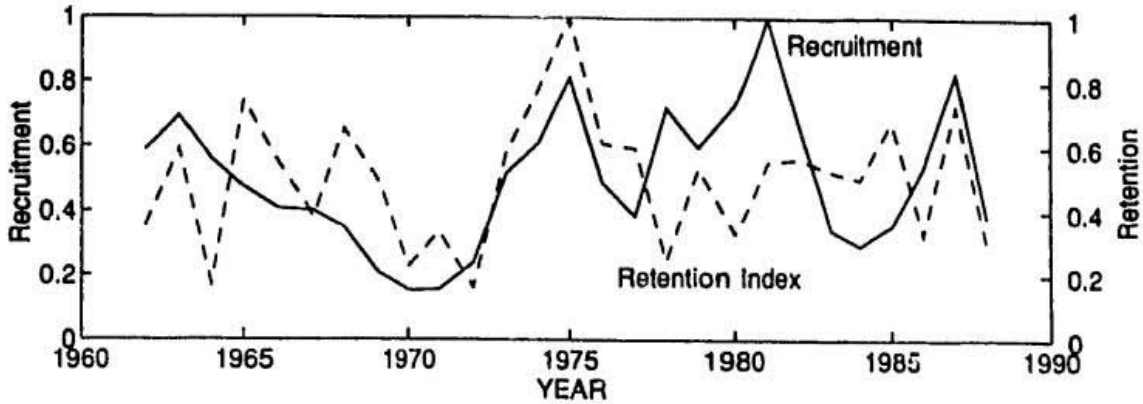

Figure 2.6: Recruitment index (solid line) and retention index $R_a v$ (dashed line) for the period spanning 1962 - 1988. These indexes have been normalised by the maximum so that indexes vary between 0 and 1. Here $R_a v$ represents model runs beginning 1 April.

2.4 Discussion of Analytical Model

We have developed a two-dimensional analytical model to simulate the time-dependent retention of eggs and larvae on the Newfoundland Shelf. The retention ratio of the model is marginally correlated with the measured recruitment of cod in the 2J3KL region of the Newfoundland shelf. These results are consistent with the recent model of de Young and Rose (1993), who argue that retention of eggs and larvae on the shelf is important for successful recruitment for cod in this region.

The analytical model developed here is similar to that of Myers and Drinkwater (1988) in that the primary factor influencing retention of larvae on the Newfoundland

Shelf is the cross-shelf Ekman component of velocity. Our model differs from Myers and Drinkwater (1988) by solving the advection-diffusion equation for a patch of larvae rather than following discrete particles. Furthermore, including along shore currents in our model allows allows us to observe that bulk Ekman flow cannot account for cod eggs and larvae to reach the coast of Newfoundland from the shelf break in the time it takes for them to drift along the entire length of the shelf.

A difficulty with the analysis presented here is that the spawning does not occur simultaneously throughout the 2J3KL region. Cod in the northern part of the region (2J) are thought to spawn earlier than those in the south (3L). Since the retention ratio will depend upon the time window that we choose, then our results may be confounded by this time variability. Unfortunately the only reliable recruitment data are for the entire 2J3KL region (de Young and Rose 1993). As well, cod populations that spawn in the same place each year may not spawn at the same time of year due to a changing environment.

Probably the most important factor ignored in this model is the influence of the vertical migration of the larvae (Sclafani *et al.* 1993, Werner *et al.* 1993), for which we have no data.

The strong cross-correlation that exists amongst almost all environmental variables in the Northwest Atlantic (Petrie *et al.* 1992) makes it difficult to develop a

mechanism for the influence of the environment upon recruitment. Our model does show significant correlation but the percentage of explained variance is small. We shall next apply a more sophisticated numerical model, which uses the diagnostic velocity field, that will allow us to consider spatial dependence of onshelf residence.

Chapter 3

Numerical modelling of drifting egg and larvae

3.1 Introduction

In chapter 2 we presented analytical solutions to the advection-diffusion equation for a spatially homogeneous current field. With a simplified topography and circulation for the Newfoundland Shelf, these analytical solutions allowed us to investigate the influence of wind-driven currents on the retention of passive cod eggs and larvae. Since the mean flow in these analytical cases is spatially uniform, a homogeneous wind affects particle drift identically regardless of particle location. The most important

criteria for retention in a homogeneous circulation field is initial distance from the shelf break. Regardless of wind-driven currents, shelf retention for a patch of larvae is high if the patch is at a sufficient distance inshore from the shelf break.

Circulation on the Newfoundland Shelf has strong spatial characteristics which include the main and the inshore branches of the Labrador Current with weak and variable flow in mid-shelf (Greenberg and Petrie 1988). Mean currents are also weak on the Grand Banks (Petrie and Isenor 1982), although there is a well defined southward transport through the Avalon Channel (Petrie and Anderson 1983). Retention of a particle on the shelf may be reduced if the wind drives it from a quiescent shelf location into the strong main branch Labrador current. However, if wind pushes particles from one quiescent shelf location to another one, shelf retention may not be appreciably altered.

To account for the spatial features of Newfoundland Shelf circulation, solving the advection-diffusion equation requires a numerical approach. This can be done either by finite differencing the advection-diffusion equation (de Young *et al.* 1994a) or by determining the advection paths of discrete particles using a Lagrangian tracking model (Bartsch *et al.* 1989). In the latter case, diffusion may be simulated by giving particles a random motion whose effect is equivalent to diffusion.

In this chapter we shall make use of a Lagrangian tracking model to examine

dispersion of cod eggs and larvae over the entire Newfoundland Shelf subject to a steady spatially dependent velocity field derived from a diagnostic calculation and a uniform wind forced time-dependent current. The Lagrangian tracking routine is effective in simulating the dispersion and advection of a patch of larvae. For small patches, it is highly efficient compared to finite differencing the advection-diffusion equation for an entire model domain. In tracking large patches of drifters, the Lagrangian tracking routine offers the possibility to backtrack and explore the dispersion of a subset of particles without rerunning the model. This cannot be accomplished when finite differencing the advection-diffusion equation. Since there remains some debate about the spawning locations for Northern Cod (Hutchings and Myers 1994), we shall explore retention of cod eggs released over the entire Newfoundland shelf region (de Young and Rose 1993). We seek to identify ideal spawning grounds based on consistency of retention.

Cod eggs are treated as passive drifters since they have no swimming ability. Egg stage duration ranges from 20 to 40 days (Page and Frank 1989). At hatching larvae feed on their yolk sack for roughly 5 days (Hempel 1972). Therefore it is reasonable to assume that eggs and larvae are passive drifters until at least 25 - 45 days after spawning. Since the Newfoundland Shelf is covered by very cold water ($0^{o}C$) during the spawning season, we shall assume egg stage duration to be 40 days,

with organisms completely passive till 45 days after spawning. Since early stages of cod larvae have limited mobility, we shall treat them as passive drifters over periods ranging from 50 to 100 days. We shall assume that cod larvae younger than 100 days have no horizontal migration ability and thus do not swim in any fixed direction for extended periods of time.

Observations of cod egg and larvae vertical distributions on the Newfoundland Shelf are few (Anderson and de Young 1994). The vertical distribution depends on vertical currents and egg & larvae buoyancy and swimming in the case of larvae. Buoyancy depends in turn on stage of development and nutritional condition. At spawning, cod eggs are released near the sea floor and rise slowly to the surface layer in 5 - 10 days (Anderson and de Young 1994). It is possible to model egg and larval vertical distributions based solely on buoyancy arguments, incorporating such a 1D model into a 3D circulation model. However, before attempting 3D modelling of larval dispersion, we aim first to understand the effects of horizontal dispersion over the Newfoundland Shelf. We shall model larval dispersion in the horizontal plane only. In this chapter we assume i) that eggs and larvae are confined to the top 50 m of the water column and ii) that the drift of all eggs and larvae is governed by the vertically averaged horizontal velocities throughout the top 50 m of the water column. It is foreseeable that Northern Cod larvae younger than 100 days may have

significant swimming speeds in the vertical direction so that their vertical distribution is not entirely passive. However, we shall neglect any vertical variations in currents or larvae distribution.

3.2 Model Description

3.2.1 Mean Flow Field

The mean flow field used by our Lagrangian tracking model is derived from a diagnostic model (de Young *et al.* 1993a) which is based upon an earlier model of Mellor *et al.* (1982). The data used by this circulation model is a density field derived from objectively analysed observations in the region, spanning the period from 1908 to 1988 (de Young *et al.* 1994b).

The model solves the steady-state linear equations of motion in sigma coordinates (i.e. x, y, σ where $\sigma = z/H$).

$$-fv = -\frac{1}{\rho_0}\frac{\partial p}{\partial x} - b\sigma\frac{\partial H}{\partial x} + \frac{1}{H^2}\frac{\partial}{\partial \sigma}\left(\nu\frac{\partial u}{\partial \sigma}\right) \tag{3.1}$$

$$-fu = -\frac{1}{\rho_0}\frac{\partial p}{\partial y} - b\sigma\frac{\partial H}{\partial y} + \frac{1}{H^2}\frac{\partial}{\partial \sigma}\left(\nu\frac{\partial v}{\partial \sigma}\right) \tag{3.2}$$

$$0 = -\frac{\partial P}{\partial \sigma} - \rho_0 b H \tag{3.3}$$

$$\frac{\partial}{\partial x}(uH) + \frac{\partial}{\partial y}(vH) + \frac{\partial}{\partial \sigma}(\Omega H) = 0 \tag{3.4}$$

where

$$b = \frac{g}{\rho_0}(\rho - \rho_r) \tag{3.5}$$

and

$$\Omega = \frac{1}{H}\left\{w - \sigma\left(u\frac{\partial H}{\partial x} + v\frac{\partial H}{\partial y}\right)\right\} \tag{3.6}$$

u, v, w, Ω are the x, y, z, σ components respectively of velocity, ν is the vertical eddy viscosity coefficient, g is the gravitational acceleration constant, ρ_0 is mean water density, ρ is water density, ρ_r is horizontal averaged water density and f is the Coriolis parameter which varies on a spherical surface.

The solution method involves calculating separately the vertical averaged horizontal components of flow (i.e. $\overline{u}$, $\overline{v}$) and the zero vertically averaged horizontal components of flow. The vertically averaged flow is calculated by solving for χ where

$$\chi = \psi - \Phi/f \tag{3.7}$$

ψ is the bulk stream function defined by

$$\overline{u}H = -\psi_y \quad \overline{v}H = \psi_x \tag{3.8}$$

Φ is proportional to the potential energy per unit area of the water column.

$$\Phi = H^2 \int_{-1}^{0} b\sigma \, d\sigma \tag{3.9}$$

Calculating χ rather than Ψ avoids explicit determination of the $JEBAR$ term which is inherently noisy. As boundary conditions, χ is set to zero at land boundaries and is specified at open boundaries. For land areas Φ is set to zero and the depth H is set at 1 metre. The σ or z component of velocity is derived from the equation of continuity once u and v are known, hence the vertical velocity may be noisy.

The horizontal steady-state flow field used in the Lagrangian tracking routine is obtained by averaging the u and v components of the diagnostic circulation field over the upper 50 m of the water column. We shall make use of the spring velocity field spanning the months of March, April and May (Figure 3.1).

This velocity field is not perfectly conservative. For the diagnostic model, the 3D continuity equation holds. In averaging the horizontal velocity components over the upper 50 m, we ignore the vertical velocities. Since these are generally non-zero, the 2D continuity equation has a small error less than 5×10^{-7} s^{-1} corresponding

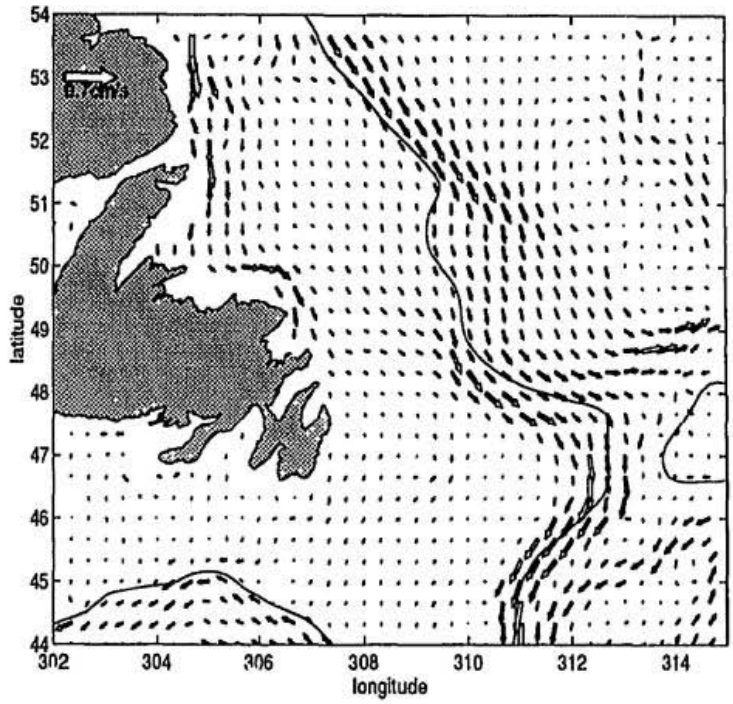

Figure 3.1: Top 50 m vertical averaged horizontal velocities from the Spring Diagnostic Model. The solid line represents the 500 m isobath.

to vertical velocities less than 25 $\mu m\,s^{-1}$. Figure 3.2 shows the contour lines for 2D divergence. Comparisons to the divergence field of the upper layer ($\sigma = 0$) of the 3D diagnostic model show that zones of convergence and divergence along the coast line originate from the diagnostic model while some convergence and divergence zones near the 500 m isobath are associated with vertically averaging of horizontal velocities. Although there are vertical velocities pumping water into and out of the

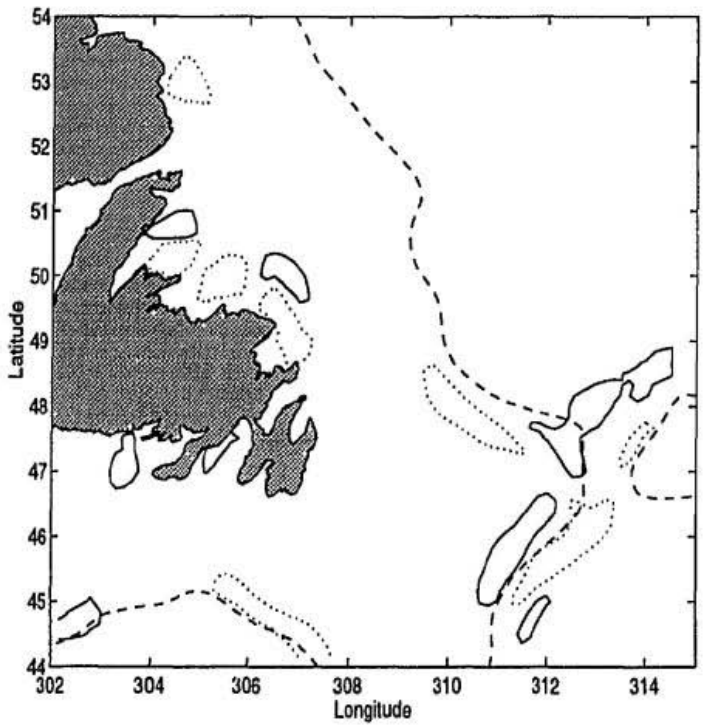

Figure 3.2: Divergence field for Figure 3.1 The solid line indicates a contour of 5×10^{-8} s^{-1} and the dotted line indicates a contour of -5×10^{-8} s^{-1}. The dashed line is the 500 m isobath.

upper layer, we do not permit the larvae and eggs to move vertically. Neglecting vertical velocities in the circulation field may cause larvae to concentrate or disperse in areas with significant vertical velocities.

3.2.2 Wind Driven Flow

In the circulation field used by the Lagrangian tracking routine, the wind-driven component of flow is derived from a slab model. We solve the vertically averaged 2D, time-dependent linear equations of motion with 3 components: the Coriolis force, linear friction and wind stress. The equations of motion governing the wind-driven component of flow are:

$$\frac{\partial u}{\partial t} - fv = \frac{\tau^x}{\rho h} - ru \tag{3.10}$$

$$\frac{\partial v}{\partial t} + fu = \frac{\tau^y}{\rho h} - rv \tag{3.11}$$

where u are v are x and y components of flow, τ^x and τ^y are the x and y components of wind stress, h is the depth of the mixed layer, ρ is the density of sea water taker as 1024 kg m^{-3}, r is the coefficient of linear friction set at 0.2 d^{-1} and f is the Coriolis parameter. For the above equations we make the f-plane approximation. This slab circulation model was originally introduced by Pollard and Millard (1970).

The Pollard-Millard model is a simple, yet realistic model of surface wind-driven flows (Pollard and Millard 1970; de Young and Tang 1989). The Pollard Millard equations (3.10 and 3.11) are solved numerically using a " leap frog in time " finite

differencing scheme. To avoid time splitting a forward timestepping scheme is used every *nft* time step where *nft* is an odd integer we set at 21. The finite differencing scheme is stable for $\Delta t < \frac{1}{2f}$. In our case the longest allowable time step is an hour and a half. The finite differencing scheme is presented in Appendix A. The finite differenced solution was tested using a constant wind stress blowing over an ocean initially at rest. The inertial oscillations induced by the introduction of wind stress decay in time, such that over the course of time, flow is south to the right of the wind as in the classic Ekman model.

Wind data used in the Pollard Millard model are from the hourly time series of wind speed observations at St. John's airport. The time series is from 1 January 1953 to 30 November 1992. Wind stress, calculated following Large and Pond (1981), is applied to the Pollard Millard model with a 1 hour timestep. Wind data were neither filtered nor smoothed. St. John's wind speed was chosen primarily due to the length and consistency of the time series. A long time series is required to look at interannual variability. As well, St. John's is situated within 250 km of the centre of our region of interest on the Newfoundland Shelf.

3.2.3 Lagrangian Tracking

Our investigation consists of tracking passive particles through a prescribed flow field of the Newfoundland Shelf region. This field is comprised of a mean background flow diagnosed from density observations and a Pollard Millard wind-driven slab model flow. Each particle is tracked individually using

$$\frac{d\vec{p}}{dt} = \vec{u} \tag{3.12}$$

where $\vec{p}$ is the particle position and $\vec{u}$ is the velocity of the water parcel at the particle position $\vec{p}$. The iterative interpolation method used to solve (3.12) through finite differencing is based on Hunter (1987), Page and Smith (1989) and presented in Appendix B. The objective of the scheme is to insure a smooth transition of particle positions from one time step to the next.

We simulate a diffusion with a diffusivity coefficient A_h of 50 m^2s^{-1} (Csanady 1982) by a random walk motion. At each timestep we add to the particle position a random vector that has a standard deviation of $2A_h\Delta t$ and a mean of zero in both the x and y direction. Δt is the model timestep set at 1 hour to coincide with the velocity field timestep. The distribution of a large group of discrete particles approaches a continuous distribution described by the advection-diffusion equation.

Particle drift onto land is prevented in this tracking routine by omitting the use of diffusion and the wind-driven component of flow for particles within ~15 km of the coast. The movement of particles is governed by three components; the mean diagnostic circulation field, the wind-driven component of flow and the random walk component. Only the diagnostic circulation field has no normal flow at land boundaries. Thus in the vicinity of land, we only use the diagnostic component of flow only and neglect simulation of diffusion. If a particle does drift onto land or is initially seeded on land it is immobilized .

3.3 Model Validation

In this section we compare the Lagrangian tracking routine output to observed drifter data on the Newfoundland shelf. Model drift paths are compared to drifter track observations collected as part of the Ocean Production and Enhancement Network (OPEN) North East Newfoundland Shelf. Drogued at 25m, drifters were initially released on the Newfoundland Shelf between 8 July and 10 July 1991 and their positions tracked for roughly 80 days. A total of 8 drifters were released from locations varying from 51.3 to 52.8 °N, and from mid-shelf to the shelf break. After 80 days, only one drifter was retained on the Newfoundland Shelf. The remaining drifters were

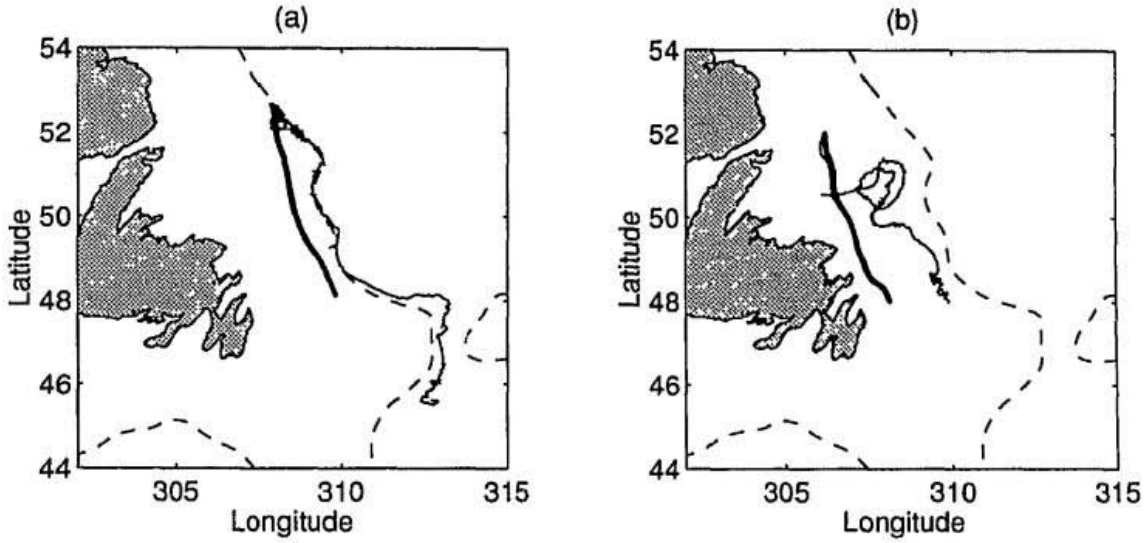

Figure 3.3: Model particle drift paths (thick line) shown with the corresponding observed drogued drifter paths (thin line). (a) using s1 from OPEN 91 drifter data. (b) using s2 from OPEN 91 drifter data.

southwards and off the shelf. One drifter crossed the Flemish Pass and moved onto the Flemish Cap. The remaining six were advected though the Flemish Pass.

For comparison, with the drifter data, the Lagrangian model is run with 8 particles seeded at observed drifter release sites. Only the mean flow field is used without any diffusion. Figure 3.3 shows the comparison of drifter paths between observed and modelled drifters for 2 drifter release sites.

Observed drifters are advected distances from their release sites between one and three times further than their model counterparts. Most modelled drifter paths are

inshore from observed tracks. Some of the observed drifters follow the 500 m isobath closely. This is not mimicked by modelled drifters (Figure 3.3a). Drogued drifters released on the shelf have a greater cross shelf displacement than their respective modelled drifters. Furthermore, the Lagrangian model does not reproduce particles reversing direction or drifter tracks crossing themselves (Figure 3.3b). Although the mean flow described by the diagnostic model mimics some features seen in the drifter data, it spreads out shelf-break flow. The model does not resolve some of the short time scale events such as storms and eddies. These factors may play an important role in drifter advection.

Since modelled drifters tend not to move into the main branch of the Labrador Current as the observed drifters, their advection velocities are consequently slower. The main branch of the Labrador Current is a 50 km narrow shelf break current whose location with respect to bottom topography is variable (Lazier and Wright 1993). The average flow over 80 years represented by the diagnostic model illustrates a diffuse, slower moving main branch current.

Diffusion and the addition of the wind component of flow may help the model better mimic observed drifter tracks. We ran the model 10 times with a random walk component for particles released for the eight observed drifter release sites. The resulting tracks for particles seeded at release sites **s1** and **s2** are plotted in Figure

3.4a. Wind data used covers a 100 day period starting 9 July. Particles were allowed to drift for 100 days.

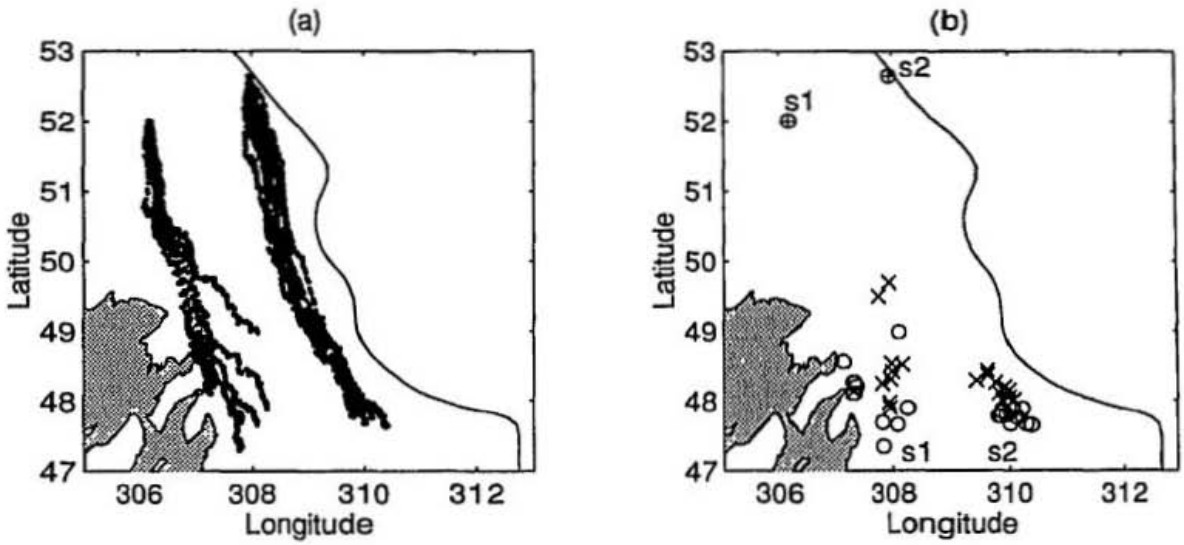

Figure 3.4: (a)10 model drifter tracks for each release site (**s1** and **s2**). (b) Initial release sites (⊕) and drifter location after 100 days. X's mark location for the no-wind case, o's mark final location for cases with wind.

The effect of diffusion is spatially dependent and linked to the mean diagnostic background flow field through which the particle is drifting. In the first 60 days particles released at **s1** show slight separation due to diffusion. As the particles approach the inshore branch of the Labrador Current the influence of diffusion is clear. A slight displacement between particles is enhanced by the flow field velocity gradients. At a 100 days, particle separation may be as much as 250 km. Particles

released at the **s2** release site are not as greatly affected by diffusion despite initial spreading due to proximity to the main branch of the Labrador Current. These particle tracks do not cross strong velocity gradients.

The wind-driven component of flow is uniform so that it cannot act directly with diffusion to enhance particle dispersion, however, the wind can move particles with respect to the mean flow field, thereby altering the spatial characteristics and timing of particle dispersion. Figure 3.4(b) shows the final location after 100 days for each of the 10 particles released at **s1** and **s2**. The X's indicate position at 100 days of particles immersed in the diagnostic flow field with a random walk component. Circles indicate final position of particles submitted to the diagnostic flow field, the wind-driven component of flow and the random walk motion. The wind-driven flow transports particles further south.

For the particles released at **s1**, wind forcing increases zonal spreading and increases the number of particles at the head of Trinity and Conception Bays from 1 to 4. Thus wind forcing and diffusion may play a role in allowing passive particles seeded on the shelf to enter the bays along the Newfoundland Coast. For particles released at the **s2** release site, wind pushes particles to final locations after 100 days of drift 25 to 100 km further to the southeast.

Wind forcing pushes model drifters further down the shelf, but not far enough

to account for the observed drifter paths. The drifters were drogued at 25 m and currents at 25 m may differ from the vertically averaged velocities over 50 m. The direction of wind-driven currents may be more windward leading to higher cross shelf advection to the main branch of the Labrador Current. Although the diagnostic model does reproduce most of the features of shelf circulation, it also weakens and broadens surface current features.

3.4 Model Results

3.4.1 Spatial Dispersion

To explore the spatial character of particle dispersion on the Newfoundland shelf we track nearly 4000 particles seeded evenly through out the entire shelf region with the Lagrangian tracking model. Particles are seeded on a grid with spacing 0.15°N by 0.15°E between latitudes 45° and 54°N and longitudes 304° and 314°E regardless of land boundaries (Figure 3.5a). Particles initially seeded on land are immobilized. Particles are tracked for a period of 100 days starting 1 April of each year. The seeding arrangement allows great flexibility as well as permitting a general overview of particle dispersion throughout the Newfoundland Shelf region.

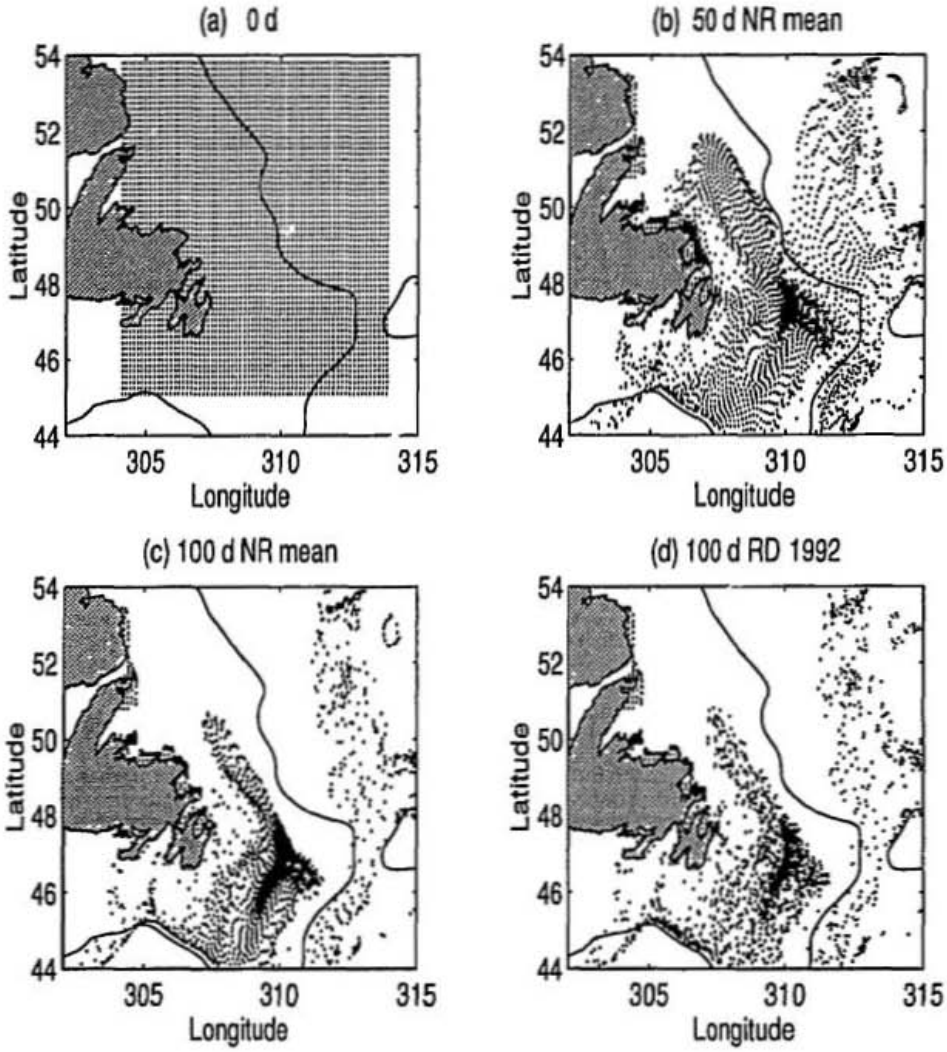

Figure 3.5: (a) Grid of the $\sim$ 4000 release locations for model particles seeded uniformly between 304° and 314°E, 45° and 54°N every 0.15°. (b) Position of particles subjected to mean current field for 50 days. (c) Position of particles subjected to mean current field for 100 days. (d) Position of particles subjected to mean current field, winds for 1992 and diffusion for 100 days.

After 50 days, locations of the 4000 particles reflects the spatial structure of the current. The absence of particles on the north end of the Newfoundland Shelf shows the influence of the inshore and offshore branch of the Labrador Current (Figure 3.5b). Further south the presence of flow through the Avalon Channel is indicated by the scarcity of particles in the region. Regions which contain concentrations of particles are the northeast Newfoundland coast, the mid shelf region south of 52°N and the Grand Banks. There are still particles over the 500 m isobath in the vicinity of the nose of the Grand Banks. Of the particles that drift eastwards from the 500 m isobath, none drift onto the Flemish Cap. However some particles do straddle its northern edge. Wind and diffusion were not included in Figure 3.5b. The regular initial particle seeding arrangement is reflected at 50 days (Figure 3.5b) by the lines formed by particles in retention areas such as the Grand Banks.

By 100 days, the pattern of particles retained shoreward of the 500 m isobath is highly visible. Only a very narrow tongue of particles are retained in the mid-shelf region. Along the eastern flank of the Grand Banks particles are retained within the 200 m isobath (Figure 3.5c). There are no particles between the 500 m and 200 m isobaths along the eastern flank. Although particles are retained throughout most of the Grand Banks region, a high concentration of particles is visible in the northeast of the Bank.

The general pattern of particle positions over the Newfoundland Shelf at 100 days does not change substantially with the addition of wind and diffusion (Figure 3.5d). The main and inshore branches are still clearly visible. Diffusion eliminates any evidence of the initial regular seeding arrangement. A high concentration of particles near the nose of the Grand Banks is still visible. The thin tongue of particles in the mid-shelf region is 20 to 30% wider than in the no-wind case.

A picture of advection patterns can be obtained by contouring the distance over which particles are displaced. Figure 3.6a is a contour plot of particle displacement from seeded origin at 50 days where the mean flow field is the only factor governing particle drift. Areas of high advection do not necessarily correspond to areas of high current velocities, but to locations where particles may reach stronger currents within a suitable period of time. On Hamilton Bank, there is a region of displacement greater than 250 km over 50 days associated with the inshore branch of the Labrador Current. Moving further offshore, particle displacement drops below 150 km in the mid-shelf region, but increases in the vicinity of the 500 m isobath to displacement values greater than 250 km. Close to land particle advection is low. Particle advection is less than 1 km a day shoreward of the inshore branch of the Labrador Current. It is interesting to note that the displacement gradient is greater between the coast and the inshore branch than between the shelf region and the main branch. Further

south the influence of the inshore branch on particle transport decreases and particle displacement gradients are weaker. Along 49°N, displacement increases continuously with eastward distance from the coast. At the north end of the Grand Banks, the displacement pattern is more intricate, with a displacement less than 100 km close to shore, in the central region and on the eastern flank of the Bank. Contour lines around the edges of the Grand Banks have been truncated due to particles leaving our model domain. In general, the eastern and southern portions of the Grand Banks have weak advection with less than 100 km displacement over 50 days. Over the northern portion of the Grand Banks, displacement over 50 days varies between 50 km and 200 km.

The displacement contours after 50 days of drift with wind forcing for the years 1984 and 1992, show resemblance of the general shelf wide displacement patterns among the wind-forced and no-wind model runs (Figures 3.6a, b and c). The displacement pattern for the year 1984 resembles that of the no-wind case, particle displacement over 50 days in 1992 may vary on the order of 50 km from the no-wind case. Near Hamilton Bank, the surface area of the region with particle displacement greater than 250 km has increased by 11 % from the no-wind case. There is also less retention in the mid-shelf region where particle displacement remains above 150 km. There are significant increases in particle transport over the northern portion of the

Grand Banks associated with 1992 winds. The overall net effect of including 1992 wind, is an increase in particle displacement.

By 100 days, the shape of the displacement contours (Figures 3.7a,b and c) is similar to those of 50 days. There are, however, differences between the 1984 wind forced case and the no-wind case; e.g. wind diminishes retention in the northern shelf sections of our domain. Along the 500 m isobath particle entrainment is slowest in the North. South of 49°N along the 500 m isobath particles leave our model domain within 100 days. From 50° to 53°N within 100 km inshore from the shelf break, particle displacement is greater than 400 km, with particles being advected into the main branch of the Labrador Current just north of the Grand Banks.

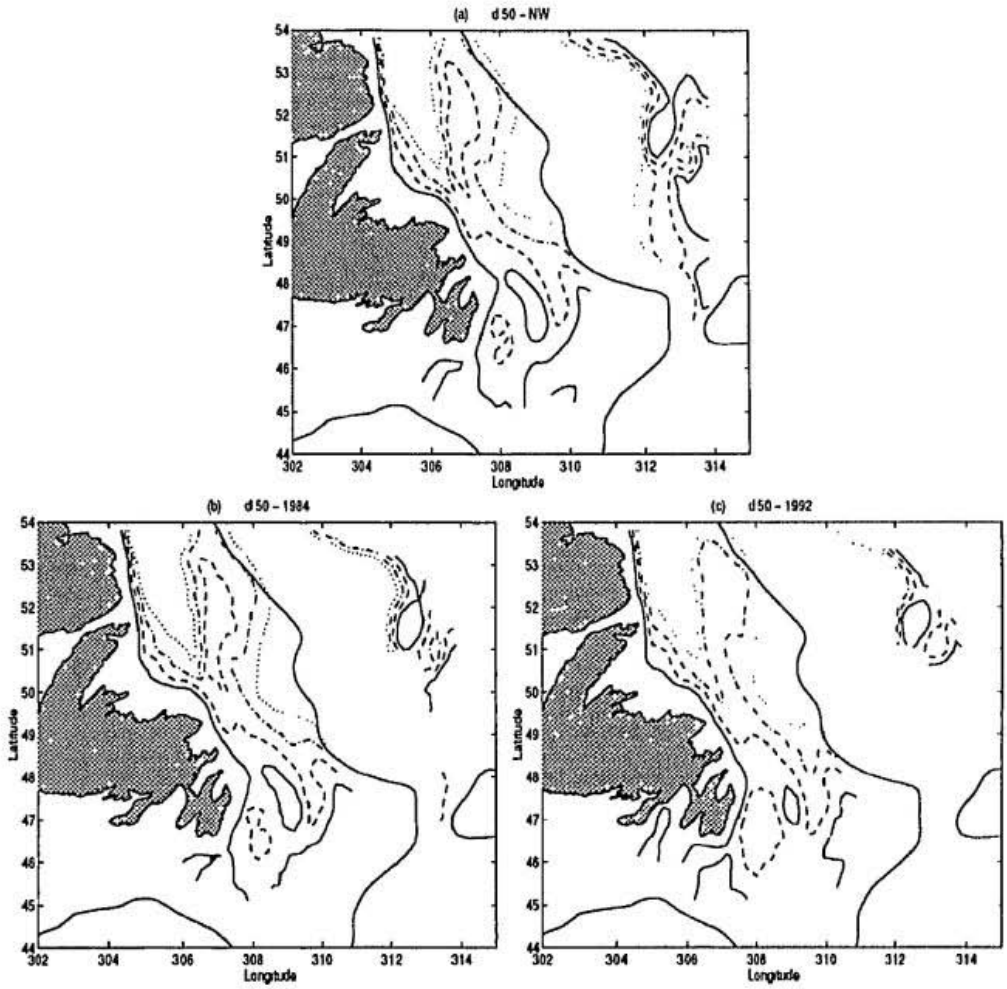

Figure 3.6: Contours of distances travelled by particles in 50 days starting 1 April. Solid line is 100 km contour, dashed line is 150 km contour, dashed-dotted line is 200 km contour and the dotted line is 250 km contour. (a) represents the mean flow case with no wind, (b) includes in addition 1984 winds and (c) includes in addition 1992 winds.

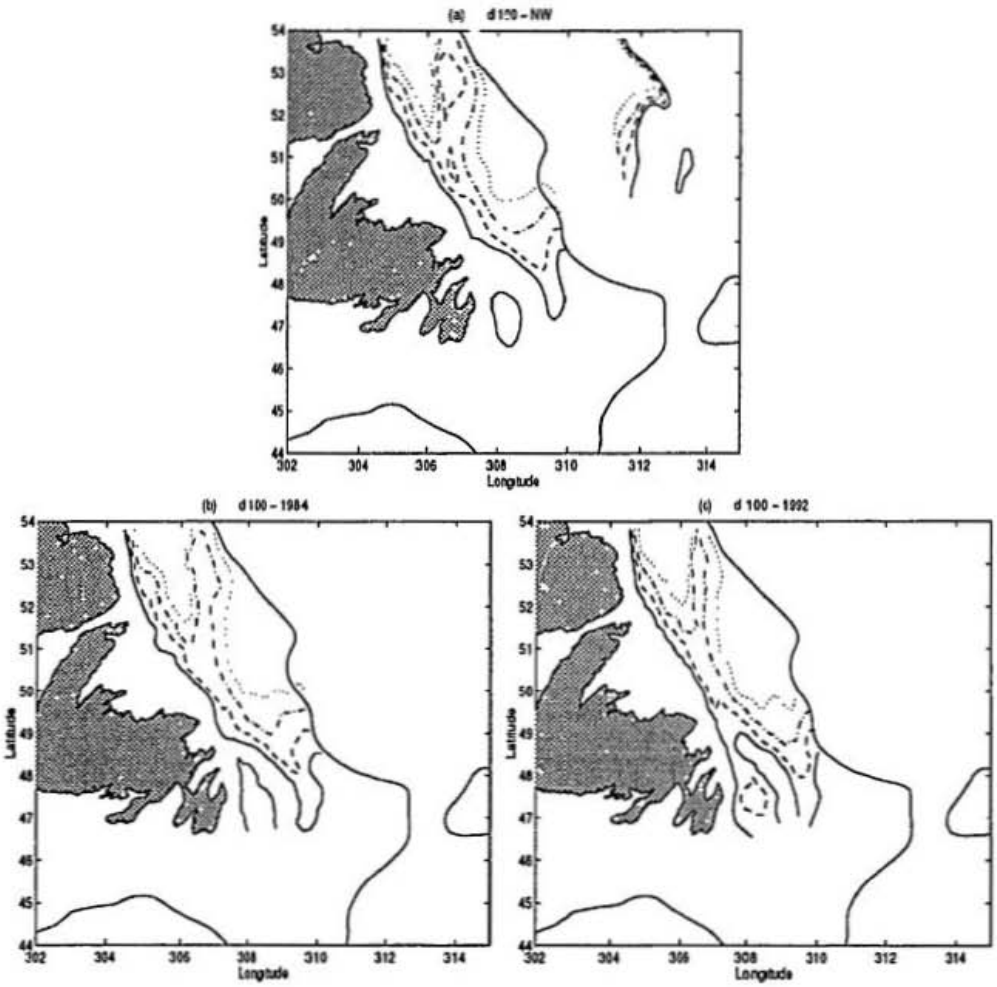

Figure 3.7: Contours of distances travelled by particles in 50 days starting 1 April. Solid line is 250 km contour, dashed line is 300 km contour, dashed-dotted line is 350 km contour and the dotted line is 400 km contour. (a) represents the mean flow case with no wind, (b) includes in addition 1984 winds, (c) includes in addition 1992 winds.

To identify particle destinations and particle origins after 50 and 100 days of drift we separate the Newfoundland shelf into 9 regions (Figures 3.8a and b). There are 7 Shelf regions and 2 'Bay' regions. Region R1 covers Hamilton Bank region, Regions R2 and R4 cover the northern and southern inner Newfoundland Shelf while regions R3 and R5 cover the northern and southern outer Newfoundland Shelf. Regions R6 and R7 represent the northern portions of the Grand Banks. The 2 bay regions were chosen to determine the origin of cod larvae that drift into coastal Newfoundland waters under passive drift. Region B1 contains Notre Dame Bay whereas region B2 contains Bonavista, Trinity and Conception Bays. In the remainder of this section we shall for simplicity describe cases with 1992 wind forcing. Roughly similar results were obtained for the 39 other years of wind forcing.

Locations after 50 days of drift for particles seeded in the various shelf regions are plotted in Figures 3.9a,b and c and 3.10a,b,c and d. Particles released in R1 range in location from Notre Dame Bay to the mid-shelf region. Particles seeded in the inshore half of R1 drift further than particles seeded in the shelfbreak half. Particles in the inshore group may extend in southward location to Newfoundland's northeast shore by 50 days. None of the particles in the shelfbreak group of R1 are advected across the shelf break. At a hundred days the particles are clearly divided into the two groups (Figure 3.11b). The inshore group is spread along the coast of

Newfoundland extending from Twillingate to the mouth of Conception Bay. The other group of particles is centred around 50°N in the mid shelf region.

Particles seeded in R2, form a distinct shoreward and mid-shelf group after only 50 days of drift (Figure 3.9b). Inshore particle distribution is already spread out from Twillingate to Cape St. Francis. By 100 days, particles in the shoreward group may be located as far south as the Avalon Channel (Figure 3.11b). The mid-shelf group is centred around 49°N and remains shoreward and southward from the R1 shelfbreak group.

By 50 days of drift, particles released in the outer shelf region R3 form a ellipse shaped patch stretched along the North-South axis inshore from the 500 m isobath (Figure 3.9c). By 100 days of drift (Figure 3.11c), particles originating in R3 form a patch that is more compact along the north-south axis than after 50 days due to particles drifting into slower moving waters on the Grand Banks.

Particles seeded in R4 drift southwards with spreading occurring in all directions. After 50 days, 11 of the 168 particles from R4 drift slowly across the head of Trinity and Conception Bays (Figure 3.10a). The rest of the particles tend to drift southwards. After 100 days (Figure 3.12a), particles are spread out over the northwest quadrant of the Grand Banks. Only 4 particles remain along the head of Trinity and Conception Bays.

Particles released from R5 concentrate in the northeast of the Grand Banks by 50 days (Figure 3.10b). Particles seeded along the southeastern edge of R5 are entrained by the main branch of the Labrador Current. By 100 days, particles seeded in the western half of R5 drift (Figure 3.12b) the furthest distances into the central regions of the Grand Banks, whereas the remaining particles are retained in the northeast of the Banks. Approximately 20 % of particles from R5 are advected out of the domain over the course of 100 days by the main branch of the Labrador Current.

From R6 particles move southeastwards towards Whale Bank (see Figure 1.1). After 100 days (Figure 3.12c) a few particles are retained in region R6 while the majority are clustered over the western edge (Whale Bank) of the Grand Banks.

Particles released from R7 near the nose of the Grand Banks move southwestwards and spread out along the direction of drift (Figure 3.10d). After 100 days particles are located near the centre of the Grand Banks(Figure 3.12d). About 5% of particles seeded in R7 are advected out of the domain by the main branch of the Labrador Current.

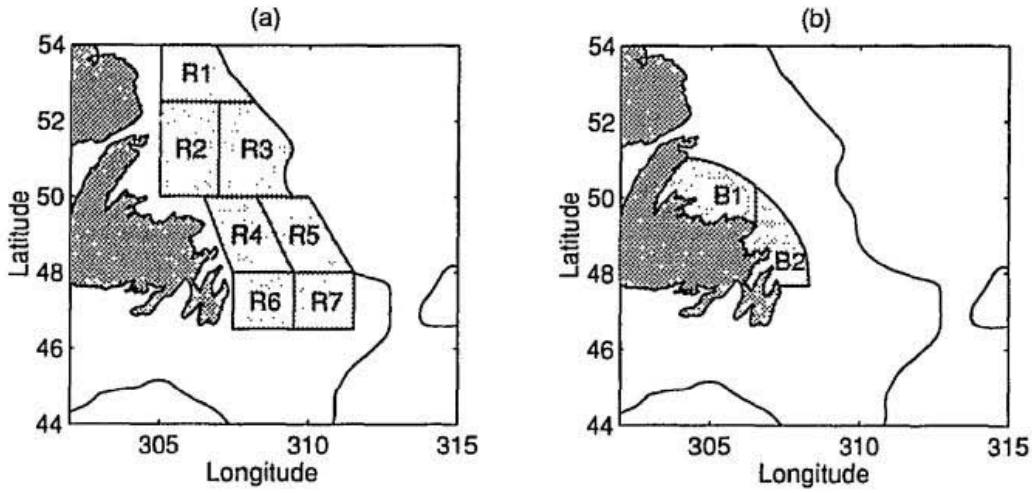

Figure 3.8: Sub-regions defined to look at the spatial character of particle dispersion. (a) regions on the shelf, (b) coastal regions.

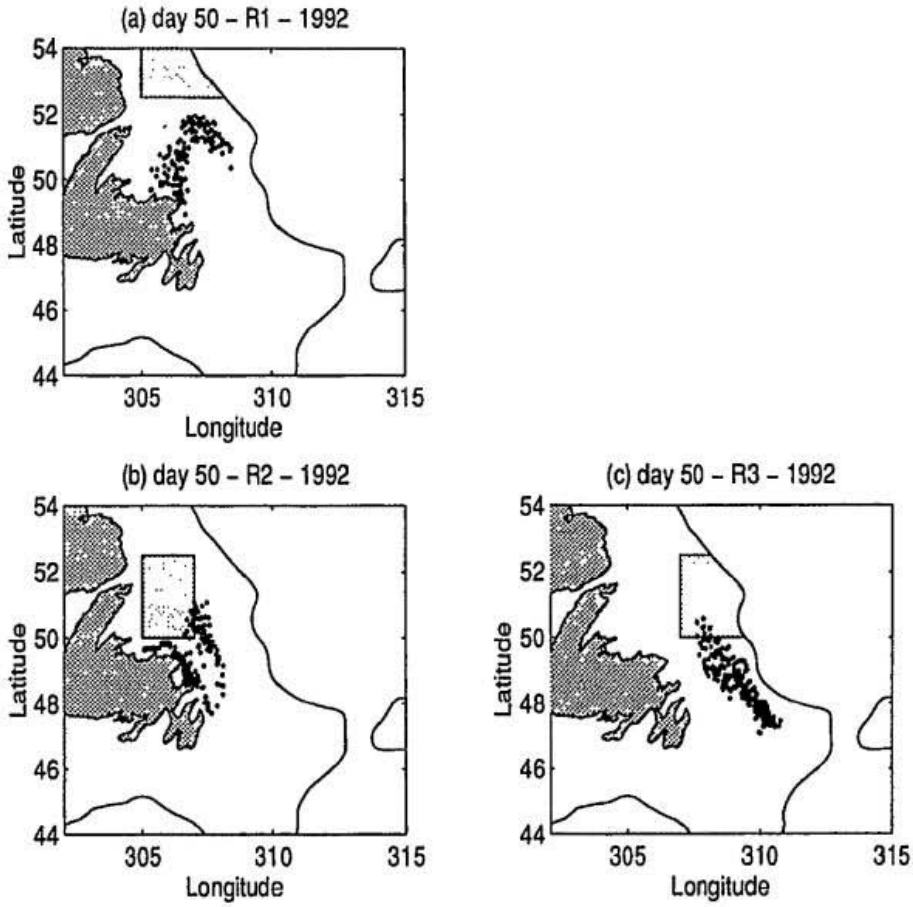

Figure 3.9: Location of particles seeded in shaded regions after 50 days of drift.

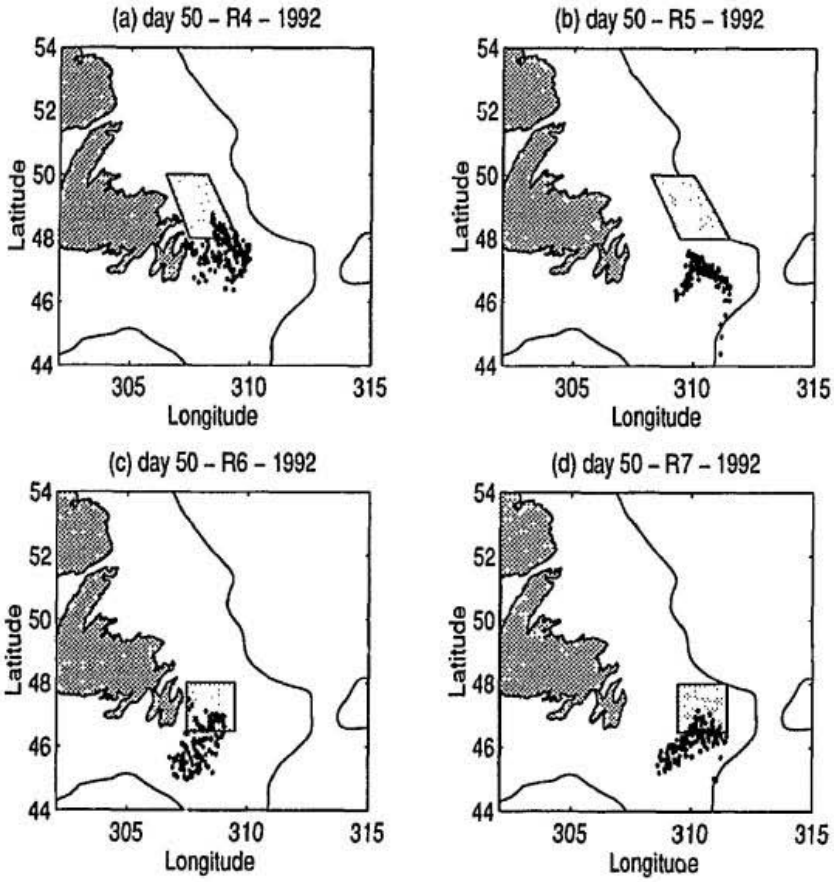

Figure 3.10: Location of particles seeded in shaded regions after 50 days of drift.

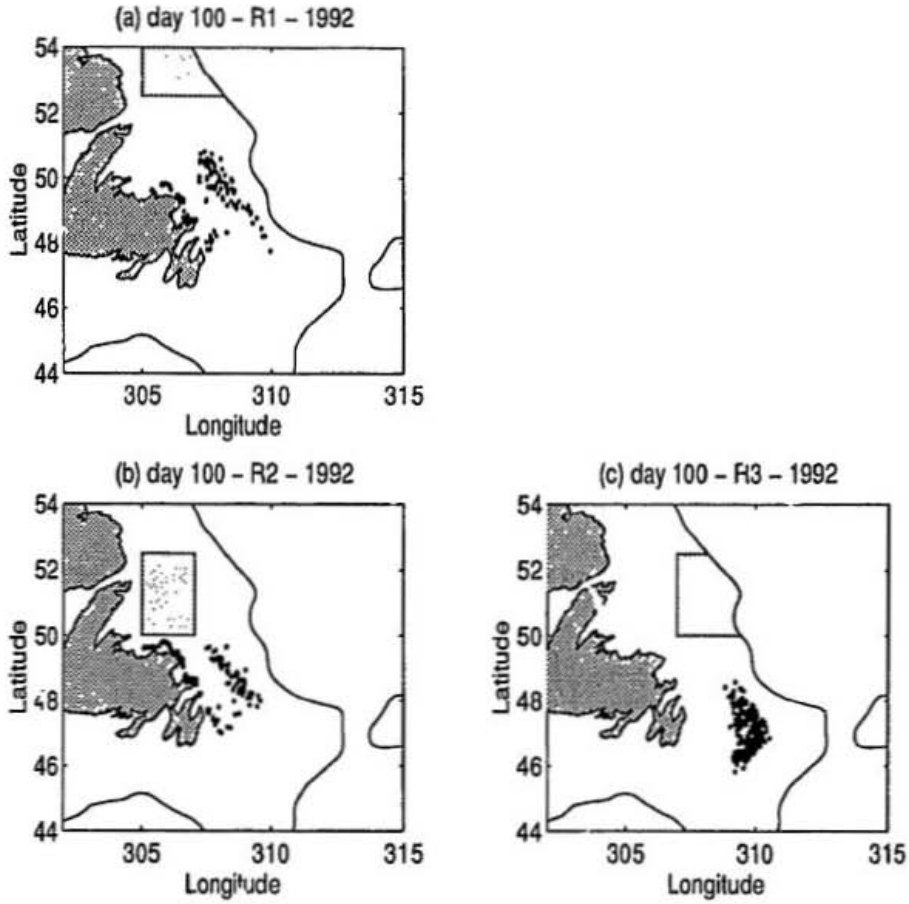

Figure 3.11: Location of particles seeded in shaded regions after 100 days of drift.

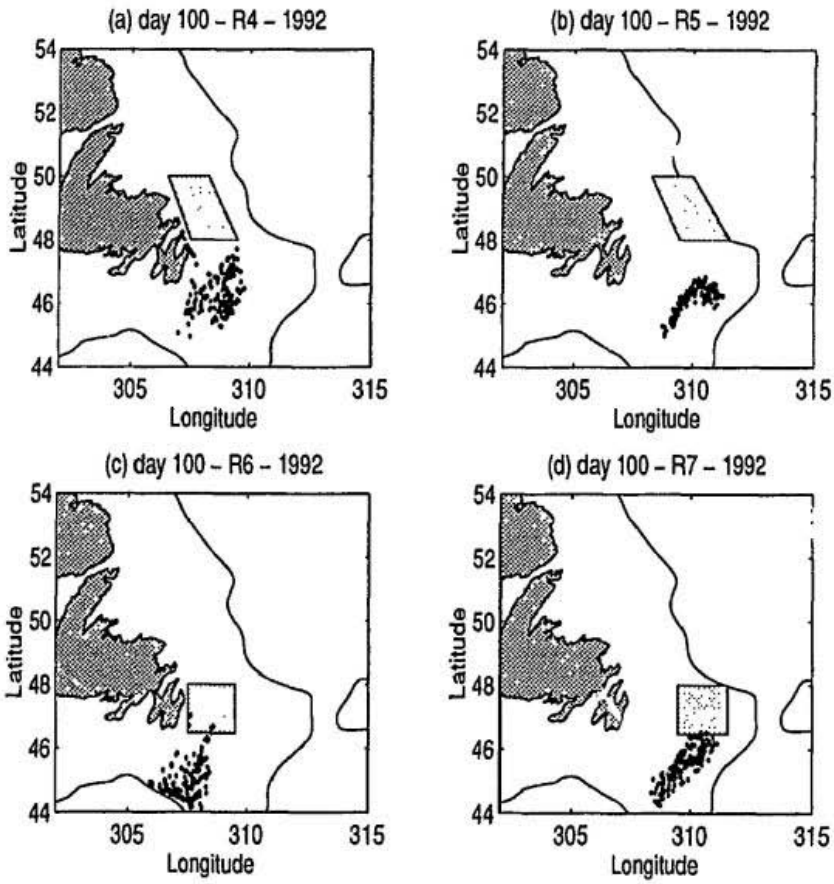

Figure 3.12: Location of particles seeded in shaded regions after 100 days of drift.

We are also interested in the origin of particles present in given regions after 50 or 100 days of drift. Figures 3.13, 3.14 and 3.15 show original location of particles that drift into each region by 50 and 100 days. Region R1 is not plotted here since no particles are present in R1 at 50 days.

Particles present in R2 at 50 d are seeded due north of R2 up to 54°N, the model's northern boundary. Two thirds of seeding locations for particles in R3 at 50 days straddle the 500 m isobath north of R3 with the remaining third of seeding locations inside the R3's northern boundary (Figure 3.13b). By 100 days region R2 is void of particles. Region R3 contains 30 to 60 particles depending on wind forcing, originating between 20 and 70 km inshore from the shelf break north of R3.

For the remaining regions R4, R5, R6, and R7 originating locations for particles in these regions at 50 and 100 days are plotted in Figures 3.13 to 3.14. Generally particles originate to the northwest of the region in question. From 50 to 100 days of the model run, the number of particles in these regions diminishes by 10 to 60 % with maximum depletion in R5 and minimum depletion in R7.

For the inner shelf regions R4 and R6 initial particle seeding locations are to the northwest with 22 and 33 % of the particles retained within the respective region over a 50 day period (Figures 3.13c,d). For particles in regions R4 and R6 at 50 days original seeding locations may extend up to 200 km to the northwest of these regions.

For particles in these regions at 100 days (Figures 3.14c,d), initial location are up to 500 km north of the respective regions.

Particles in region R5 at 50 days are located along a narrow area stretching from the northwest corner of the region across the 500 m isobath to a location 100 km seaward from the shelf break at 54°N. Initial location of particles present in R5 at 100 days, are clumped around the 500 m isobath in the northern section of our model domain. Some particles seeded in the mid-shelf region also manage to reach R5 by 100 days.

R7 is a region that contains the highest concentration of particles. Initial location of particles in this region at 50 days are along the 500 m isobath up to 600 km north of the region. At 100 days , initial particle location is along the 500 m isobath with roughly 95 % of locations north of 50°N. Nearly half of the seeding locations are seaward of the 500 m isobath.

For the Notre Dame Bay region B1, seeding locations for particles in the domain at 50 and 100 days are almost identical in distribution. Most particles seeded in B1 remain in the region through out the 100 day model run. As well a band of particles seeded roughly 70 km wide along the axis of the inshore branch up to 54°N are advected into B1.

Initial locations of particles in region B2 at 50 and 100 days differ slightly.

Particles seeded close to shore are retained in B2. There also is a narrow band of particles seeded 70 km wide along longitude 306°E from region B2 to 54°N, however for particles present in B2 at 50 days, initial particle locations extend only to 53°N.

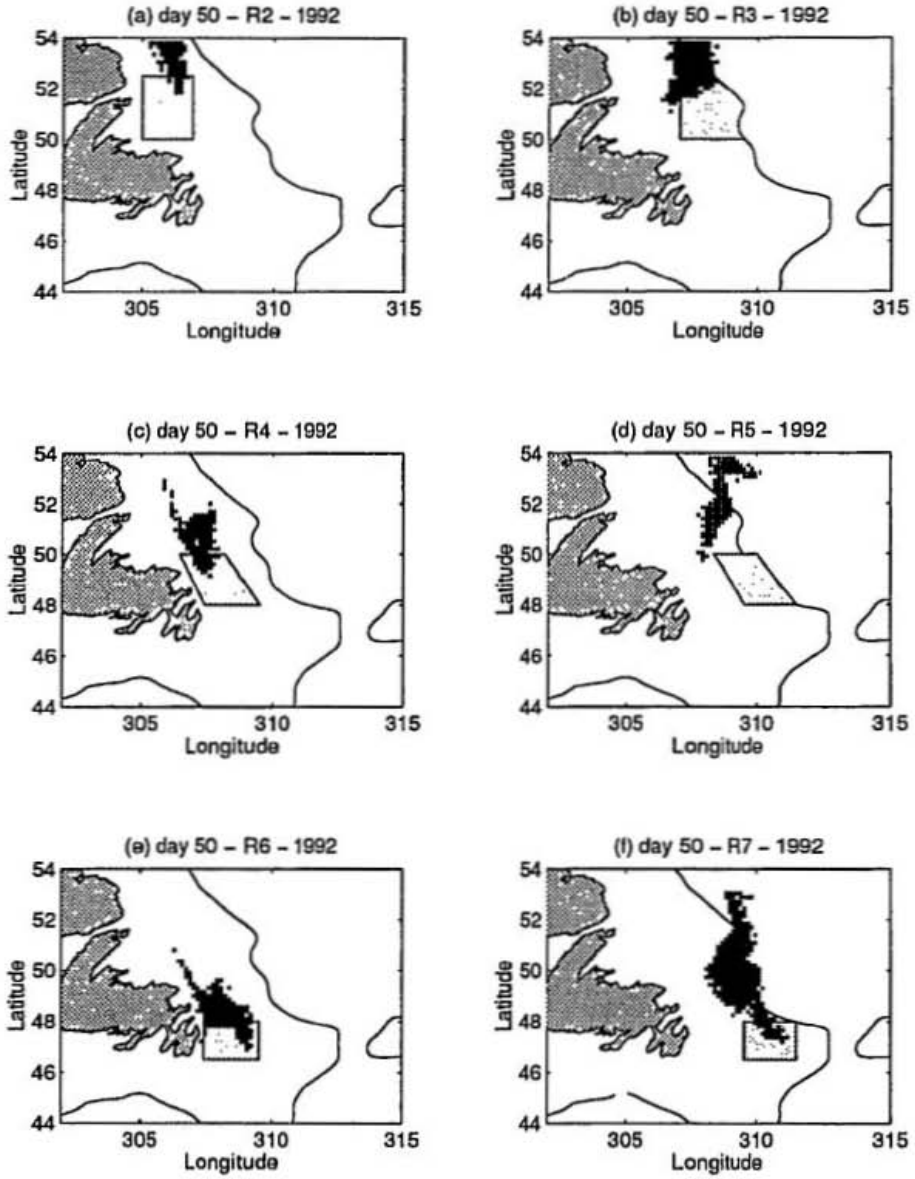

Figure 3.13: Initial location of particles that are in shaded regions at 50 days.

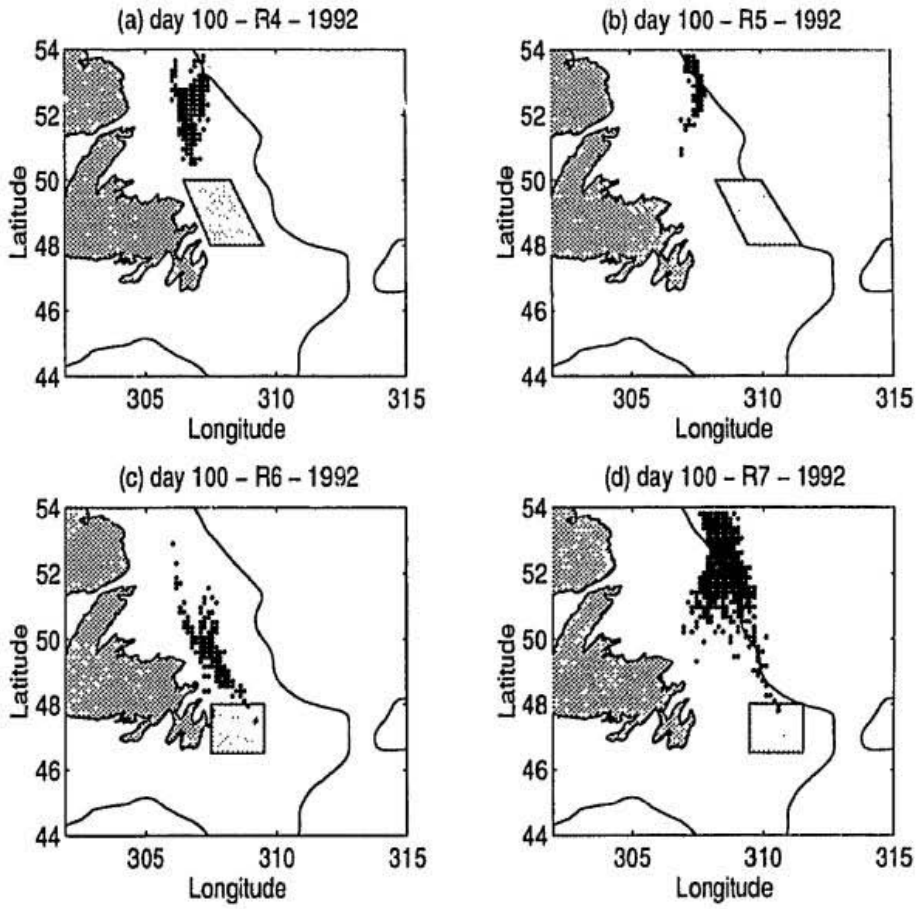

Figure 3.14: Initial location of particles that are in shaded regions at 100 days.

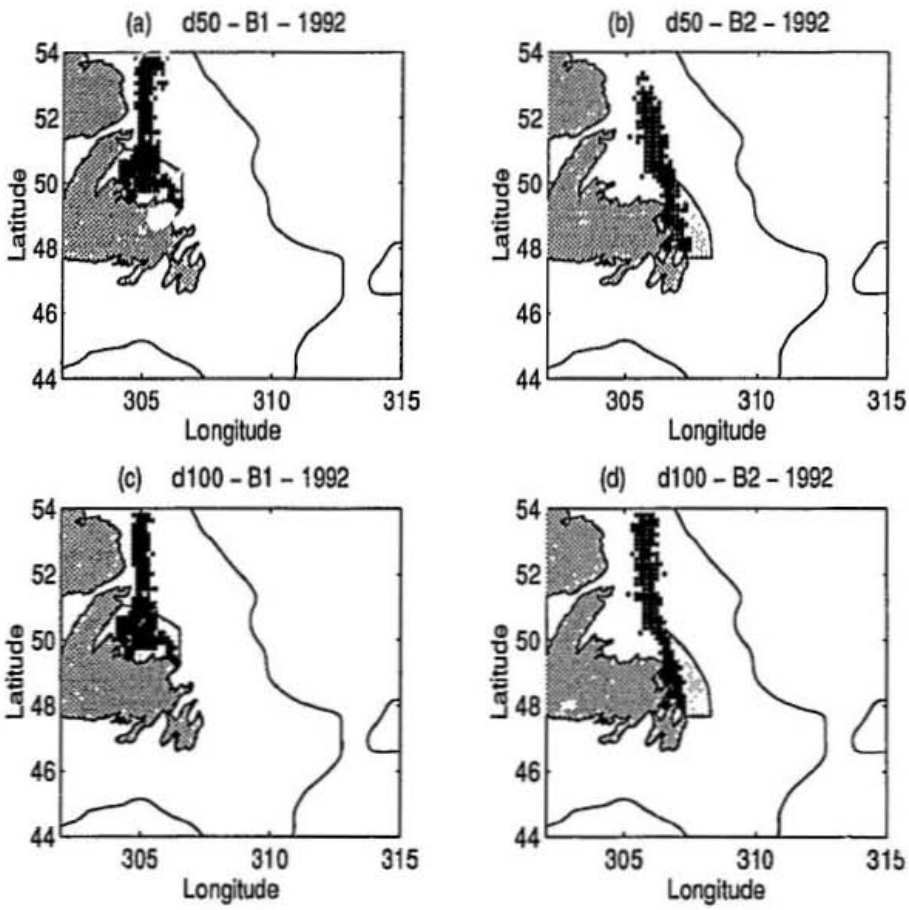

Figure 3.15: Initial location of particles in shaded regions B1 and B2 at 50 days (a and b) and at 100 days (c and d).

3.4.2 Interannual Variability in Dispersion

The number of particles advected into a region at a given time after release varies with wind forcing, and can thus be used as a tool for understanding variability of particle drift induced by variability in the wind-driven component of flow. For a general overview, we plot the number of particles in a given region after a given period of drift against the 40 years in which run the model using wind forcing. We make use of the shelf regions R1, R2, R3, R4, R5, R6 and R7 as well as the bay regions B1 and B2 defined in Figures 3.5a and b. To ensure that observed drift phenomenon are wind forced effects and not effects of random walk, we run the Lagrangian model in each of the 40 years 10 times. Figures 3.16 and 3.17 present the mean of 10 realisations of the model for particle numbers in each region against year. Figures 3.18 and 3.19 present all 10 realisations for the number of particles versus year in each region at 50 and 100 days.

Over all years, the wind-driven component of flow on its own may account for a southward particle transport of 40 to 90 km over a period of 100 days. Over the same period of time, east-west transport by the wind-driven component of flow may vary between 60 km westwards and 40 km eastwards throughout the years. As foreseen, the effect of homogeneous wind forcing on particle drift is spatially dependent. This

spatial dependency stems from the spatial variability in the mean background flow. On average, the wind-driven flow reduces the number of particles present at 50 and 100 days in the outer shelf regions R3, R5, and R7 as well as in the inner shelf region R2. The southerly transport by wind is significantly negatively correlated with the number of particles in these regions at 50 and 100 days with correlation coefficients r ranging from -0.62 to -0.96 (Table 3.1 and 3.2). In contrast, the wind-driven current generally increases numbers of particles present in the inner shelf regions R4 and R6 as well as in the bay regions B1 and B2. Southerly transport by wind is significantly correlated to the numbers of particles in B1 for 50 and 100 days. The number of particles in R4 at 50 days also varies significantly with southerly wind-driven transport with an r value of 0.62. For particle numbers in regions R6 at 50 and a 100 days there is no correlation with the southern component of wind-driven flow ($r \leq 0.07$).

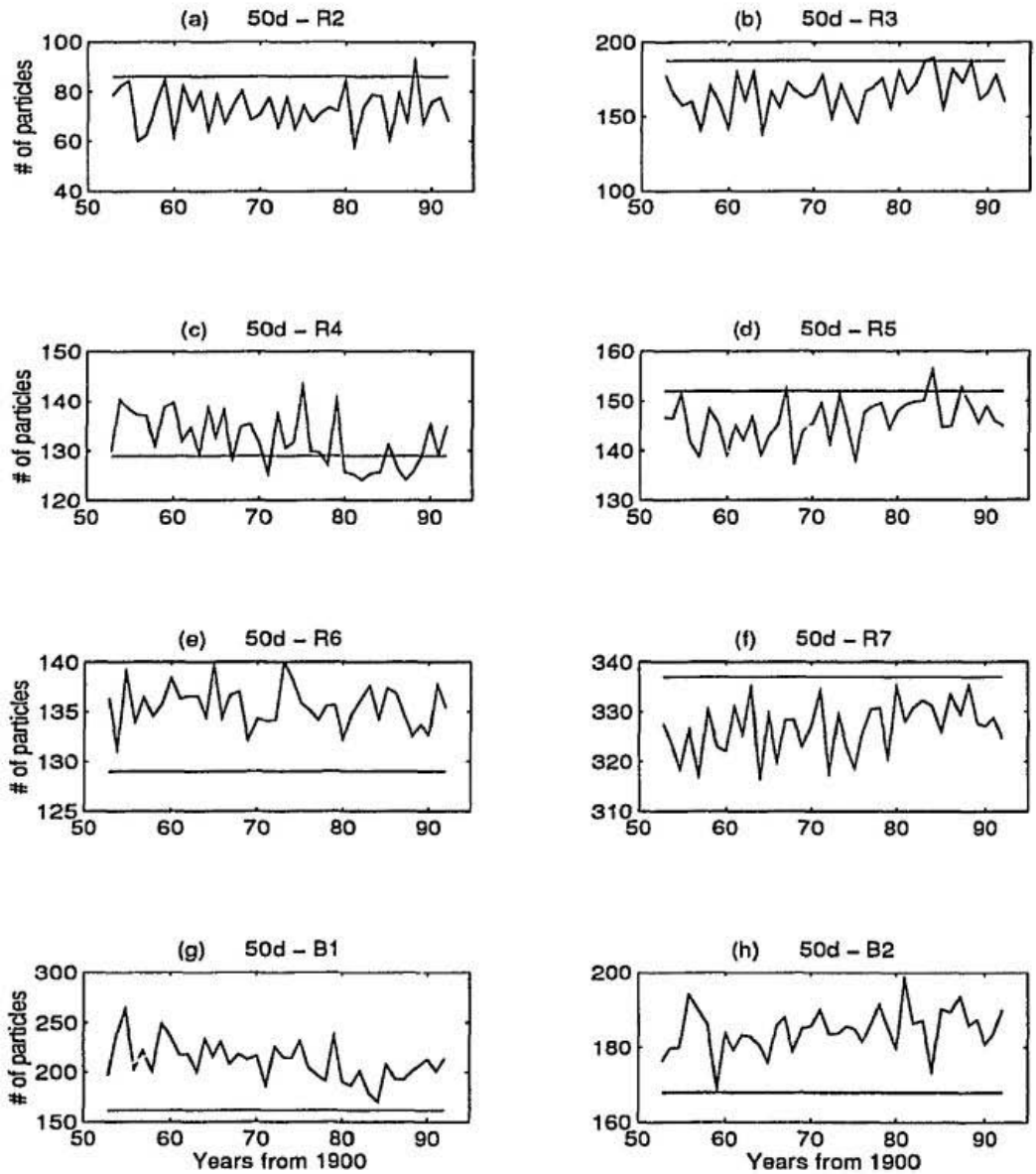

Figure 3.16: Number of particles inside different regions after 50 days. The graph represents the mean of 10 realisations. The horizontal line indicates the number of particles in the region in the absence of wind forcing and diffusion.

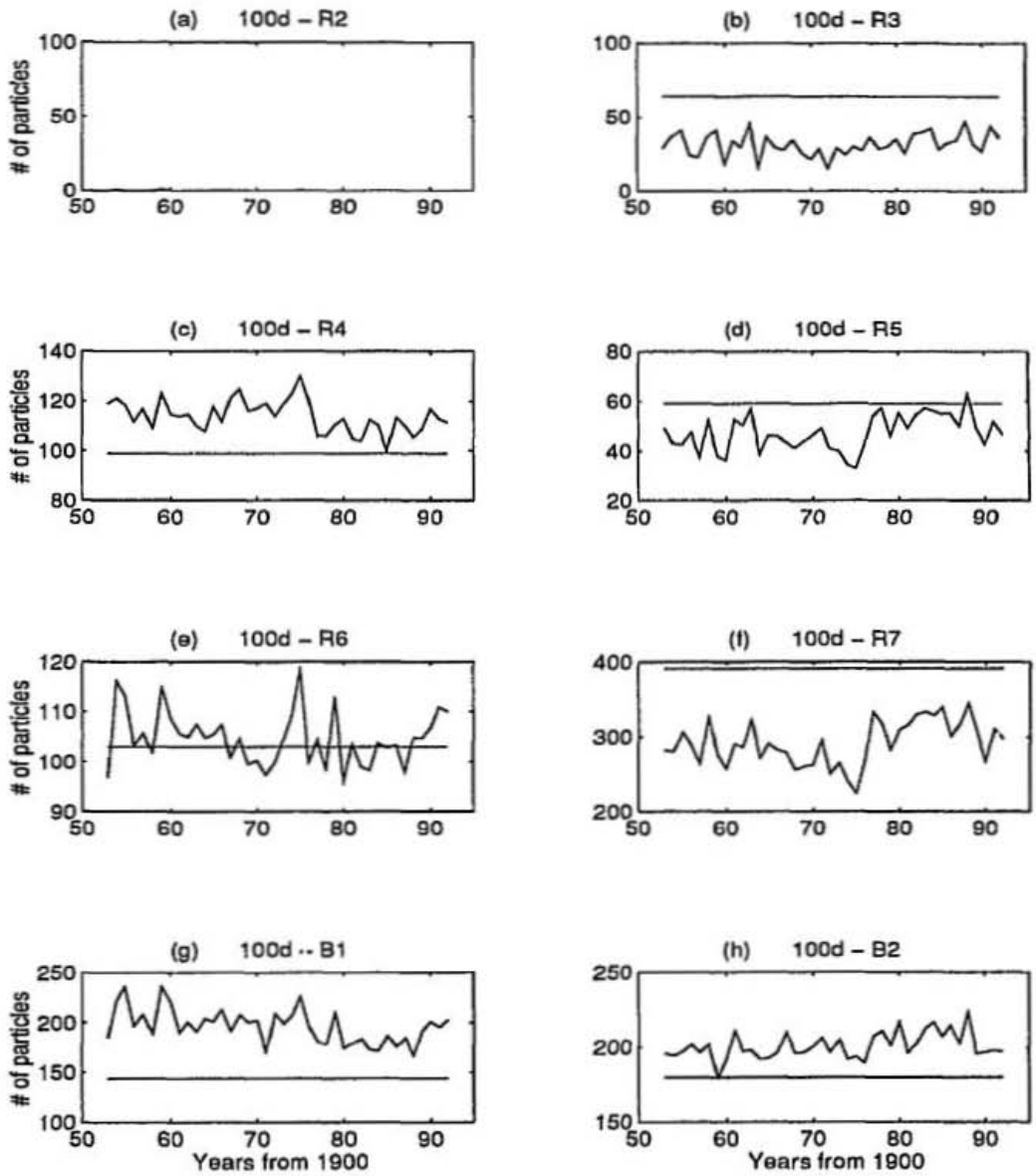

Figure 3.17: Number of particles inside specific regions at 100 days. The graph represents the mean of 10 realisations. The horizontal line indicates the number of particles in the region in the absence of wind forcing and diffusion.

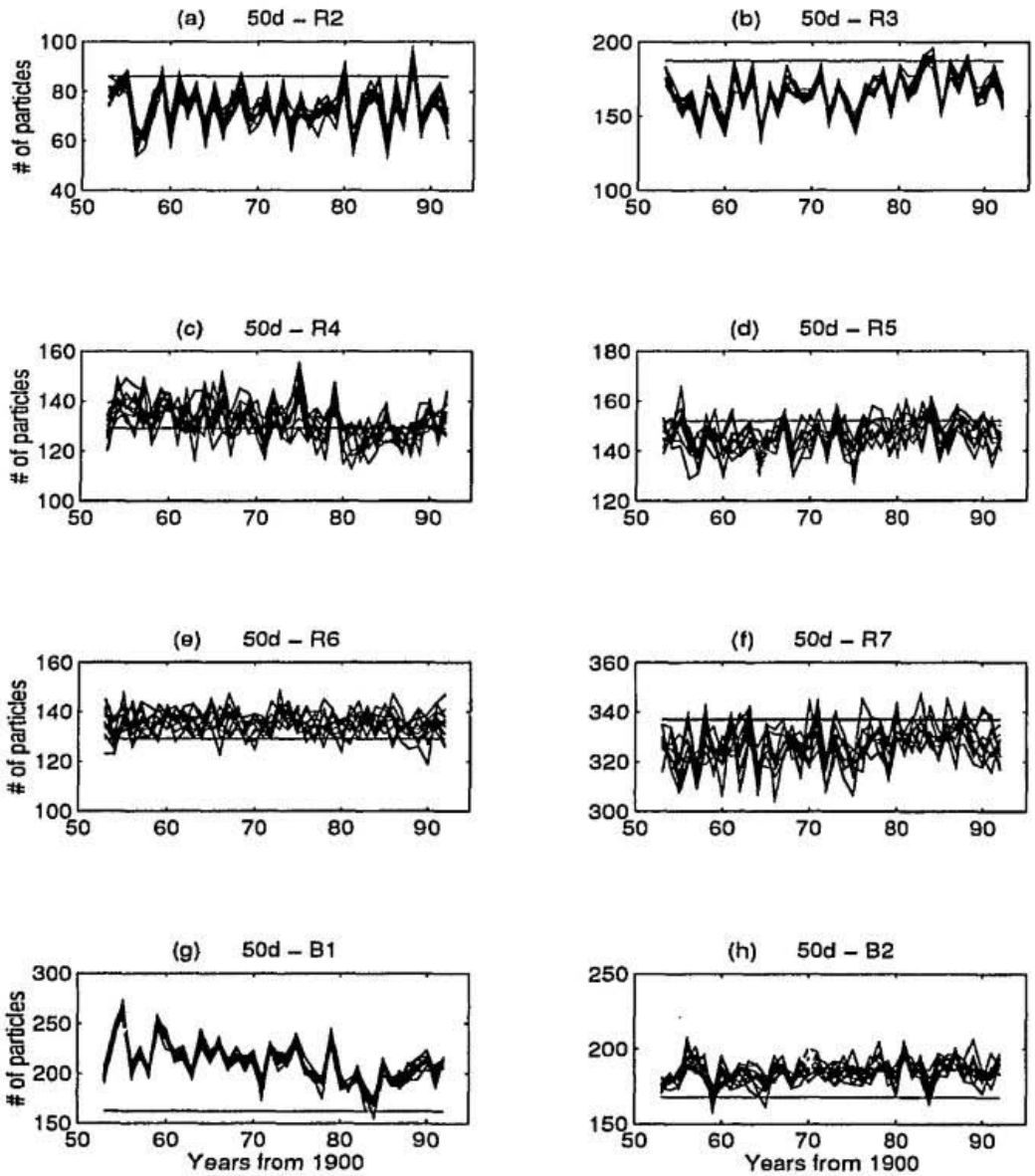

Figure 3.18: Number of particles inside specific regions at 50 days for 10 realisations. The horizontal line represents the no-wind case.

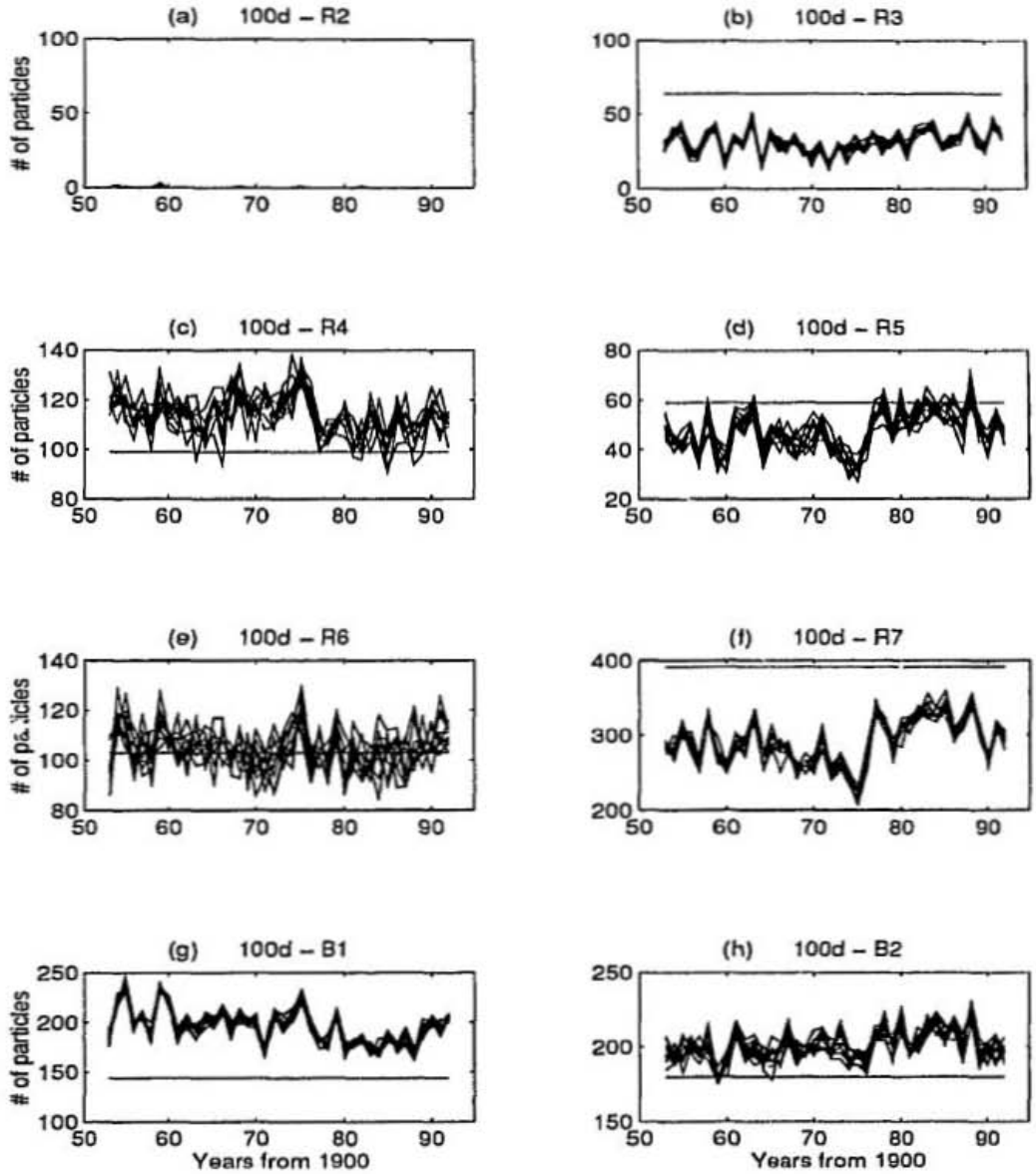

Figure 3.19: Number of particles inside specific regions after 100 days for 10 realisations. The horizontal line represents the no-wind case.

Inner-shelf regions R4, R6 and B1 are dependent on the westward component of wind-driven flow. There is a significant negative correlation between the numbers of particles inside inner shelf regions R4, R6 and B1 at 100 days and eastward wind-driven transport (Table 3.2). The same correlation is significant for particles in these regions at 50 days with the exception of region R6. This illustrates the importance of timing of the wind-driven component of flow with respect to particle position in the mean velocity field. At a fixed time, the wind-driven transport of a particle may be effective in altering its position or advection to a region depending on the location of the particle in the mean velocity field.

Eastward wind-driven transport is significantly correlated at 100 days with the number of particles present in R5, R7 and B2. Eastward wind-driven transport is negatively correlated to the number of particles in R3 at 100 days (Table 3.2), but there is no significant correlation between particle numbers in R3 at 50 days (Table 3.1) and eastward wind-driven transport. There is, however, no significant correlation between eastward wind driven transport and the number of particles in R3, R5 and R7 at 50 day...

Tables 3.3 and 3.4 are correlograms of cross correlation coefficients of particle numbers inside a region at 50 and 100 days. There is significant and high coherence between the interannual variation of particle numbers across the shelf break regions

R3, R5 and R7 as well as the inner shelf region R2. Wind forcing reduces the number of particles in all of these regions. A high and significant correlation also exist for particle drift into regions R4, R6 and B1. These regions depend on southward and westward wind-driven transport for particles retention. In region B1, the additional southward drift allows particles to cross the east flowing inshore branch of the Labrador Current into slow moving coastal waters of the southern coast of Notre Dame Bay. Wind increases the retention of particles inside B1.

There is a significant negative correlation between the number of particles in B1 and the number of particles in B2 at 100 days. Westward wind-driven flow favours particle transport into B1, whereas eastward wind-driven flow favours particle transport into B2. Further indication of this is given by the significant negative correlation between eastward wind driven transport and particle numbers in B1 at 50 and 100 days. and the significant positive correlation between eastward wind-driven transport and number of particles in B2 at 50 and 100 days. Although the mean winds increase particle transport into B1 and B2, variability in the wind causes opposite responses from particle transport into these 2 regions.

The wind-driven component of flow is not as effective at increasing particle numbers in regions R6 and particularly R4, as in the bay regions B1 and B2. These regions have an open southern boundary past through which particles may exit. Wind

driven flow enhances southeast particle transport into these regions. Wind has a greater influence in R6 than R4 due to the generally weak steady current in R6.

Long term trends over the 40 years can be detected in particle numbers present in a given region throughout the years. The mean number of particles inside B1 at 50 and 100 days from one decade to the next is decreasing throughout the 40 year run. Between the first decade (1953 - 1962) and the last decade (1983-1992), particle numbers at 50 days decrease from 225 to 197. Such a decreasing trend is also present in R4. The decreasing trend in B1 and R4 is caused by an increased eastward wind-driven transport from one decade to the next.

Southward transport also modulates long term trends, particularly in the outer-shelf regions R3, R5 and R7. The interdecadal variability in particle numbers present in these regions at 100 days follows the same trend as interdecadal southerly wind-driven transport variability. In each of the 4 decades of the model run, southerly wind transport is 51, 56, 51 and 29 km respectively. This pattern is mimicked by decadal binned particle numbers inside outer shelf regions at 100 days. Region R7 for example has a mean of 285, 267, 283 and 312 for particle numbers in the regions at 100 days for each decade.

The effects of diffusion in each region is visible in Figures 3.18 and 3.19. Here 10 realisations of particles inside each region at 50 and 100 days is plotted against year.

At 50 days diffusion does not change results for regions R3 and B1. The shape of the mean curve is visible. However for regions R4, R5, R6 and R7 diffusion camouflages the mean curve as shown in Figures 3.16 and 3.17. This is particularly true at 50 days in R6 where there is no clear observable trend among the 10 realisations. At 100 days the diffusion plays an important role in R4, R5 and R6. For the other regions the mean trend is clearly visible (Figure 3.17). Regions R4 and R6 are particularly sensitive to diffusion. Region R6 can be categorised as the region with the slowest moving currents. Diffusion may play a more important role where currents are weaker.

Table 3.1: Cross correlation coefficient r between number of particles ending inside different regions at 50 days and wind-driven transport. dS is southward wind-driven transport measured as the net distance between a particle's final and initial location using only the wind-driven component of flow. dE is the eastward wind driven component of flow. The 95% significance level is 0.31. Bold notation denotes correlations coefficients greater than 0.4

dS	**-0.81**	**-0.95**	**0.62**	**-0.65**	0.07	**-0.81**	**0.52**	0.24
dE	**-0.59**	0.09	**-0.54**	0.09	-0.15	0.27	**-0.68**	**0.55**
REG	R2	R3	R4	R5	R6	R7	B1	B2

Table 3.2: Cross correlation coefficient r between numbers of particles ending inside different regions at 100 days and wind-driven transport. Presented the same as in Table 3.1

dS	**-0.96**	0.20	**-0.71**	0.02	**-0.72**	**0.43**	**-0.49**
dE	-0.31	**-0.64**	**0.47**	**-0.78**	**0.42**	**-0.76**	0.34
REG	R3	R4	R5	R6	R7	B1	B2

Table 3.3: Cross correlation coefficient r between number of particles ending inside different regions at 50 days. The 95 % significance level is 0.31.Bold font indicates correlations above 0.40.

R2	1.00							
R3	**0.62**	1.00						
R4	-0.19	**-0.79**	1.00					
R5	0.34	**0.70**	**-0.68**	1.00				
R6	0.00	-0.09	0.02	-0.10	1.00			
R7	**0.48**	**0.90**	**-0.83**	**0.55**	-0.07	1.00		
B1	-0.01	**-0.73**	**0.86**	**-0.49**	0.18	**-0.77**	1.00	
B2	**-0.57**	-0.05	-0.29	0.06	-0.09	0.09	-0.36	1.00
REG	R2	R3	R4	R5	R6	R7	B1	B2

Table 3.4: Cross correlation coefficient r between numbers of particles ending inside different regions at 100 days. Results are presented as in Table 3.3.

R3	1.00						
R4	-0.11	1.00					
R5	**0.56**	**-0.69**	1.00				
R6	0.21	0.35	**-0.46**	1.00			
R7	**0.62**	**-0.77**	**0.89**	-0.31	1.00		
B1	-0.22	**0.57**	**-0.80**	**0.73**	**-0.66**	1.00	
B2	0.32	**-0.44**	**0.75**	**-0.45**	**0.60**	**-0.76**	1.00
REG	R3	R4	R5	R6	R7	B1	B2

3.5 Dispersion of Egg and Larvae Patches

To investigate the advection of cod eggs spawned at the shelf break we seed 5 patches of 9 particles in each of the 40 years of the model run. Each of the 5 patches p1, p2, p3, p4 and p5 covers an area roughly 20 km by 30 km and is centred along the 500 m isobath between 49 °N and 53.5 °N (Figure 3.20a). We define the 'extended patch' as the set of all particles seeded in a given patch over all 40 years of the model run (i.e. 9 particles × 40 years). The extended patches after 25 days of drift are plotted in Figure 3.20b. Also shown in Figure 3.20b is the contouring polygon used to estimate the area of each extended patch (Appendix C). After 25 days of drift the area of the extended patches proceeding southwards from p1 to p5 are 2.2, 2.8, 3.8, 2.4 and 4.6 thousand square kilometres respectively. This corresponds to extended patch areas 3 to 6 times larger than their corresponding initial patch area. With the exception of patch p4, extended patch areas after 25 days of drift increase in area with southerly location.

For the patches seeded at the shelf break, we show the results at 25 days only. After longer drift periods some of the extended patches overlap with each other. After 100 days of drift, the only extended patch retained on the Newfoundland Shelf is that of p1, the most northern seeded patch at 53.5°N. The other extended patches are

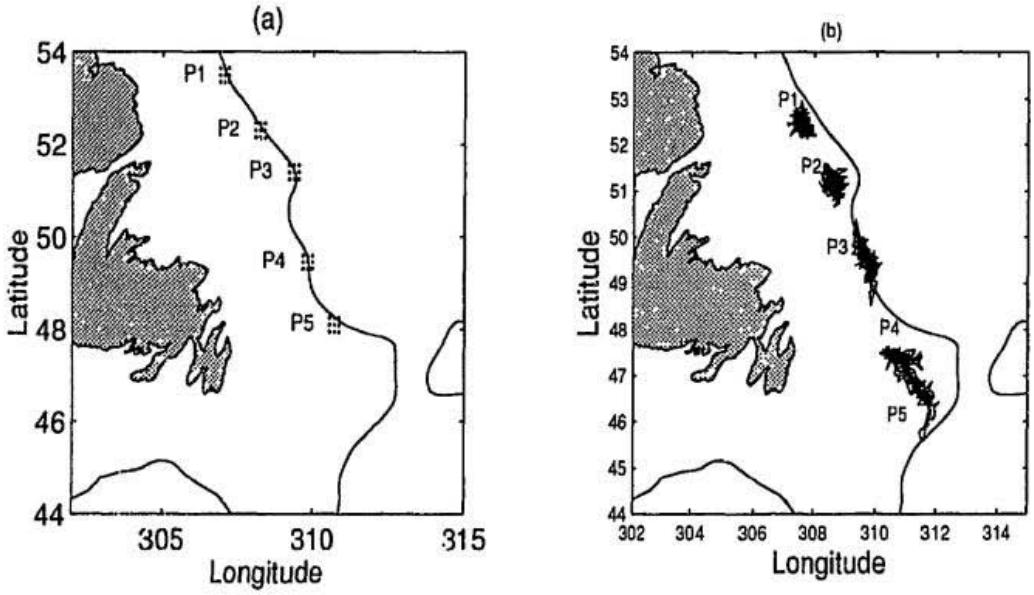

Figure 3.20: (a) Release locations of particle patches. (b) Location of 'extended patch' for p1, p6 and p7 after 25 days of drift. The 'extended patch' is the set of all points in a patch released in all 40 years of the 100 day model drift runs. The 'extended patches' are encompassed by a polygon from the geometric area routine (see Appendix C).

advected onto the the eastern flank of the Grand Banks and cover large areas due to particles being entrained into the main branch of the Labrador Current and out of the domain.

Having looked at particle patch dispersion at the shelf break we now proceed to compare dispersion for 3 patches of particles seeded at various cross shelf locations. We shall compare drift for patches p1 which has been previously defined, p6 seeded due north of Cape Freels near 52°N (Figure 3.21b) and p7 seeded near the inshore

branch of the Labrador Current in Notre Dame Bay (Figure 3.21a). The extended patch of p7 drifts across the inshore branch of the Labrador Current into coastal waters near Cape Freels. After 75 days of drift the extended patch of p7 stretches along the coast from Conception Bay to 50 km northwest of Cape Freels. The extended patch of p6 is located due south of the seeding area by 25 and 50 days with some of the particles reaching the coastline near Bonavista Bay by 50 days. After 75 days of drift particles in the extended patch of p6 are concentrated in two groups with one group along the eastern coast of Newfoundland between Cape Bonavista and Cape St. Francis, and the other, further north in the mid-shelf area east of Cape Freels (Figure 3.21h),

To estimate the area of the extended patches, we make use of a contouring polygon for each patch (Appendix C) which is also shown in Figures 3.21a to i. The area of the extended patches evolve with drift time and are plotted in Figures 3.22a. Figures 3.22a shows the evolution of the area of the extended patches for p1, p6 and p7 with drift time. The extended patch of p7 covers the smallest area. This is due to the inshore location of its particles after 50 days of drift. Although the extended patch area of p1 initially expands at the same rate as that of p7, it continues to expand while the extended patch area of p7 levels off after 50 days of drift. The extended patch area for p6 expands the fastest. By 100 days of drift the extended

patch area of p6 is roughly five times greater than that of p7 and two times greater than that of p1. This greater extended patch area for p6 is due to the dispersion of particles over the inshore and mid-shelf area.

The evolution of the extend patch areas for the shelf break patches p1, p2, p3, p4 and p5 are shown in Figure 3.22b. As the extended patches drift over the eastern flank of the Grand Banks with some particles entrained into the Labrador Current, the areas measured with the contouring polygon may fluctuate. Figure 3.22b shows the extended patch area for all the particles in the extended patch that are in the domain. Particles isolated from the rest of the patch are removed subjectively to avoid a large measurement of area due to the presence of a single particle. Particles out of the domain are not included in the extended patch area measurement. This may lead to some of the fluctuation caused in extended patch areas particularly for p3, p4 and p5. After 80 days of drift the extended patch of p2 has the lowest surface area. Particles from this patch are retained on the northeastern flank of the Grand Banks.

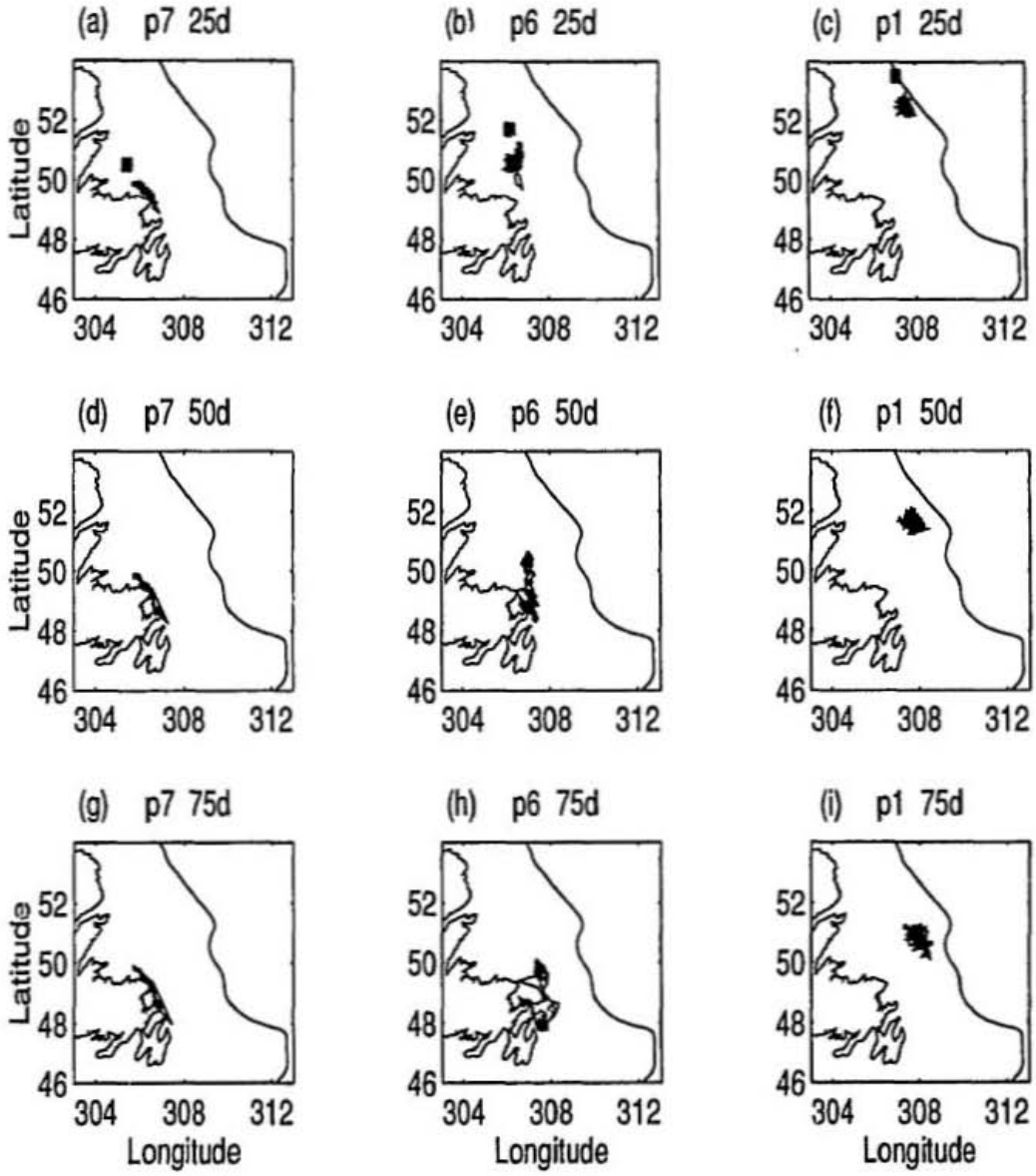

Figure 3.21: Location of 'extended patch' for patches p1, p6 and p7 (small dots) after 25, 50 and 75 days of drift. Initial patch location (thick dots) is shown for the 25 day plots (a,b and c). The 'extended patch' is the set of all points in a patch released over the 40 year model run.

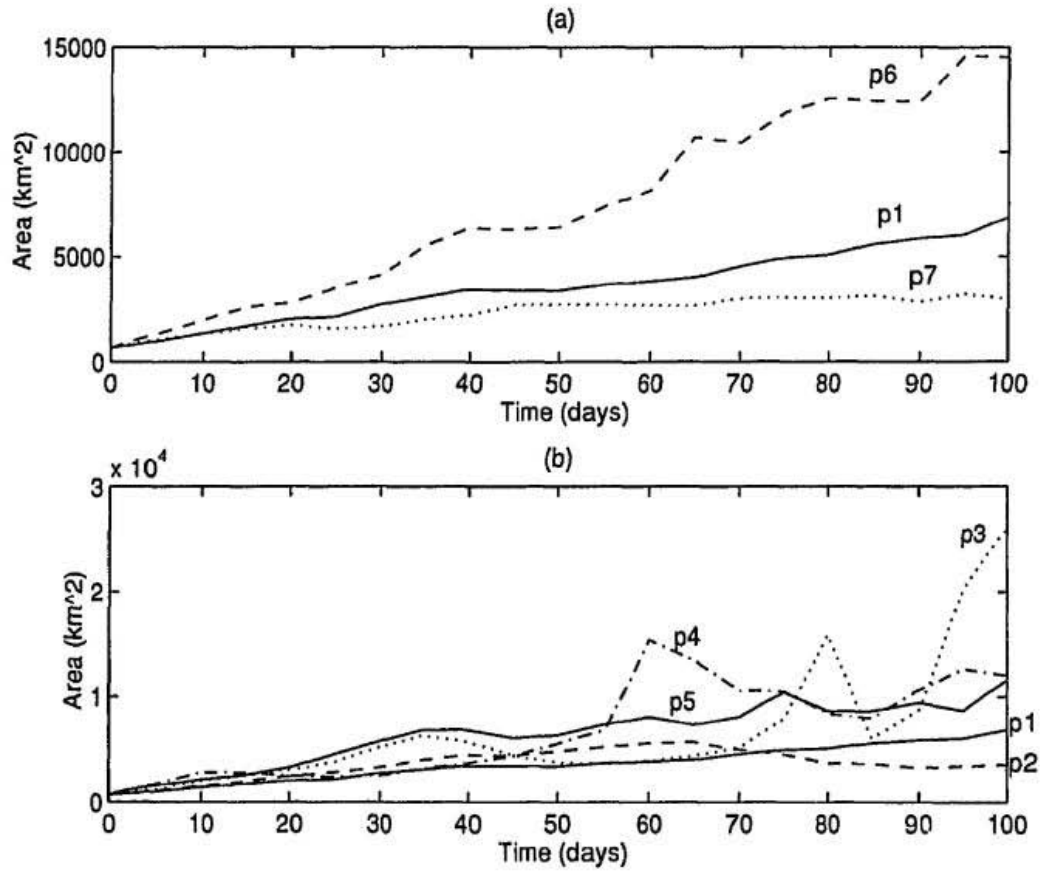

Figure 3.22: Surface area (see Appendix C) of extended patches versus day of model run. (a) for extended patches of patches p1, p6 and p7. (b) for extended patches of patches p1, p2, p3, p4 and p5.

3.6 Discussion

In this Chapter we have described the spatial drift pattern of passive particles on the Newfoundland Shelf. We also link changes in the wind-driven component of flow to changes in particle drift and retention of particles in various regions of the shelf. Our objective is to infer from modelling passive drift, favourable spawning ground locations for northern cod.

Comparisons of modelled drift with observed drifters show reasonable agreement. The southward transport of observed drifters is reproduced by the model. The addition of the wind driven component of flow can improve resemblance of model drift tracks to observed drift tracks. After 80 days the net displacement between final and initial observed drifter locations is roughly between 1 to 3 times further than the displacement reproduced by the model although the actual length of the drifter tracks is on the order of 2 to 5 times greater than model drift tracks. The model does not reproduce particles reversing direction, as is sometimes observed. Model particles have a tendency to be retained on the shelf whereas observed drifters tend to drift into the main branch of the Labrador Current. The reduced advection rates in the model are caused partly by a circulation field with broader and slower moving hydrographic features such as the main branch of the Labrador Current. Our model

does permit a number of interesting observations on passive particle drift relating to advection of cod eggs and larvae and improves greatly on the analytical model of Chapter 2 by including spatial dependence in the circulation field.

Passive particles drifting into the inshore bay regions B1 and B2 originate from further north, east of 307°W. Region B1 represents Notre Dame bay and B2 represents Bonavista, Trinity, and Conception Bays. The inshore branch of the Labrador Current is an important influence on the advection of particles into coastal waters of Newfoundland. The wind-driven flow increases the number of particles crossing the inshore branch of the Labrador current into coastal waters. If nursery grounds for northern cod are the bays of northeastern Newfoundland, then, based on passive drift over periods ranging from 50 to 100 days, corresponding spawning grounds for northern cod may lie anywhere north and west of Cape Freels as well as near the coast. The wind-driven component of flow increases the number of cod larvae that enter the bay regions. Since the seeding arrangement in our model is regularly spaced, the number of particles advected into the bay regions is proportional to the surface area of the originating particle locations. Thus the wind-driven component of flow may increase the size of suitable spawning grounds for cod whose larvae thrive in the bays of northeast Newfoundland.

Another approach for identifying suitable spawning grounds is to identify re-

gions of retention where the displacement of seeded particles is low, comparatively to most of the Newfoundland Shelf. From contours of particle displacement in Figures 3.5 and 3.6, an obvious zone of retention throughout the years would be the inshore regions of Newfoundland. These would be regions where spawning grounds would coincide with nursery grounds due to the low current velocities. However the topography and the model resolution of of $\sim$ 20 km does do not permit good resolution of the current within 10 to 20 km of the coast of Newfoundland and in the bays. A more detailed model of the advection of cod eggs and larvae in a coastal circulation model or a bay circulation model is needed to study the passive drift of larvae into and out of bays. The present model does allow us to observe that wind increases particle advection towards the northeast Newfoundland coast.

A second region of retention on the Newfoundland Shelf would be the mid-shelf area north of 51 °N, between the inshore and offshore branches of the Labrador Current. In this region, seeded particles are advected distances less than 3 km per day in the no-wind case and less than 3.5 km per day in the wind forced case. From observation of particle drift, particles seeded in this region are retained on the Newfoundland Shelf during the 100 day model run and do not drift onto the Grand Banks in that period of time. Thus 50 to 100 day old larvae on the Newfoundland Shelf just north of the Grand Banks could be spawned in this mid-shelf spawning site.

Another region of retention identified by our model, is the north end of the Grand Banks as well as the nose of the Grand Banks. These areas are contained in regions R6 and R7 and have transport under 2 km per day (Figures 3.6a,b and c). It should be noted that particles in R7 along the eastern boundary are advected into the main branch of the Labrador Current. Some of the particles seeded in R6 drift over 100 days as far as the 500 m isobath on the southwestern flank the Grand Banks. The most favourable location for spawning along the northern section of the Grand Banks based on 100 day drift runs would be region R7. The majority of particles from R7 drift into the centre of the Grand Banks over this period. Based on these model predictions, cod spawning in the northern section of the Grand Banks could form a self sustaining population.

There is a discrepancy between our model runs of passive drifters and those by Helbig *et al.* (1992). Helbig *et al.* used the barotropic circulation model of Greenberg and Petrie (1988) (GP) to look at advection of passive particles seeded on the Newfoundland Shelf. They also looked at the effects of idealised wind forcing including idealised storms. Using the GP model as the mean current flow field, Helbig *et al.* observed that model drifters seeded on the Newfoundland Shelf are advected around the Grand Banks and not onto it as occurs with our model (Figure 3.12a and b). Furthermore drifters from the 1991 field program of OPEN are observed to be

advected through the Flemish Pass around the Grand Banks.

The Lagrangian model drift studies help illustrate the fate of cod eggs and larvae spawned at the shelf break along the 500 m isobath. Advection along the shelf break is high with particle displacement greater than 5 km per day. Northerly spawning along the shelf break inshore from the southern Labrador Coast is the most suitable spawning ground. Here advection rates are lowest with the model indicating that particles drift onto the shelf. Among particle patches seeded at the shelf break (Figure 3.20), only the most northerly seeded patch of larvae remain on the Newfoundland Shelf after 100 days of drift. The remainder drift onto the Grand Banks with a portion of particles advected around the banks and out of the domain. Our model shows that in all the years of the model run, no particle seeded along the shelf break may reach the coastal waters of Newfoundland. Thus based on our model of passive particle drift up to 100 days, for a cod population spawning at the shelf break, its nursery grounds are unlikely to be the bays of eastern Newfoundland.

While permitting us to identify suitable spawning grounds based on retention, the model also permits investigations of the effect of wind, such as regions where wind is an important factor regarding drift. The wind-driven component of flow increases the number of particles drifting into inner shelf regions while reducing the number of particles drifting into outer shelf regions. The variability of the southerly wind-

driven component of flow is strongly negatively correlated with particle drift into the outer-shelf regions and positively correlated with drift into inner shelf regions. Thus the wind-driven component of flow in any given year may favour particle drift into one region at the expense of another.

Chapter 4

Summary & Conclusions

In this thesis we have presented an analytical and a numerical model regarding retention and advection of cod eggs and larvae on the Newfoundland Shelf. Initially our objective was to relate an index of retention of larvae on the shelf to recruitment of Northern Cod, thereby determining if Northern Cod recruitment is sensitive to physical advection at the egg and larval stage.

Our analytical approach consisted of solving the advection diffusion equation for a patch of eggs and larvae immersed in a time-dependent, spatially homogeneous flow field. As a shelf retention index we use the proportion of larvae on the shelf averaged over a given drift period (R_{av}). The analytical model suggested that retention of larvae is sensitive to parameters such as the size of a larval patch and wind parameterisation,

particularly when spawning occurs at the shelf break. Furthermore, retention for a patch of eggs seeded in the shelf break is highly variable. Over the course of 100 days, wind driven cross-shelf displacement of a patch of larvae is between 50 km offshore and 50 km inshore depending on the year.

Comparing the retention index with recruitment for the entire 2J3KL regions produced correlations that were at most marginally significant. While the 2J3KL recruitment data set is the most comprehensive for Northern Cod, it also covers the entire 2J3KL cod stock. With the analytical model we were exploring the retention of a patch of larvae initially released at the shelf break. Thus our index R_{av} may not properly represent the retention of larvae over the entire Newfoundland Shelf. We also note tha the Labrador Current has strong spatial characteristics and that eggs and larvae drift is governed by the *in situ* flow and not the vertical averaged flow. When we assume that cod eggs and larvae drift according to the bulk Ekman flow, we propose that eggs are evenly distributed in the upper column, and that we are following the mean drift of particles seeded over the entire water column. Including the vertical distribution of the wind driven component of flow and larvae would increase diffusivity.

Our Lagrangian drift model proved to be an efficient tool at determining the drift of passive particles seeded though out the entire shelf. One of our aims was to

determine possible spawning and nursery grounds for Northern Cod.

For cod whose larvae develop in the bays of northeastern Newfoundland, modelling of passive drift over periods of 50 to 100 days suggest that the corresponding spawning grounds for these nursery areas would be the nursery areas themselves as well as the region stretching northwards from Notre Dame Bay to the Southern Coast of Labrador and west of Cape Freels. The mid-shelf area at Hamilton Bank would be favourable for spawning, with low advection rates between the inshore and main branch of the Labrador Current. Eggs spawned in this regions are retained on the shelf for at least 100 days. For a cod population spawning at the shelf break, based on our modelling of passive drift, it is unlikely that larvae would reach the coast of Newfoundland. However northerly spawning near 54°N would be more suitable than southerly spawning since eggs and larvae would be retained on the Newfoundland Shelf. Spawning along the shelf break further south would have eggs and larvae drift onto the Grand Banks or over the nose of the Grand Banks and into the main branch of the Labrador Current.

Although we use a slab-model for the wind-driven flow, the effect of wind on the retention of larvae is spatially dependent. In general, while the wind increases particle drift into inshore and inner-shelf regions, it also reduces particle retention in outer-shelf regions. Furthermore, over the course of the 40 years of the model run,

southward wind-driven transport is decreasing and eastward wind driven transport is increasing. The resulting retention of particles in inshore and inner-shelf regions with the exception of B2 is decreasing and retention in outer-shelf regions is increasing. The negative correlation between particles drifting into region B1 and B2, suggest that the wind driven component of flow may favour particle drift into one bay region at the expense of particle drift into the other.

It should be noted that all our model results are based on a 2-D circulation field, where we assume that cod eggs and larvae are distributed in the top 50 meters of the water column and that these eggs and larvae drift according to the top 50 m vertically averaged flow. Further study of larval cod advection on the Newfoundland Shelf will require a 3 dimensional circulation model, and use of a specified or dynamically modelled vertical distribution of eggs and larvae. An important improvement from 2-D to 3-D passive drift modelling would be the vertical shear in the wind driven component of flow which would advect surface particles faster in a different direction than particles at depth. Thus sensitivity to winds would be increased with vertical distribution playing an important role in the horizontal drift of eggs and larvae (Bartsch *et al.* 1989). Detailed modelling of drifting larvae at the shelf break will require a time dependent baroclinic model to resolve eddies.

The circulation field constrains the ability of Lagrangian drift models in repro-

ducing egg and larval drift of northern cod. In our model, we used a diagnostic flow field representing the mean flow during the spring season over 80 years. Comparison to drifter data suggest that our model overestimates retention of larvae on the shelf. One rather simplistic assumption of our model is that the wind is treated as uniform over the entire shelf. Helbig *et al.* (1992) demonstrated that spatially varying wind fields such as storms could influence drift of larvae from shelf regions to inshore regions. Better parameterisation of the wind driven component of flow is undoubtedly important. Varying vertical diffusivity may allow wind-induced vertical currents (Werner *et al.* 1993) which change the vertical distribution and thus the horizontal drift of larvae. Temporal variations in the vertical diffusivity coefficient could modulate the magnitude of the wind driven component of flow with time. Also, as has been noted by Lazier and Wright (1993), overall transport of the Labrador Current undergoes seasonal fluctuations due to fresh water runoff. Time of spawning with respect to variations in the strength of the Labrador current may also vary retention. Thus there are a number of other factors that must be considered for inclusion in future biological/physical models of this region.

The wind-driven and mean components of flow allow eggs seeded north and west of Cape Freels to drift into coastal Newfoundland. Eggs spawned near the shelf break, are advected along the shelf by the mean and wind-driven circulation and

are not carried towards the coast. In our model, eggs and larvae may drift from the Newfoundland Shelf on to the Grand Banks, contrary to the drifter modelling of Helbig *et al.* (1992). Based on regions of reduced advection, suitable spawning grounds would be the mid shelf area north of 52°N and the north end of the Grand Banks.

Since the majority of cod are thought to spawn at the shelf break a question to be answered by future models is: how the shelf break can be a suitable spawning ground? Based on the two models presented in this thesis, the shelf break is not an ideal spawning ground. It remains to be seen if future models can show how eggs and larvae seeded at the shelf break can reach coastal Newfoundland or are retained over the shelf. If modelling advection cannot validate shelf retention of larvae spawned at the shelf break, then we will need to readdress the question of suitable nursery grounds for northern cod populations spawning at the shelf break.

Appendix A

Finite Differencing the Pollard Millard Model

The model that we apply was developed by Pollard and Millard (1970).

We solve the following equations numerically.

$$\frac{\partial u}{\partial t} - fv = \frac{\tau^x}{\rho h} - ru \tag{A.1}$$

$$\frac{\partial v}{\partial t} + fu = \frac{\tau^y}{\rho h} - rv \tag{A.2}$$

where u are v are x and y components of flow, τ^x and τ^y are the x and y components of wind stress, h is the depth of the mixed layer, ρ is the density of sea water, r is

the coefficient of linear friction and f is the Coriolis parameter.

The above differential equations are solved using a leap frog in time differencing scheme.

$$u^{n+1} = 2\Delta t \left\{ \left(\frac{\tau^x}{\rho h} \right)^n - r u^n + f v^n \right\} + u^{n-1} \tag{A.3}$$

$$v^{n+1} = 2\Delta t \left\{ \left(\frac{\tau^y}{\rho h} \right)^n - r u^n - f u^n \right\} + u^{n-1} \tag{A.4}$$

Superscript n refers to the time step at time $n\Delta t$ where n is a integer.

A problem occurring with the leap frog in time differencing is time splitting. Since the solution of velocities at time step $n+1$ is solved by adding a factor to the velocity solution at time step $n-1$, the solution from one time step to the next may drift apart such that after many time steps the solution of velocities at even n time steps no longer resembles the solution at odd n time steps. To ensure that even and odd solutions do not drift apart, we use a forward time stepping scheme every *nft* timesteps. Here *nft* is an odd integer chosen arbitrarily. The forward in time solutions of the differential equations are:

$$u^{n+1} = \Delta t \left\{ \left(\frac{\tau^x}{\rho h} \right)^n - r u^n + f v^n \right\} + u^n \tag{A.5}$$

$$v^{n+1} = \Delta t \left\{ \left(\frac{\tau^y}{\rho h} \right)^n - r u^n - f u^n \right\} + u^n \tag{A.6}$$

If $d << f$ Stability in the model solutions is assured by

$$\Delta t < \frac{1}{2f} \tag{A.7}$$

Appendix B

Lagrangian Tracking Routine

In this section we describe the Lagrangian tracking routine used in this thesis. We present a simple iterative procedure for determining the position of a passive particle advected through a 2 dimensional time-dependent flow field defined on a finite difference mesh.

The velocity of a passive drifter is equal to the instantaneous velocity of the fluid at the drifter's current location. The velocity field is known only at discrete intervals in space and time, whereas discrete particles drift through the velocity field continuously in space and time. Therefore we interpolate the velocity field to a particle location to find its advection velocity. To ensure smoothness in particle paths we implement an iterative time averaging method for determining particle positions

at the next time step.

At time t, a particle has position $\vec{p}(t)$ in a surrounding fluid of velocity $\vec{u}(\vec{p}(t), t)$. The position of the particle at time $t+dt$ is then derived from:

$$\frac{\vec{p}(t+dt) - \vec{p}(t)}{dt} = \vec{u}\,(\vec{p}(t), t) \qquad (B.1)$$

where dt is the duration of the time step and is identical to the time step of the circulation field.

To reduce displacement errors generated by spatial and temporal gradients in the Eulerian velocity field, a scheme of averaging the velocity at the previously estimated particle position at time t with the velocity at the current estimated particle position at time $t+dt$ is implemented.

For the first iteration we have

$$\vec{p}_1(t+dt) = \vec{p}(t) + \vec{u}\,(\vec{p}(t), t)\; dt \qquad (B.2)$$

For subsequent iterations:

$$\vec{p}_i(t+dt) = \vec{p}(t) + \left\{\overline{\vec{u}_i}\right\} dt \qquad (B.3)$$

where

$$\overline{\vec{u}_i} = \frac{1}{2}\left\{\vec{u}(p(\vec{t}), t) + \vec{u}(\vec{p}_{i-1}(t+dt), t+dt)\right\}$$

The convergence criterion to stop the iteration is that

$$\|u_i - u_{i-1}\| < 0.1\ cm/s$$

The scheme is stable for:

$$dt\ <\ 2/\left\|\frac{d\vec{u}}{d\vec{p}}\right\|_{\max}$$

The interpolation scheme used is bilinear interpolation. When a particle is advected out of the domain, the particle is ignored and its position assigned an out-of-bounds value.

Appendix C

Geometrical method for calculating the area covered by a set of points on a spherical surface

We wish to develop a geometrical method to calculate the area of a given set of points $\vec{P}$ (Figure C.1) situated on a spherical surface. We start with a simple polygon $\vec{C}$ (Figure C.3) based upon modification of the convex hull (Figure C.2) of the set of points $\vec{P}$. The area of the polygon $\vec{C}$ describes the area of the given set of points $\vec{P}$. Here we present the algorithm for measuring the area of a set of points on a spherical

surface, evaluate imposed constraints and discuss the utility of the method.

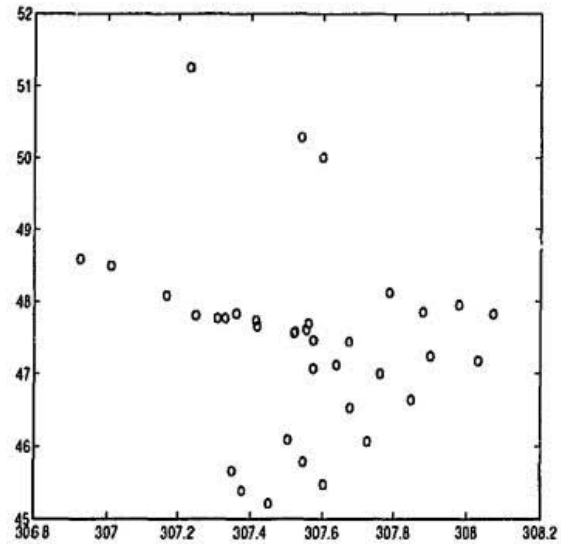

Figure C.1: Points $\vec{P}$ (circles) which span an area measured on the earth's surface. The axes are in degrees East and North.

The algorithm starting point is a convex hull surrounding the set of points (Figure C.2). A convex hull of a set of points is a convex polygon surrounding the set. For details on building the convex hull see Preparata and Shamos (1985). Since the area surrounded by a convex hull can be severely increased by having just one point located far from the others in the set, we cannot use the convex hull as a measure for the area of the set of points $\vec{P}$. Therefore we create a polygon $\vec{C}$ that contains more vertices and thus depends on a larger subset of points in $\vec{P}$. The construction of $\vec{C}$ is done by replacing the longest edge of the convex hull by two new edges which

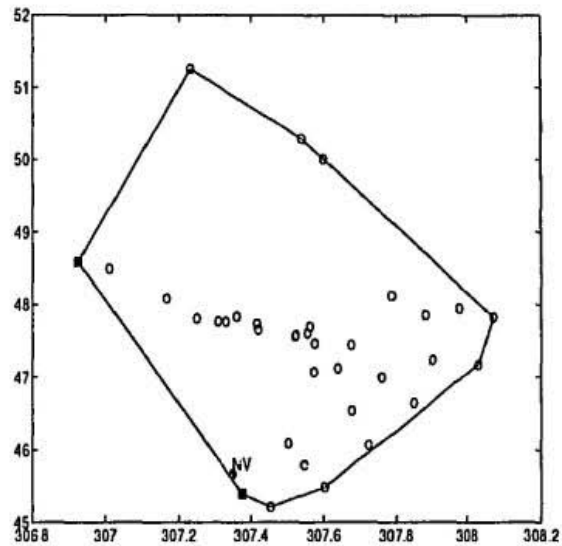

Figure C.2: The Convex Hull of $\vec{P}$: The two vertices marked by * refer to the longest edge. *NV* refers to the next interior point to be added to the Convex Hull. The axes are the same as in Figure C.1.

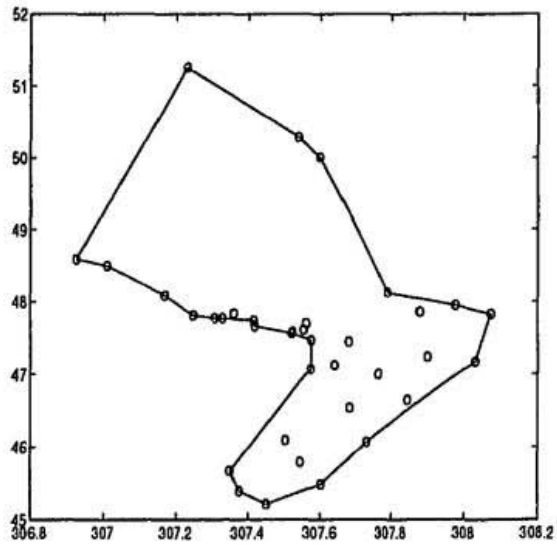

Figure C.3: Final polygon $\vec{C}$ surrounding the set of points $\vec{P}$. The area of the polygon represents the area of the set of points $\vec{P}$. The axes are the same as in Figure C.1.

include a new vertex NV taken from the interior points. We iterate this process always seeking to replace the longest segment of the contouring polygon by two new segments. Once the number of vertices of the contour reach a specified fraction of the total number of initial points in $\vec{P}$ we stop the iteration.

Before we discuss the conditions governing the adding of new vertices to the convex hull we explore the notation used in this algorithm. Any set of points on a plane can be defined by a vector with imaginary notation. The real part of each element of the vector represents the abscissa of the point, the imaginary part represents the ordinate. The vector list $\vec{P}$ describing the initial set of points in the plane has no

particular order. However the vector list $\vec{C}$ describing a simple polygon surrounding $\vec{P}$ is in counterclockwise order such that two consecutive vertices of $\vec{C}$ represent an edge of the polygon. The first and last element of $\vec{C}$ represent the same point so that all the edges are specified. For a contouring polygon with n points, the size of $\vec{C}$ is n+1 (i.e. $\vec{C} = (C_1, C_2, C_3, ..., C_n, C_{n+1})$ where $C_1 = C_{n+1}$) . Since the first and last element of $\vec{C}$ represent the same point, all edges are specified by $\overline{C_iC_{i+1}}$ where $i \in (1, ..., n)$.

In this algorithm we make use of two coordinate systems. Initially the points to be contoured are on a spherical plane. Polygon edge lengths are calculated on the spherical plane while the choice of new points to add to the polygon boundary is done in Cartesian coordinates. Evaluation of an area bounded by a closed geometrical object on a spherical plane shall be accomplished in spherical coordinates.

Initially $\vec{C}$ is the convex hull of the initial set of points. At this stage $\vec{P}$ represents the interior points not on the convex hull boundary. We select the longest edge $\overline{C_iC_{i+1}}$ in $\vec{C}$. To search for a new vertex NV we transform $\vec{C}$ and $\vec{P}$ into Cartesian coordinates so that C_i is at the origin and $\overline{C_iC_{i+1}}$ has an angle of zero. We require that any new vertex NV that we add to $\vec{C}$ must be situated between $x = 0$ and $x = real(C_{i+1})$. We also require that the two new edges defined with the new vertex

NV (i.e. $\overline{C_iNV}$ and $\overline{NVC_{i+1}}$) do not form an interior angle less than β ($\beta = 10^o$) with other edges, intersect the existing boundaries or result in any points being outside the new contour $\vec{C}$. We also require that none of the new edges formed be longer than the edge they are replacing. We choose the point having the smallest ordinate that satisfies this criterion.

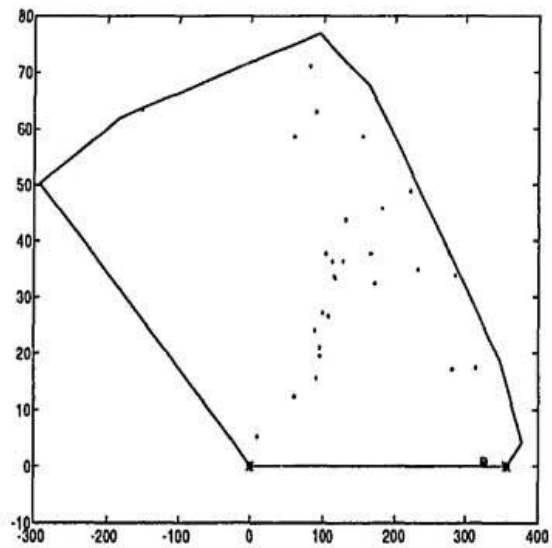

Figure C.4: Replacing the longest edge of the convex hull (1st iteration). Axes are in Cartesian coordinates of km. C_i is at the origin. C_{i+1} is on the horizontal axis. The dotted circle represents the closest interior point that satisfies the new vertex criterion for the longest edge $\overline{C_iC_{i+1}}$.

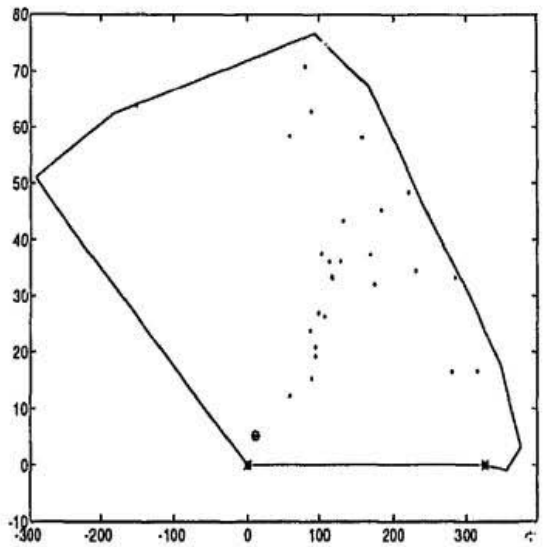

Figure C.5: Replacing longest edge of the convex hull (2nd iteration)

If a suitable new vertex is found we add it between the appropriate vertices in $\vec{C}$ and delete it from the interior points $\vec{P}$. If no suitable vertex is found for the longest edge we eliminate that edge from further consideration for replacement. The procedure of defining two new edges for the longest edge of $\vec{C}$ is repeated until the number of vertices in $\vec{C}$ corresponds to an arbitrary fraction of the initial number of given points in $\vec{P}$. Further more, if there are no more interior points that satisfy conditions to become vertices, the iteration stops. Further discussion on the stop criterion is found at the end of the appendix.

Next we wish to calculate the area of the polygon defined by $\vec{C}$. For this $\vec{C}$ must be in spherical coordinates (latitude and longitude coordinates). $\vec{C}$ lies on a spherical surface with radius R (R = 6321 km). We first calculate the area of the convex hull. From this we subtract the area of the spherical triangles that we have eliminated from the convex hull to form the final contouring polygon $\vec{C}$ (Figure C.6).

To calculate the area of the convex hull we triangulate it (Preparata and Shamos 1985) and then apply spherical triangle area calculations. Figure C.7 illustrates the coordinates used for calculating the area of a spherical triangle and the appropriate equations are given below.

The angle θ_i covered by the great circle route between two vertices on the sphere can be calculated from the projection of one vertex over the other.

$$\cos\theta_i = \frac{\vec{p_j} \bullet \vec{p_k}}{\| \vec{p_j} \| \| \vec{p_k} \|} \qquad (C.1)$$

The following two relations for spherical triangles are given in Weast et Al. (1964). The interior angles α_i of the spherical triangle can be derived from :

$$\cos\alpha_i = \frac{\cos\theta_i - \cos\theta_j \cos\theta_k}{\sin\theta_j \sin\theta_k} \qquad (C.2)$$

Where $i, j, k \in (1, 2, 3)$ and i, j, k all differ.

The area of a spherical triangle is a function of the sum of its interior angles.

$$AREA(p_{1,2,3}) = (\sum_{i=1}^{i=3} \alpha_i - \pi) R^2 \qquad (C.3)$$

Thus to calculate the area of a set of points, we construct its convex hull, add vertices to achieve a polygon that gives a better geometrical fit to the points, triangulate and apply spherical triangles relations to calculate the total area of the polygon.

We evaluate our polygon routine by comparing it to two other methods for estimating the area of a set of points. These are the area of the standard deviation ellipse and the area of the convex hull. We will also discuss and illustrate the fine tuning of the number of vertices needed to represent accurately a set of points. This

includes a comparison between two sets of initial points of different size.

In the Standard Deviation Ellipse Method we fit a line by linear regression to the set of points $\vec{P}$. The standard deviation along this line is σ_x, perpendicular to this line the standard deviation of the set of points is σ_y. The mean location of the points is given by $\hat{P}$. We then draw an ellipse with σ_x as the major axis along the fitted line, σ_y as the minor axis and $\hat{P}$ as the centre. The area of this ellipse is given by $\pi\sigma_x\sigma_y$ and represents the area of the set of points.

The main advantage of the polygon is that its perimeter can mould itself to the different patterns encountered in a set of points. The shape of the standard deviation ellipse is rigid. The convex hull's shape depends on the distribution of the set of points, however its area can depend heavily on an isolated point in the set.

In Figures C.8 through C.11 we illustrate the three methods for different sets of points. The total number of initial points are 72, the minimum interior angle β is 10^o and the ratio of vertices to total points is $\frac{1}{3}$. These points indicate the position of a set of model drifters in an experiment. An array of drifters placed on a square grid is left free to be advected by the current.

After 20 days the set of drifters is still well ordered (Figure C.8). In this case the convex hull gives the best looking contour for the set of points. Our method of the polygon in this case reduces the area slightly but may lead to a jagged boundary.

The polygon routine "searches too much" for the boundary of a well ordered set of points. As for the ellipse method, it consistently underestimates the area. On Figure C.9 we see a weakness in our polygon contouring routine. The creation of the polygon relies on conditions imposed on points to add to the longest edge. However it may happen that a new vertex to the longest edge may be very close to another edge in the contour. There is no direct mechanism for giving preference of an interior point to a particular edge due to geometric proximity. However increasing the minimum size (β) of any interior angle avoids the problem.

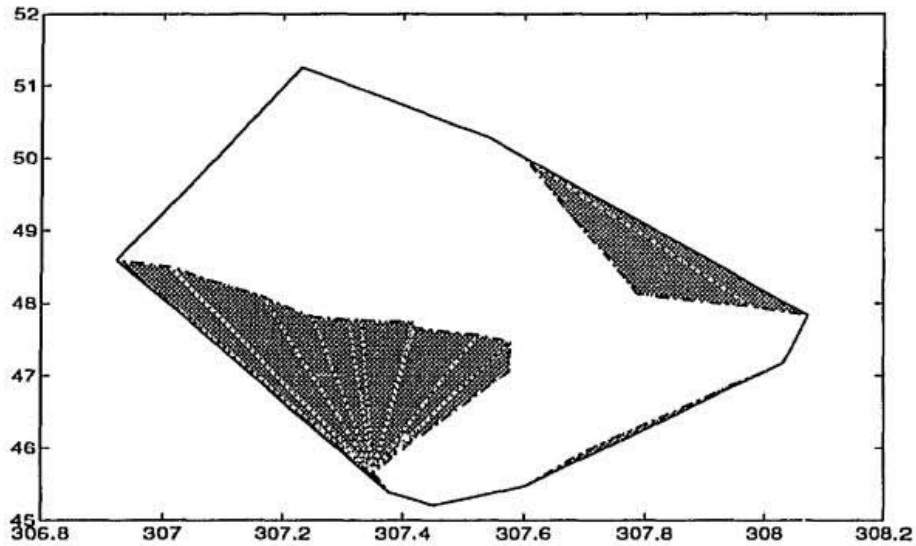

Figure C.6: Area Calculation: The area of the polygon $\vec{C}$ (dotted dashed line) is calculated by subtracting the triangular shaded areas from the area of the convex hull (solid line).

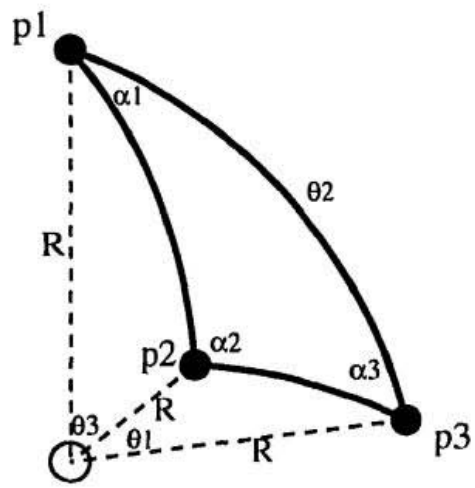

Figure C.7: A spherical triangle: The circle represents the sphere's centre, α_i's are the interior angles of the spherical triangle, θ_i's are the angles of the great circle route between two vertices on the spherical triangle and $\vec{p_i}$'s are the vertices of the spherical triangle. $\vec{p_i} = (\lambda_i, \phi_i, R)$ where $i \in (1, 2, 3)$.

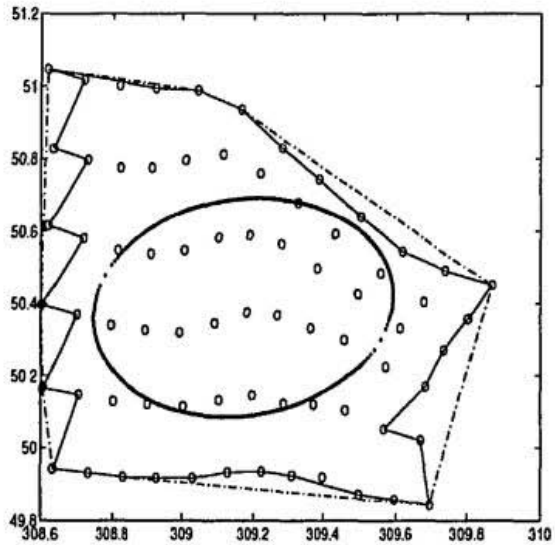

Figure C.8: 20 days after release, area of polygon 7738 km^2 (solid line), area of convex hull 8965 km^2 (dashed dotted line), area of standard deviation ellipse 3153 km^2 (dots).

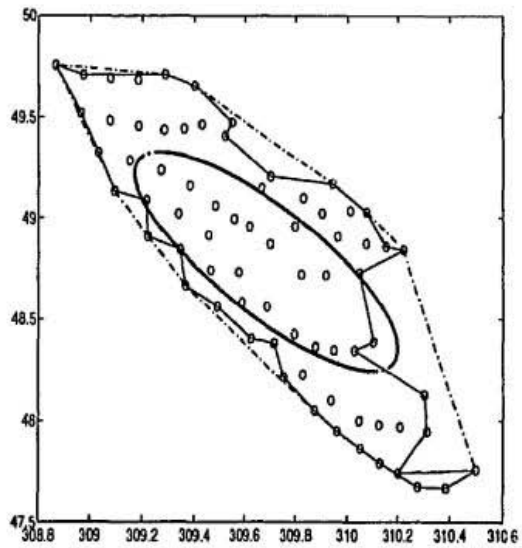

Figure C.9: 50 days after release, area of polygon 9009 km^2 (solid line), area of convex hull 11610 km^2 (dashed dotted line), area of standard deviation ellipse 4216 km^2(dots).

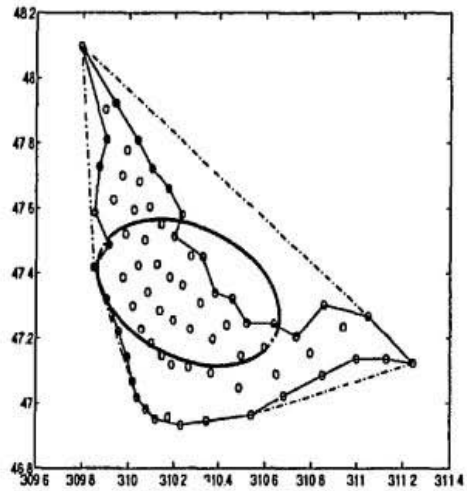

Figure C.10: 80 days after release, area of polygon 4194 km^2 (solid line), area of convex hull 6771 km^2 (dashed dotted line), area of standard deviation ellipse 2241 km^2 (dots).

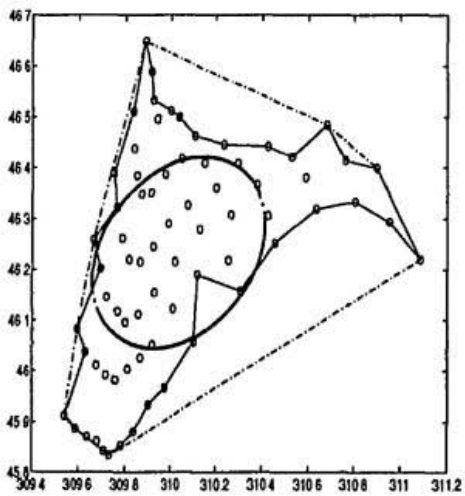

Figure C.11: 120 days after release, area of polygon 3518 km^2 (solid line), area of convex hull 6014 km^2 (dashed dotted line), area of standard deviation ellipse 1817 km^2 (dots).

Here we discuss the specifics of the parameters chosen in the polygon. We will discuss the number of points in the set, the ratio of vertices to total number of points, the maximum length of new edges criterion as well as the minimum angle β criterion.

The criterion we set for eligibility of a interior point as a new vertex on the polygon boundary determine the final characteristics of the polygon. In Figures C.12 to C.17 we present the contouring polygon for 4 different ratios of boundary points over total points in the set. For this case the total number of points is 36 or 72 and the most suitable ratio is $\frac{2}{3}$. Suitability is determined by the ability of the polygon to outline the shape of the set of points without adding unnecessary detail and is decided subjectively. We can see in Figure C.15 where all the points lie on the boundary that the shape of the polygon no longer represents the general shape of the points. The polygon is almost divided into two.

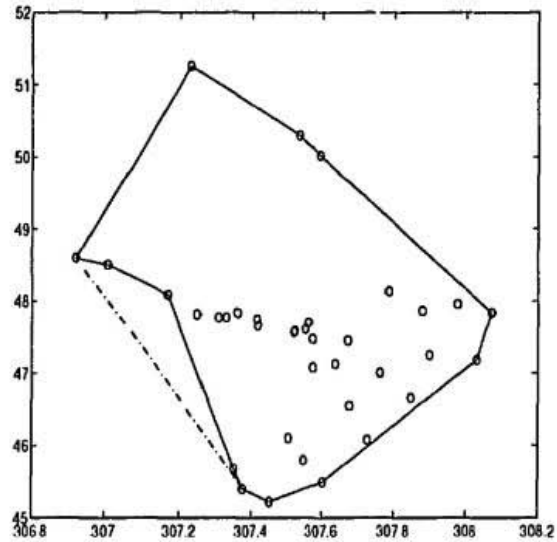

Figure C.12: Ratio of $\frac{1}{3}$, 12 vertices out of 36 points

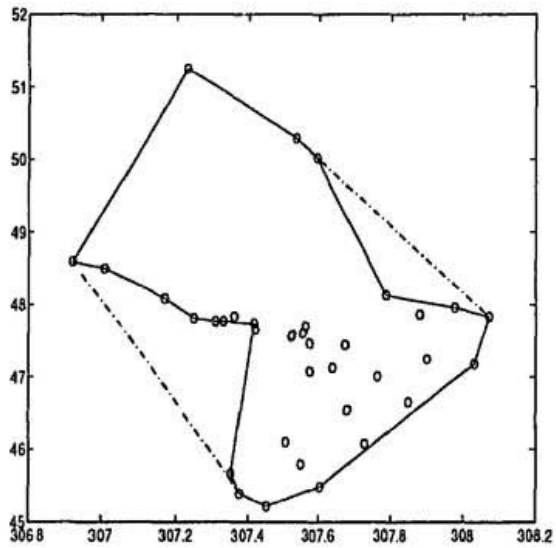

Figure C.13: Ratio of $\frac{1}{2}$, 18 vertices out of 36 points

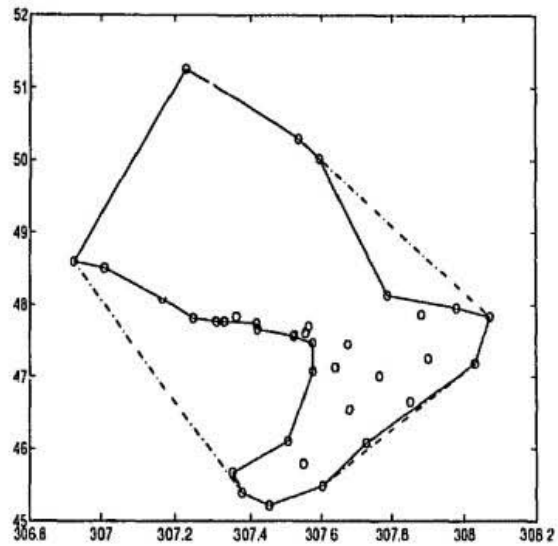

Figure C.14: Ratio of $\frac{2}{3}$, 24 vertices out of 36 points

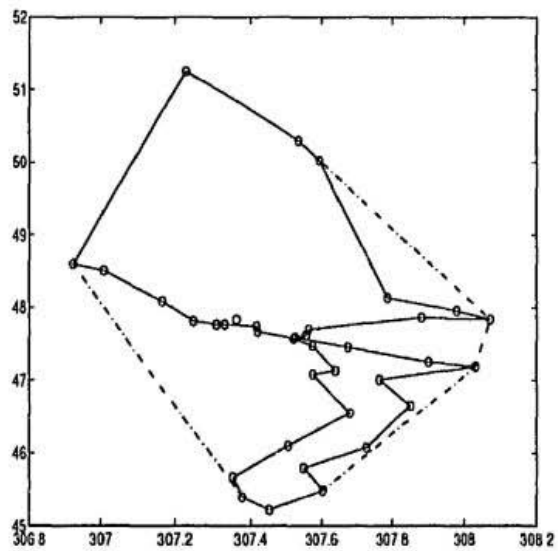

Figure C.15: Ratio of 1, 35 vertices out of 36 points

To illustrate the difference that the total number of initial points makes on the choice of the ratio of boundary points, we choose to contour a set of 72 points (Figures C.17 to C.21). Here, however, the choice of the other parameters comes into play. For a ratio of $\frac{1}{3}$ the polygon represents the geometry of the points well. For higher values the boundary becomes too jagged. As we increase the number of points we wish to have on the boundary we discover a limit of 52 points for the set shown. Thus the criterion by which we choose a new vertex constrains in some cases the polygon to a maximum number of points on the polygon. For a set of 36 points a ratio of $\frac{2}{3}$ was suitable whereas for a set of 72 points a ratio of $\frac{1}{3}$ was suitable. Also the greater the ratio, the smaller the overall area covered by the resulting polygon.

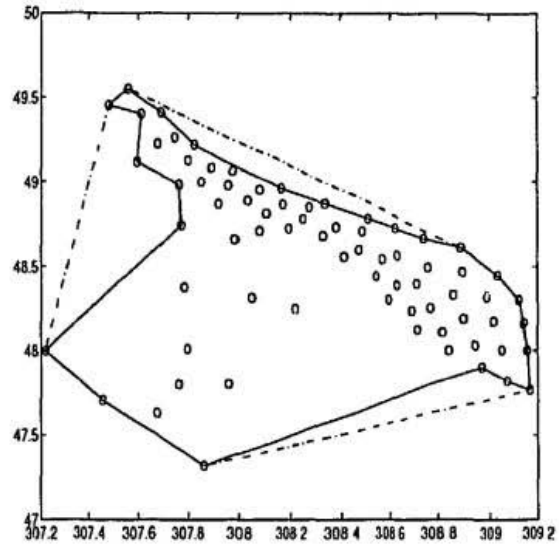

Figure C.16: Ratio of $\frac{1}{3}$, 24 vertices out of 72 points, area:

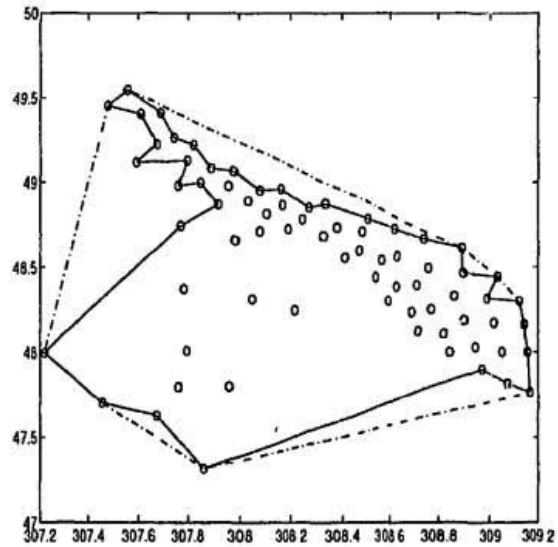

Figure C.17: Ratio of $\frac{1}{2}$, 36 vertices out of 72 points

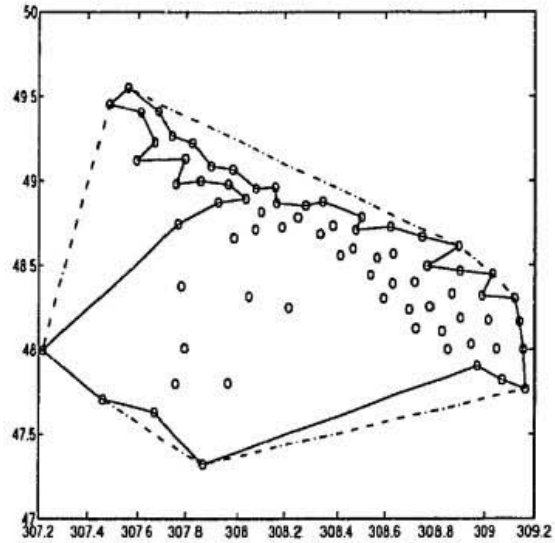

Figure C.18: Ratio of $\frac{2}{3}$, 42 vertices out of 72 points. Here it is the new vertex criterion that limit the number of vertices and not the ratio.

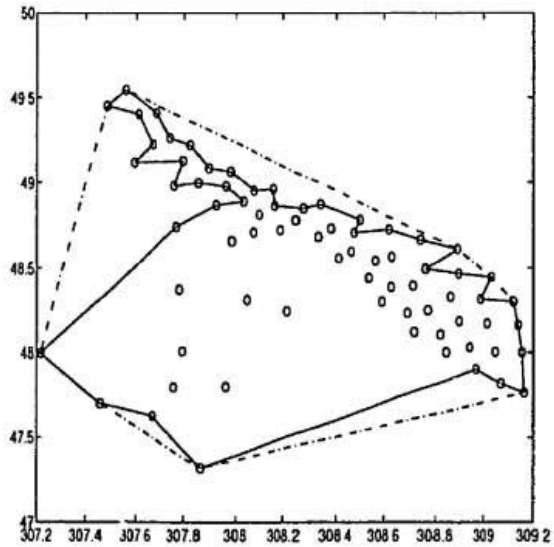

Figure C.19: Ratio of $\frac{1}{1}$, 42 vertices out of 72 points; Here it is the new vertex criterion that limit the number of vertices and not the ratio.

Finally, we present in Figure C.21 the effect of the minimum interior angle β. Increasing β may increase the polygon's surface area by approximately 10%. Furthermore, a larger β smoothes the shape of the bounding polygon. However the polygon routine is not as sensitive to the interior angle limit as it is to the ratio of vertices over total number of points.

The polygon routine working on a set of points distributed on an evenly spaced rectangular grid can represent the rectangular geometry of the points. The convex hull would initially consist of the 4 corner points. The polygon routine would then proceed adding points that are on the initial 4 vertices of the convex hull. At this point, the regular spacing ensures that any interior point would form an edge with a vertex that is longer than the edge it replaces. Since this is not permitted by our algorithm, the polygon routine outputs the shape of the rectangular convex hull.

The polygon contouring routine constitutes a geometrical method for calculating the area of a set of points. Our method is an improvement over that of the convex hull of a set of points for area calculations since it allows more vertices on the boundary. For cases in which the set of points are regularly spaced, the resulting boundary of the polygon routine is the convex hull. The polygon routine is a method for measuring the area of a set of points in a consistent manner.. It works well when the number of points to be contoured is a constant. The parameters to be used in

the model depend on the total number of points. This routine has been developed to be used operationally. It's application demands that the choice of parameters be verified with comparison of the contouring polygon and the distribution of the set of points. For applications in this thesis single points whose presence increase the area significantly are removed before application of the polygon routine.

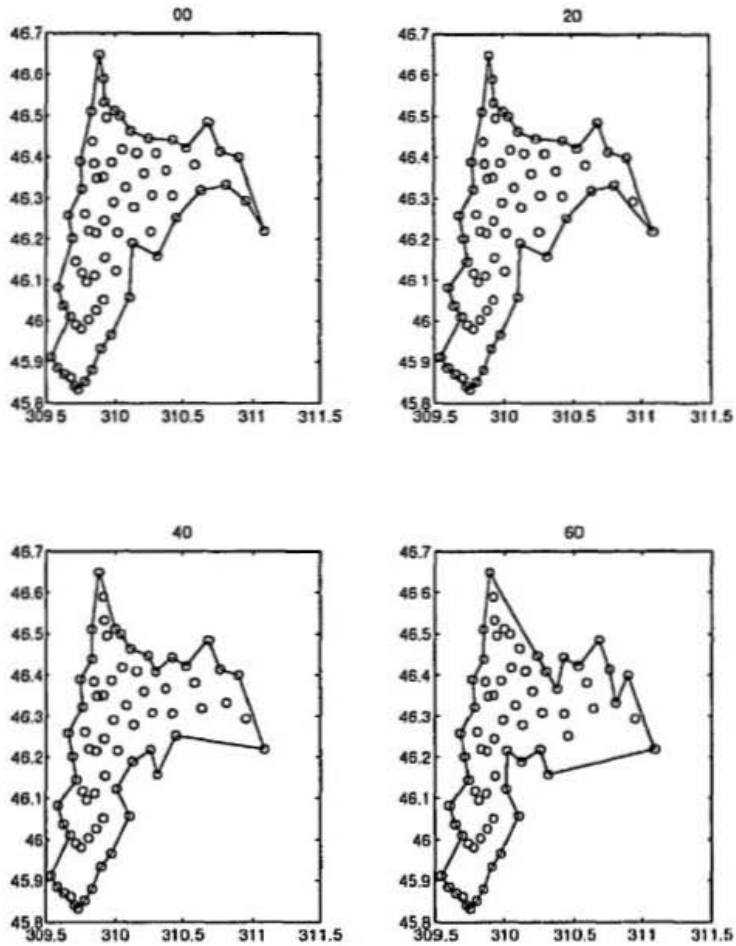

Figure C.20: Polygon routine for 4 different minimum interior angles β. β = (0°, 20°, 40°, 60°). The change in area of the polygon with respect to the polygon with $\beta = 0°$ is 1% for $\beta = 20$, 4% for $\beta = 40$ and 12% for $\beta = 60$.

References

Allen, A. A. 1979. Current variability at the offshore edge of the Labrador Current, M.Sc. thesis, Dalhousie University.

Anderson, C. 1986. Motions driven by buoyancy forces and atmospheric stresses in the Avalon Channel, Newfoundland, Canada, Institute of Oceanography, Ph.D. thesis, McGill University, 196pp.

Anderson, J., and B. de Young, 1994. Application of a 1-dimensional model of vertical distributions to cod eggs and larvae on the NE Newfoundland shelf, *Can. J. Fish. Aquat. Sci.*, submitted.

Akl, S. G., 1979. Two remarks on a convex hull algorithm. *Info. Proc. Lett.*, 8: 108-109.

Bailey, W. B. 1961. Annual variations of temperature and salinity in the Grand Banks region, Fish. Res. Board Canada, Manuscript Rep. Ser. No 74. 30pp

Baird, J., C. A. Bishop, W. B. Brodie and E. F. Murphy, 1992. An assessment of the cod stock in NAFO divisions 2J3KL. *CAFSAC Res. Doc.* 92/75, 76 pp.

Bakun, A., J. Beyer, D. Pauly, J. G. Pope, and G. D. Sharp, 1982. Ocean Sciences in Relation to Living Resources, *Can. J. Fish. Auat. Sci.*, 39: 1059-1070

Bartsch, J., K. Brander, M. Heath, P. Munk, K. Richardson and E. Svendsen, 1989. Modelling the advection of herring larvae in the North Sea, *Nature*, 340: 632-636.

Brown, J. A., P. Pepin, D. A. Methaven and D. C. Somerton, 1989. The feeding growth and behaviour of juvenile cod, *Gadus Morhua*, in cold water environments, *J. Fish. Biol.*, 35:373-380.

Chapman, D. C. and R. C. Beardsley, 1989. On the origin of shelf water in the Middle Atlantic Bight, *J. Phys. Oceanogr.*, 19:384-391.

Csanady, C. T. 1982. Circulation in the Coastal Ocean. Reidel, Amsterdam, 274 pp.

de Young, B., J. Anderson, R. J. Greatbatch, and P. Fardy, 1994a Advection-diffusion modelling of capelin larvae in Conception Bay, Newfoundland, *Can. J. Fish. Aquat. Sci.*, (In press).

de Young, B. and F. Davidson, 1994. Modelling retention of cod (*Gadus Morhua*) eggs and larvae on the Newfoundland Shelf. ICES *J. Mar. Sci.*, (In press).

de Young, B., Perry, F., and R. J. Greatbatch, 1994b. Objective analysis of hydrographic data in the Northwest Atlantic, *Canadian Data Report of Hydrographic and Ocean Sciences*, 93pp. (In press).

de Young, B., R. J. Greatbatch and K. B. Forward, 1993a. A diagnostic coastal circulation model with application to Conception Bay Newfoundland, *J. Phys. Oceanogr.* , 23.12:2617-2635.

de Young, B., T. Otterson and R. J. Greatbatch, 1993b. The local and nonlocal response of Conception Bay to wind forcing, *J. Phys. Oceanogr.* , 23.12:2636-2649.

de Young, B., and G. Rose, 1993. On recruitment and distribution of Newfoundland cod (*Gadus morhua*), *Can. J. Fish. Aquat. Sci.*, 50:2729-2741.

de Young, B., and C. L. Tang, 1990. Storm-Forced Baroclinic Near-Inertial Currents on the Grand Bank, *Can. J. Phys. Oceanogr.*, 20.11:1725-1741.

Fortier, L., M. E. Levasseur, R. Drolet and J. C. Therriault, 1992. Export production and the distribution of fish larvae and their prey in a coastal jet frontal region, *Mar. Ecol. Prog. Ser.*, 85:203-218.

Harris, L., 1991. Independent Review of the state of the Northern Cod Stock, Department of Fisheries and Oceans, Ottawa, ON.

Hilborn, R. and C. Walters, 1992. Quantitative Fisheries Stock Assessment, Chapman and Hall, New York, N.Y., 570 pp.

Gill, A.E. 1982. Atmosphere-Ocean Dynamics, Academic Press, New York, N.Y., 662 pp.

Goddard, S. V., M. H. Kao and G. L. Fletcher, 1992. Antifreeze production of juvenile nothern Atlantic cod (*Gadus Morhua*), *Can. J. Fish. Aquat. Sci.*, 49:516-522

Greenberg, D. A. and B. D. Petrie, 1988. The mean barotropic circulation on the Newfoundland shelf and slope, *J. Geophys. Res.*, 93: 15541-15550.

Gulland, J. A. 1983. Fish Stock Assessment: A Manuel of Basic Methods, John Wiley and Sons, 223pp

Helbig, J. H., G. Mertz, and P. Pepin, 1992. Environmental influences on the recruitment of Newfoundland/ Labrador cod, *Fish. Oceanogr.*, 1: 39-56.

Hempel, G. 1972. Early life history of marine fish: the egg stage, Washington Seagrant Publications, Seattle, Wa., 70 pp.

Hjort, J. 1914. Fluctuations in the great fisheries of northern Europe. *Rapp. P.-v. Réun. Cons. Int. Explor. Mer.*, 20: 1-228.

Hunter, J. R. 1987. The application of lagrangian particle tracking techniques to modelling dispersion in the sea, p 257-269 In J. Noye: *Numerical Modeling: applications to marine systems*, Elsevier Science Publishers B.V. (North Holland).

Hutchings J. A., R. A. Myers, G. R. Lilly, 1993. Geographic variations in the spawning of Atlantic Cod *Gadus Morhus*, *Can. J. Fish. Aquat. Sci.*, 50:2457-2467.

Iles, T. D. and M. Sinclair, 1982. Atlantic Herring: Stock Discretness and Abundance, *Science*, 215: 627-633.

Jarvis, R. A. 1973. On the identification of the convex hull of a finite set of points in the plane, *Info. Proc. Lett*, 2: 18-21

Kasai, A., M.J. Kishi and T. Sugimoto, 1992. Modeling the transport and survival of Japanese sardine larvae in and around the Kuroshio Current, *Fish. Oceanogr.*, 1:1-10.

Kjesbu, O. S., 1989. The spawning activity of cod, *Gadus morhua* L. *J. Fish. Biol.*, 34:195-206

Kollmeyer, R. C., D.A. McGill and N. Corwin, 1967 Oceanography of the Labrador Sea in tthe vicinity of Hudon strait in 1965, *Bull. U.S. Cst. Guard*, 19:1-34

Large, W.G. and S. Pond, 1981. Open ocean momentum flux measurements in moderate to strong winds, *J. Phys. Oceanogr.*, 11:324-336.

Lazier, J. N. and D. G. Wright, 1993. Annual velocity variations in the Labrador Current, *J. Phys. Oceanogr.*, 23.4:659-678.

Lynch, D. R., F. E. Werner, D. A. Greenberg and J. W.Loder, 1991. Diagnostic model for baroclinic, wind-driven and tidal circulation in shallow seas, *Continental Shelf Research*, 12.1:37-64

McLellan, H. J., 1957. On the distinctness and origin of the slope water off the Scotian shelf and its easterly flow south of the Grand Banks, *Fish. Res. Board Can.*, 14:213-239

Matthews, D. J., 1914 Report on the work carried out by the S.S. Scotia, 1913. Ice observation, meteorology, and oceanography of the North Atlantic Ocean. Darling and Son. Publ., London.

May, A. W. 1966. Biology and fishery of Atlantic cod, *Gadus morhua* from Labrador . Ph.D. Thesis, McGill University, Montreal, 225 pp.

Mellor, L. M., C. R. Mechoso and E. Keto 1982. A diagnostic calculation of the general circulation of the Atlantic Ocean, *Deep-Sea Research*, 29.10A:1171-1192.

Moynihan, M. J. and M. S. Anderson, 1971. Oceanography of the Grand Banks Region and the Labrador Sea - April-June,August and October 1969, *U.S. Cst. Guard Rep.*, 48 CG 378-48:1-259.

Myers, R. A., S. A. Akenhead and K. Drinkwater, 1990. The influence of Hudson Bay runoff and ice-melt on the salinity of the inner Newfoundland Shelf, *Atmosphere-Ocean*, 28.2:241-256

Myers, R. A., G. Mertz, and C. A. Bishop, 1993. Cod Spawning in Relation to physical and Biological cycles of the Northern Northwest Atlantic. *In press*

Myers, R. A. and K. F. Drinkwater, 1988. Offshelf Ekman transport and larval fish survival in the Northwest Atlantic, *Biological Oceanography*, 6:45-64.

Nelson, W. R., M. C.Ingham, and W. E. Schaaf, 1977. Larval transport and year-class strength of Atlantic Menhaden, *Brevoortia Tyrannus. Fishery Bulletin*, 75.1:23-41.

Page,F. H. and P. C. Smith, 1989. Particle Drift in the Surface Layer off Southwest Nova Scotia: Description and Evaluation of a Model, *Can. J. Fish. Aquat. Sci.* , 46(Suppl. 1):21-43.

Page,F. H. and K. T. Frank, 1989. Spawning time and egg stage duration in Northwest Atlantic Haddock (Melanogrammus aeglefinus) Stocks with Emphasis on Georges and Browns Bank, *Can. J. Fish. Aquat. Sci.* , 46(Suppl. 1):68-81.

Petrie, B., J. W. Loder, J. Lazier and S. Akenhead, 1992. Temperature and salinity variations on the Eastern Newfoundland Shelf: The residual field, *Atmosphere-Ocean*, 30: 120-139.

Petrie, B. and C. Anderson, 1983. Circulation on the Newfoundland continental shelf, Atmosphere-Ocean, 21: 207-226.

Petrie, B. D. 1985. Mean and variable current : over the Grand Banks, BIO review'85, DFO, pp38-40.

Petrie, B. D. and A. Isenor, 1985. The near surface circulation and exchange in the Newfoundland Grand Banks Region, *Atmosphere Ocean*, 23.3:209-227.

Pepin, P. and R. A. Myers, 1991. Significance of egg and larval size to recruitment variability of temperate marine fish, *Can. J. Fish. Aquat. Sci.* , 48:1820-1828.

Pitcher, T. J. and P. J. Hart, 1982. Fisheries Ecology, Chapman and Hall, 414 pp.

Pinhorn, A. T. and R. G. Halliday, 1990. Canadian versus international regulation of northwest atlantic fisheries: Management practices, fishery yields, and resource trends, 1960-1986. *N. Am. J. fish. Man.*, 10:154-174.

Pollard, R. T, 1970. On the generation of inertial waves in the ocean, *Deep Sea Res.*, 17:795-812.

Pollard, R. T. and R. C. Millard, 1970. Comparison between observed and simulated wind-generated inertial oscillations, *Deep Sea Res.*, 17:813-821.

Preparata, P. P. and M. I. Shamos, Computational Geometry: an Introduction, Springer Verlag, Berlin, 1985. 376pp

Rose, G. A., 1993. Cod spawning on a migration highway in the north-west Atlantic, *Nature*, 366:458-461.

Scalfani, M., C. T. Taggart and K. R. Thompson, 1993. Condition, buoyancy and the distribution of larval fish: implications for vertical migration and retention, *Journal of Plankton Research* , 15.4:413-435.

Scott, W. B. scott and M. G. Scott, 1988. Atlantic fishes of Canada, Can. Bull. Fish. Aquat. Sci. 219:731pp.

Smith, E. H., F. M.Soule and O. Mosby, 1937. The Marion and General Greene expeditions to Davis Straight and Labrador Sea, *Bull. Coast Guard*, 19, 259pp.

Sutcliffe, W. H., R. H. Loucks, K. F. Drinkwater and A. R. Coote, 1983. Nutrient flux onto the Labrador Shelf from Hudson Strait and its biological consequences, *Can J. Fish. Aquat. Sci.*, 40:1692-1701.

Templeman, W., 1981. Vertebral Numbers in Atlantic Cod, *Gadus Morhua*, of the Newfoundland and adjacent areas, 1947-1971, and their use for delineating cod stocks, *Northwest Atlantic Fish. Sci.*, 2:21-45.

Templeman, W. 1966. Marine resources of Newfoundland. Fisheries Research Board of Canada, Ottawa, Bulletin no. 154: 170 pp.

Weast, R. C. (editor), 1964. CRC Standard Mathematical Tables (Student Edition), The Chemical Rubber Co.

Werner, F. E., F. H. Page, D. R. Lynch, J. W. Loder, R. G. Lough, R. I. Perry, D. A.Greenberg and M. M.Sinclair, 1993. Influences of mean advection and simple behaviour of cod and haddock early life stages on Georges Bank. *Fisheries Oceanography* , 2.2: 43-64.